MULTI-YEAR TIME SERIES CROP MAPPING

A THESIS SUBMITTED TO
THE GRADUATE SCHOOL OF INFORMATICS OF
THE MIDDLE EAST TECHNICAL UNIVERSITY

BY

MUSTAFA TEKE

IN PARTIAL FULFILLMENT OF THE REQUIREMENTS
FOR
THE DEGREE OF DOCTOR OF PHILOSOPHY
IN
THE DEPARTMENT OF INFORMATION
SYSTEMS

JANUARY 2020

MULTI-YEAR TIME SERIES CROP MAPPING

Submitted by MUSTAFA TEKE in partial fulfillment of the requirements for the degree of **Doctor of Philosophy in Information Systems Department, Middle East Technical University** by,

Prof. Dr. Deniz Zeyrek Bozşahin
Dean, **Graduate School of Informatics** _____

Prof. Dr. Sevgi Özkan Yıldırım
Head of Department, **Information Systems** _____

Prof. Dr. Yasemin Yardımcı Çetin
Supervisor, **Information Systems Dept., METU** _____

Examining Committee Members:

Assoc. Prof. Dr. Banu Günel Kılıç
Information Systems Dept., METU _____

Prof. Dr. Yasemin Yardımcı Çetin
Information Systems Dept., METU _____

Assoc. Prof. Dr. Behçet Uğur Töreyin
Informatics Institute, İstanbul Technical University _____

Prof. Dr. Alptekin Temizel
Multimedia Informatics Dept., METU _____

Prof. Dr. İlhami Bayramin
Soil Science and Plant Nutrition Dept., Ankara University _____

Date:

I hereby declare that all information in this document has been obtained and presented in accordance with academic rules and ethical conduct. I also declare that, as required by these rules and conduct, I have fully cited and referenced all material and results that are not original to this work.

Name, Last name: Mustafa Teke

Signature :

ABSTRACT

MULTI-YEAR TIME SERIES CROP MAPPING

Teke, Mustafa

Ph.D., Department of Information Systems

Supervisor: Prof. Dr. Yasemin Yardımcı Çetin

January 2020, 101 pages

Recent automated crop mapping via supervised learning-based methods have demonstrated unprecedented improvement over classical techniques. However, most crop mapping studies are limited to same-year crop mapping in which the present year's labeled data is used to predict the same year's crop map. Classification accuracies of these methods degrade considerably in cross-year mapping. Cross-year crop mapping is more useful as it allows the prediction of the following years' crop maps using previously labeled data. We propose Vector Dynamic Time Warping (VDTW), a novel multi-year classification approach based on the warping of angular distances between phenological vectors. The results prove that the proposed VDTW method is robust to temporal and spectral variations compensating for different farming practices, climate and atmospheric effects, and measurement errors between years. We also describe a method for determining the most discriminative time window that allows high classification accuracies with limited data. We carried out tests of our approach with Landsat 8 time-series imagery from years 2013 to 2015 for classification of corn and cotton in the Harran Plain, and corn, cotton, and soybean in the Bismil Plain of Southeastern Turkey. In addition, VDTW was tested with corn and soybean in Kansas, the US for 2017 and 2018 with the Harmonized Landsat Sentinel data. The VDTW method improved the cross-year overall accuracies by 3% with fewer training samples compared to other state-of-the-art approaches including spectral angle mapper (SAM), dynamic time warping (DTW), time-weighted DTW (TWDTW), random forest (RF), support vector machines (SVM) and deep long short-term memory (LSTM).

Keywords: time series, crop mapping, phenology, multi-year classification, dynamic programming

ÖZ

ÇOKLU-YIL ZAMAN SERİSİ ÜRÜN HARİTALAMA

Teke, Mustafa
Doktora, Bilişim Sistemleri Bölümü
Tez Yöneticisi: Prof. Dr. Yasemin Yardımcı Çetin

Ocak 2020, 101 sayfa

Son yıllarda geliştirilen öğreticili makine öğrenme yöntemleri klasik yöntemlere göre benzeri görülmemiş iyileştirme sağlamışlardır. Ancak, ürün sınıflandırma çalışmlarının çoğu aynı yıla ait verinin yine aynı yıla ait eğitim verisi kullanmaktadır. Bu yöntemlerin farklı yıllara ait eğitim verisi kullandığı durumlarda sınıflandırma sonuçları önemli ölçüde düşmektedir. Yıllar arası ürün eşlemesi, daha önce toplanmış verileri kullanarak sonraki yıllardaki ürün deseni haritalarını tahmin edilmesine izin verdiği için daha kullanışlıdır. Bu çalışmada, fenoloji vektörleri arasındaki açısal mesafeye göre bükme gerçekleştiren vektör dinamik zaman bükme algoritması geliştirilmiştir. Testler, önerilen VDTW yönteminin farklı tarım uygulamalarını, iklim ve atmosferik etkileri ve yıllar arasındaki ölçüm hatalarını telafi eden zamansal ve spektral değişimlere karşı gürbüz olduğunu göstermektedir. Ayrıca, sınırlı veri ile yüksek sınıflandırma doğruluklarına izin veren optimal zaman penceresini belirlemek için bir yöntem de geliştirilmiştir. Testlerde, 2013-2015 yılları arasında Harran Ovası'nda pamuk ve mısır, Bismil Ovası'nda mısır, pamuk ve soya fasülyesi ürünlerini içeren zaman serisi Landsat 8 uydu görüntüleri kullanılmıştır. Bunun yanında, 2017 ve 2018 yıllarında ABD, Kansas'taki VDTW mısır ve soya fasulyesini Harmonize Landsat Sentinel (HLS) verileriyle testler gerçekleştirildi. VDTW yöntemi, spektral açı eşleştiricisi (SAM), dinamik zaman bükme (DTW), zaman ağırlıklı DTW (TWDTW), rastgele orman (RF), destek vektör makineleri (SVM) ve derin uzun kısa süreli bellek (LSTM) dahil olmak üzere diğer en başarılı yaklaşımlara kıyasla daha az veri kullanarak yıllar arası doğrulukları %3 iyileştirdi.

Anahtar Sözcükler: zaman serisi, fenoloji, çoklu-yıl sınıflandırma, dinamik programlama

To My Beloved Family

ACKNOWLEDGMENTS

I would like to express my deepest gratitude to my supervisor, Prof. Dr. Yasemin Yardımcı Çetin, for her guidance, encouragement, and support during the preparation of this thesis. I will never forget her assistance and positive approach during my Ph.D. studies.

I owe my deepest gratitude to Assoc. Prof. Dr. Banu Günel and Assoc. Prof. Dr. Behçet Uğur Töreyin for their contributions and comments during the thesis. I would like to extend my gratitude to Prof. Dr. Alptekin Temizel and Prof. Dr. İlhami Bayramin for their valuable comments, suggestions, and evaluations.

I am deeply grateful to F. Fehmi Şimşek for his fantastic help in providing and preparing ground truth.

I would like to thank my friends in the Information Technologies department and colleagues at TÜBİTAK UZAY Space Technologies Research Institute for their friendship and encouragement.

I can not state how the support from my family was invaluable, and I am indebted a lot of time to spend together with my wife Elif, my daughter Rana and my son Emirhan.

TABLE OF CONTENTS

LIST OF TABLES

TABLE

LIST OF FIGURES

FIGURE

LIST OF ABBREVIATIONS

DL	Deep Learning
DoY	Day of Year
DTW	Dynamic Time Warping
EVI	Enhanced Vegetation Index
GNDVI	Green NDVI
HLS	Harmonized Landsat Sentinel
LSTM	Long Short-Term Memory
ML	Machine Learning
MSAVI	Modified Soul Adjusted Vegetation Index
NDVI	Normalized Difference Vegetation Index
NIR	Near-Infrared
NRF	National Registry of Farmers
OSAVI	Optimized Soil Adjusted Vegetation Index
PA	Producer's Accuracy
PVDTW	Partial Vector Dynamic Time Warping
RF	Random Forest
SAM	Spectral Angle Mapper
SAR	Synthetic Aperture Radar
SAVI	Soil Adjusted Vegetation Index
SGF	Savitzky-Golay Filtering
SVM	Support Vector Machine
TWDTW	Time Weighted DTW
UA	User's Accuracy
VDTW	Vector Dynamic Time Warping
VI	Vegetation Index
WDRVI	Wide Dynamic Range Vegetation Index

CHAPTER 1

INTRODUCTION

The world population has been increasing so that it is expected to be over nine billion in 2050(United Nations, 2015). Providing the necessary amount of food for the increasing human population is a significant concern. On the other hand, advanced agricultural technologies, such as precision agriculture and precision irrigation are rapidly emerging to optimize water, fertilizers, and pesticides, thereby enabling higher crop yield. Remote sensing is a critical technology that would enable us to observe the growth of field crops. Satellite imagery is a standard method to monitor large areas.

Advanced applications, such as precision agriculture or crop yield estimation, require accurate crop mapping. Early-season crop yield estimates are a vital factor for food security. Crop maps are also required for statistical purposes to analyze annual changes in agricultural production. There are a variety of field crops with similar phenologies and spectral signatures or the same crop may have distinct growing periods due to climate differences in the same country.

There are various organizations that focus on crop monitoring. Group on Earth Observation's (GEO) Global Agriculture Monitoring (GEOGLAM), European Commission's Monitoring Agricultural Resources (MARS) Crop yield forecasting system (MCYFS), USDA Foreign Agriculture Services (FAS), Chinese Cropwatch System are examples of global crop monitoring systems (Rembold & Maselli, 2006). Recently, Waldner, et al. (2016) developed a global cropland layer at 250m resolution(Waldner et al., 2016). Kotera, et al. presented a global cropland and water index map from time-series MODIS imagery (Kotera, Berberoglu, Nagano, & Cullu, 2015). One of the most notable examples of crop mapping systems is CropScape. CropScape enables the USDA National Agricultural Statistics Services to map US data for statistical purposes in collaboration with George Mason University (Han, Yang, Di, & Mueller, 2012).

European Commission allocates agricultural subsidies under Common Agricultural Policy to farmers and farming businesses. Land Parcel Identification System is the basis of the distribution of subsidies that amounted to around €41 billion in 2011 (Jansen, Badea, Milenov, & Moise, 2014). Turkey also maintains an LPIS system:

Farmer Registration System (Turkish: Çiftçi Kayıt Sistemi, ÇKS). Yearly agricultural subventions up to $3 billion are distributed through declarations through ÇKS. Even a fractional improvement in the LPIS based subvention system could have very high returns.

Turkey is an ecologically diverse country. Many types of crops are grown in different regions of the country. Some field crops usually have similar reflectance, while their phenology and physical structures cause differences in electro-optical systems. A major tool to differentiate among crops is the use of multi-temporal or time-series satellite imagery classification. Time-series satellite image classification involves extracting features defining the growth of the crops, e.g., maximum NDVI or time between sowing and harvest.

The multi-year classification of crops is conducted in the Harran Plain, Şanlıurfa, Turkey. Corn and cotton are major crops of the Harran Plain (Çelik & Gülersoy, 2013). Corn is planted after the harvest of winter wheat. These crops have similar phenological periods.

Crop mapping from satellite or aerial data by using remote sensing methods is an intensely studied area. In our past studies, we considered the use of multispectral, hyperspectral, and synthetic aperture radar (SAR) in crop classification. The increasing temporal resolution of earth observation satellites allows us to collect time-series data: Landsat 8 has a 16-day temporal resolution. On the other hand, recently launched Sentinel-1(a/b) and Sentinel-2(a/b) satellites will have a 5-day temporal resolution. The availability of high temporal resolution satellite imagery has enabled researchers to develop advanced time-series satellite imagery classification applications.

Field surveys are the most basic method of crop mapping. However, they are expensive and may not cover all fields (Esetlili et al., 2018). Furthermore, crop field surveying is prone to human errors (Şimşek, Fatih Fehmi ;Teke, Mustafa;Altuntaş, 2016). An effective multi-year crop mapping methodology is required to monitor the status of crops, verify and monitor subventions, forecast crops, ensure price stability, and obtain agricultural statistics. Remote sensing is a critical technology that would allow us the mapping of field crops by using aerial and satellite imagery from various sources and modalities. Crop mapping methods may use single, multi-temporal and time-series satellite imagery. These algorithms typically require field data collection for each year of interest. Hence, they are expensive. Cross-year crop mapping enables the use of previous field surveys for the present year, thereby reduces the effort needed to training sample collection.

Governments need to forecast crop yields to feed their population. This task becomes a challenge for large countries by only using information declared by farmers. Also, governments and the food industry need to estimate foreign crop yields to plan international trade. In addition to crop yield estimates, governments support farmers depending on the type of crop they plant in the farmlands.

Remote sensing is the primary tool to classify large vegetation areas quickly and efficiently. However, the capability of discriminating vegetation types with multispectral imagery is limited.

Phenology is described as the study of periodic plant and animal life cycle events and how these are influenced by seasonal and interannual variations in climate, as well as habitat.

The common method to estimate the type of vegetation and crop yield is to use vegetation phenology computed from time series of remote sensing data. Vegetation phenology uses multispectral data and detects the existence of vegetation by checking the value NDVI and other vegetation indices. Vegetation planting, growing and harvesting times are predicted then results are compared with vegetation phenology information to classify the crop. However, phenological classification requires capturing data regularly to monitor the growth of the crop. Continuous acquisition of images of the same area may not be feasible: due to cloud cover or long revisit time intervals of the satellites. Also, there may a phenological shift of the same crop due to the effects of climate, soil, or date of planting.

In this study, it is aimed to develop an efficient cross-year crop mapping algorithm that uses a limited number of training samples and resistant to annual measurement and growth variations.

The main contribution of the study is the novel vector distance-based optimal time warping algorithm: VDTW. VDTW method overcomes difficulties in cross-year crop classification in which training and test data are selected from different years: spectral shifts due to changes in illumination at the observation moment and temporal shifts in growth due to yearly climate variations or farming practices. We simulated different cases of illumination and growth changes. Furthermore, we tested our methodology in a multi-year approach in two regions (the Bismil and the Harran Plain) with distinct cropping practices. The proposed approach requires a lesser number of training samples compared to other methods; thus, it reduces the costly collection of field data.

In our second contribution, we focused on exploiting crop phenologies to use fewer and effective image acquisitions. A method that automatically determines the optimal time window in which crops have discriminative phenological features was developed. This optimal time windows selection algorithm allows mid-season crop classification enabling early accurate prediction of crop yields. In this way, the necessary precautions for transport, storage as well as price volatility could be taken.

Chapter 1 of the study presents the introduction, the statement of the problem, the purpose of the study, the significance of the study, research questions, the assumptions, limitations, delimitations, the definitions of terms, and organization of the study.

Chapter 2 is a review of recent literature.

Chapter 3 provides information on data.

Chapter 4 presents the methodology that will be used in the study, including a description of the data collection procedures and validation of results.

Chapter 5 is the results and findings of the developed method.

Chapter 6 is a discussion of the conclusions of the study.

CHAPTER 2

LITERATURE REVIEW AND BACKGROUND

2.1. Analysis of the Literature

We surveyed multi-temporal and time-series crop mapping literature with an emphasis on cross-year crop mapping. Land use/land cover (LULC) is an extensively studied research area (Gómez, White, & Wulder, 2016)(R. Congalton et al., 2014)(García-Mora, Mas, & Hinkley, 2012). Moreover, crop mapping is a sub-research area of LULC. Multi-temporal and time-series electro-optical satellite imagery were used in the majority of the studies in crop mapping that we surveyed. Multi-temporal images, which are less frequently acquired than time-series imagery, were also commonly used in crop mapping studies.

2.1.1. Phenological and Time Series Vegetation Classification

Twenty-six periodic AVHRR data acquired in the year 1992 of western Great Plains, USA, is analyzed to classify wheat, milo, corn, fallow and grass by Jakubauskas et al. (Jakubauskas, Legates, & Kastens, 2002). NDVI time-series information is processed with Fourier analysis and amplitude, and phase values are obtained. Harmonics (first, second, etc.) are extracted from the signal. In the study, the stepwise discriminant analysis is used as a classifier. To measure the classification results of AVHRR data, labeled land use information of Landsat satellite imagery is downscaled to 1000 m resolution. They were able to acquire 52% classification accuracy.

Twenty-meter resolution AVIRIS data were collected in May, June, and September between 1998 and 2002 from California to discriminate spectra of five different vegetation and impervious surfaces are considered in (Dennison & Roberts, 2003). Dennison and Roberts address the problem of selecting vegetation as training data at different seasons for classification and obtaining a unique spectral signature from multiple observations. To overcome this challenge, they developed end member average root mean square method (EAR) to select endmembers for multiple spectral mixture analysis; this method selects a spectral signature from multiple training samples that were acquired at different seasons. They found out that images with water surplus were modeled 8-16% better than images with water deficit. Modeled spectra

are tested for each year: classification accuracy varies between accuracies for soil water surplus images are between 59% and 90%, while classification accuracies for soil water deficit images are between 52% and 81%.

Nidamanur and Zbell studied the classification of winter rape with HyMap hyperspectral imagery (Nidamanuri & Zbell, 2011). In this study, spectral signatures of crops (winter rape, winter barley, winter rye, alfalfa) which co-exist with winter rape at four distinct growing seasons. They also collected spectral data with in-situ measurements to develop spectral libraries. Spectral angle mapper (SAM) and spectral feature fitting (SFF) methods are used for classification. In their study, they found out that winter rape has a unique vegetation characteristic while other crops studied have common less distinct characteristics. They suggest that every vegetation type should be considered as different cases while characterizing their spectra.

36 10-days MODIS images to classify forest into evergreen, deciduous, and shrubs (Yu, Zhuang, Chen, & Hou, 2004). In the study, Yui et al. applied the unsupervised classification to time series analysis of phenology data: the mean NDVI, first- and second-order amplitude and phase are used to produce unsupervised classification map.

In (Wardlow, Egbert, & Kastens, 2007), 12-month time series 250m MODIS data for the state of Kansas are analyzed by using NDVI and EVI indices to find the type of crops at 2000 crop sites. Alfalfa, corn, sorghum, soybeans, and winter wheat spectra are analyzed. Wardlow et al. found out that vegetation indices of the crops consisted of each vegetation general multi-temporal signature. However, there are some minor differences in the phenology of the crops in some regions, depending on climate and planting differences. They also found out that most vegetation NDVI and EVI responses were similar in the growing season, but they began to differ in the senescence phase of the crops. In (Wardlow et al., 2007), Wardlow and Egbert used MODIS data to classify alfalfa, corn, sorghum, soybeans, winter wheat, fallow in Kansas. They used decision trees as a classifier; all classification accuracies are higher than 84%.

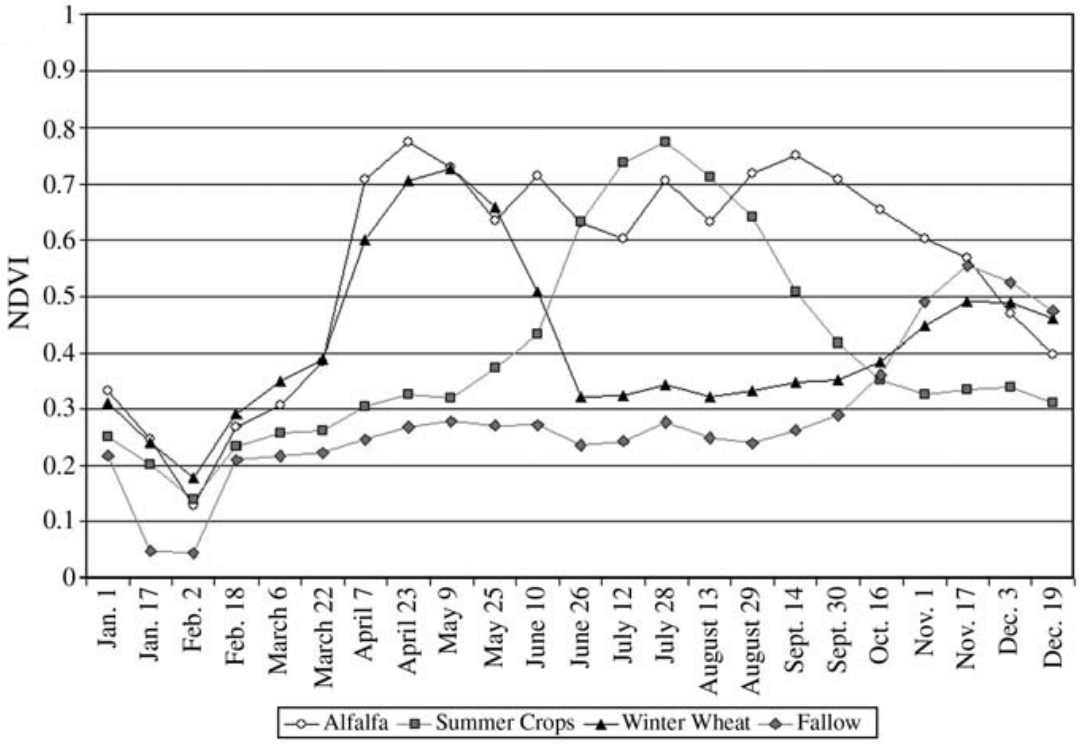

Figure 1: Change of NDVI values through a year (Wardlow et al., 2007).

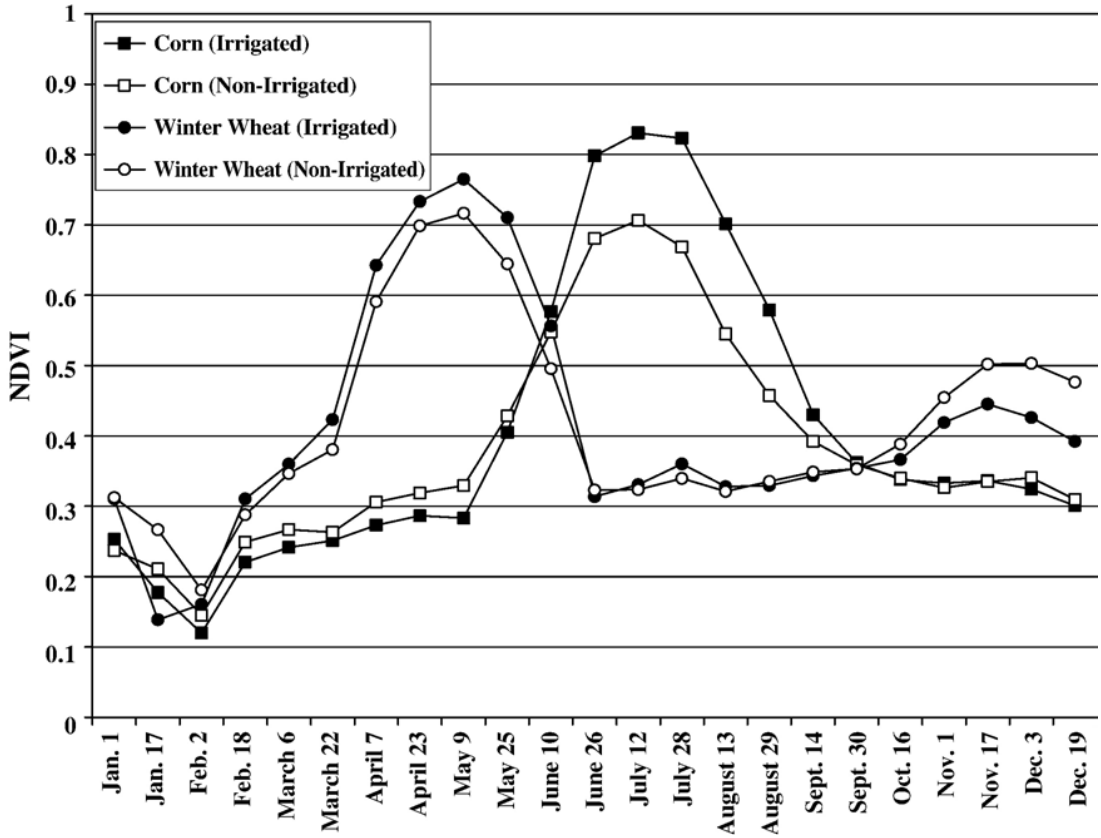

Figure 2: Effect of irrigation on NDVI values, irrigated crops have higher NDVI values(Wardlow et al., 2007).

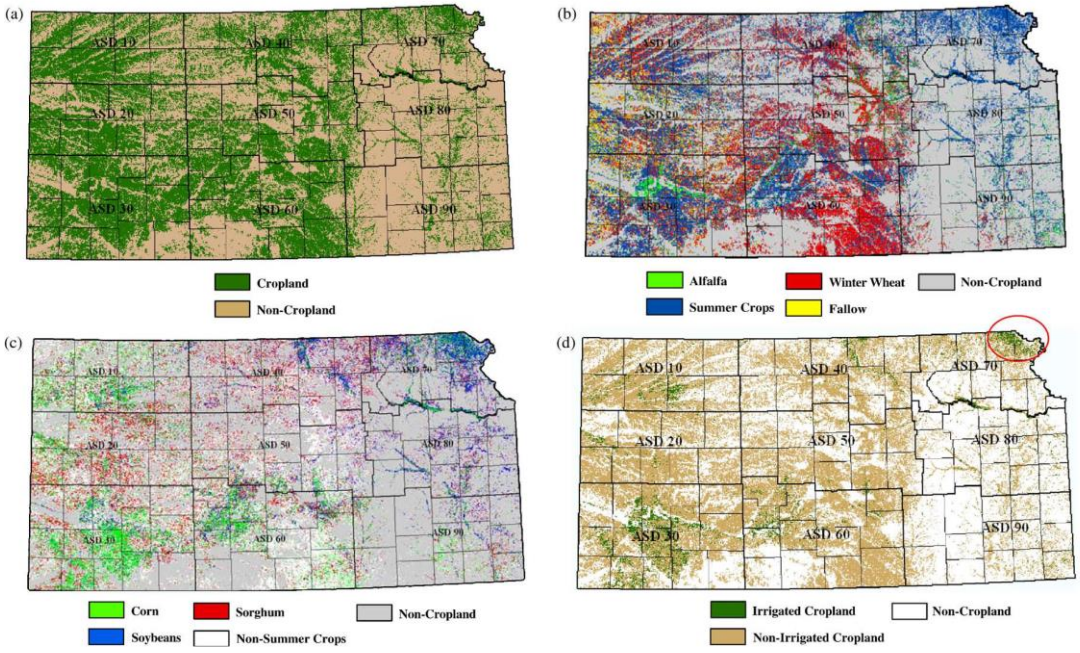

Figure 3: Classification results for nine Agricultural Statistics Districts (ASDs) of the State of Kansas(Wardlow et al., 2007).

In another study, 12 crop types in Germany using 35 Landsat TM/ETM images acquired between the years 1987 and 2002 were used imagery are classified by a spectral and temporal approach (S. Foerster, Kaden, Foerster, & Itzerott, 2012). In the study, Foerster et al. used a spectral and temporal approach to classify crop types by using a hierarchical classification method and compared its performance against maximum likelihood classifier. They also used meteorological information as weather conditions could accelerate or delay vegetation of crops. This classification is conducted by using NDVI values acquired at different seasons of the year. A hierarchical method is used to classify vegetation by first classify vegetation into coarse groups of summer, winter, and perennial grass/fallow land. In subgroups, a fine classification is applied by using phenological information: phenological information obtained by NDVI analysis is matched for classification. However, the study reaches a lower performance value of 65.7% while the Maximum Likelihood classifier has 72.8% accuracy. The research suggests that timing and the number of image acquisitions are essential for vegetation classification using phenological information.

12 Landsat scenes from Landsat-5 and Landsat-7, which were acquired at different dates from 2002 to 2004, are analyzed to classify crops (Soybeans, Corn, Sugarcane, Pasture, and Riparian forest) in (Leite et al., 2011). Leite et al. deployed Hidden Markov Models (HMM), where the growth stages are states. Properties of vegetation are modeled as state transition parameters of the HMM model. Images are segmented before classification and are used for training and test areas. Classification using HMM was able to reach 85% average accuracy. Phenological stage (Prepared Soil, Growth

phase, Adult phase, Post-Harvesting) average accuracy is found to be 81%, and growth phase accuracy is determined as 55%.

Common reeds and submerged macrophytes which are wetlands vegetation are classified by using SPOT-5 time series data which was acquired at different times of the year between 2005 and 2006 in (Davranche, Lefebvre, & Poulin, 2010) by Davranche et al. In the study, they used near-infrared band between March and June, the Optimized Soil Adjusted Vegetation Index in December, and the Normalized Difference Water Index (NDWI) in September for common reeds. Submerged macrophyte was classified with the shortwave-infrared band in December, the NDWI of September, the red band in September, and the Simple Ratio index in March. These vegetation indices and band values are used in classification trees. The accuracy of the classification is of 98.6% in 2005 and 98.1% in 2006 for common reed, and 86.7% in 2005 and 85.9% in 2006 for submerged macrophytes. They note that with a small training size (N=25), classification trees are potent tools to discriminate vegetation types.

Another application of analyzing time-series data is to estimate vegetation area of winter wheat by using the MODIS Enhanced vegetation index (Y. Pan et al., 2012). In this study, data belongs to two representative regions in China: one around Tongzhou, Beijing (TZ), and the other located around Shuyang, Jiangsu (SY). MODIS data are 16-day composite EVI products from September 2006 to June 2007 (for TZ) and September 2008 to June 2009 (for SY). In the study, Pan et al. developed a Crop Proportion Phenology Index (CPPI) which expresses time-series MODIS Enhanced Vegetation Index (EVI) data and area of winter wheat in China. Crop areas which are needed to determine winter wheat areas for constructing test data are collected by using high-resolution multispectral sensors (Landsat and SPOT) as MODIS has a very low resolution. EVI is less susceptible to biases from haze and clouds; however, EVI time-series information is further filtered by a Savitzky–Golay filter to reduce the effects of cloud cover and other sources of noise. CPPI is computed from phenological state change points. Calculate accuracies for two different sites are 90.5% and 93.8%. The study concludes that the value of EVI and the area of winter wheat are correlated. The authors conclude CPPI could be applied to further crop types by using a limited number of training samples.

2.1.2. Time Series Crop Classification

Maus et al. proposed time-weighted dynamic time warping (TWDTW), which is an improvement over DTW by incorporating time difference between samples as an additional cost (Maus et al., 2016). TWDTW method has two different time costs: linear and logistic function-based. TWDTW method improved the cross-year classification performance compared to the DTW method. In another study, pixel-based and object-based TWDTW methods were compared with Random Forest (RF) with Sentinel-2 time series data. Object-based TWDTW acquired comparable results to the RF method (Belgiu & Csillik, 2018).

Zhong et al. used Landsat TM and ETM+ images of 2006-2010 to classify maize and soybean in central USA (Zhong, Gong, & Biging, 2014). They developed a phenology-based multi-year classifier. In addition to phenology, spectral features are used. Images are first segmented into individual fields. Spectral features are computed from the mean value of segments. Spectral, phenological, Pheno-spectral, Pheno-index, and Accu-heat (Accumulated Heat is used). Phenology of crops is extracted from EVI. Pheno-spectral variables are spectral values at specific phenological transition dates. Pheno-indices are NDSVI (normalized differential senescent vegetation index (SWIR1, Red)) and NDTI (normalized difference tillage Index (SWIR1, SWIR2)) at phenological transition dates (Dates where phenological transitions occur: growing starts or holds, etc). Values at transition dates are interpolated by using curve fitting functions. Accumulated heat is a new variable introduced by the study. Accumulated heat is cumulative of heat values obtained at five different growing periods. Selected feature groups are used in random forest classifier. Classification performed over the same year and cross-year data. Several combinations of input variables are compared in the tests. Phenology based classification shows comparable performance to other methods that use combined features.

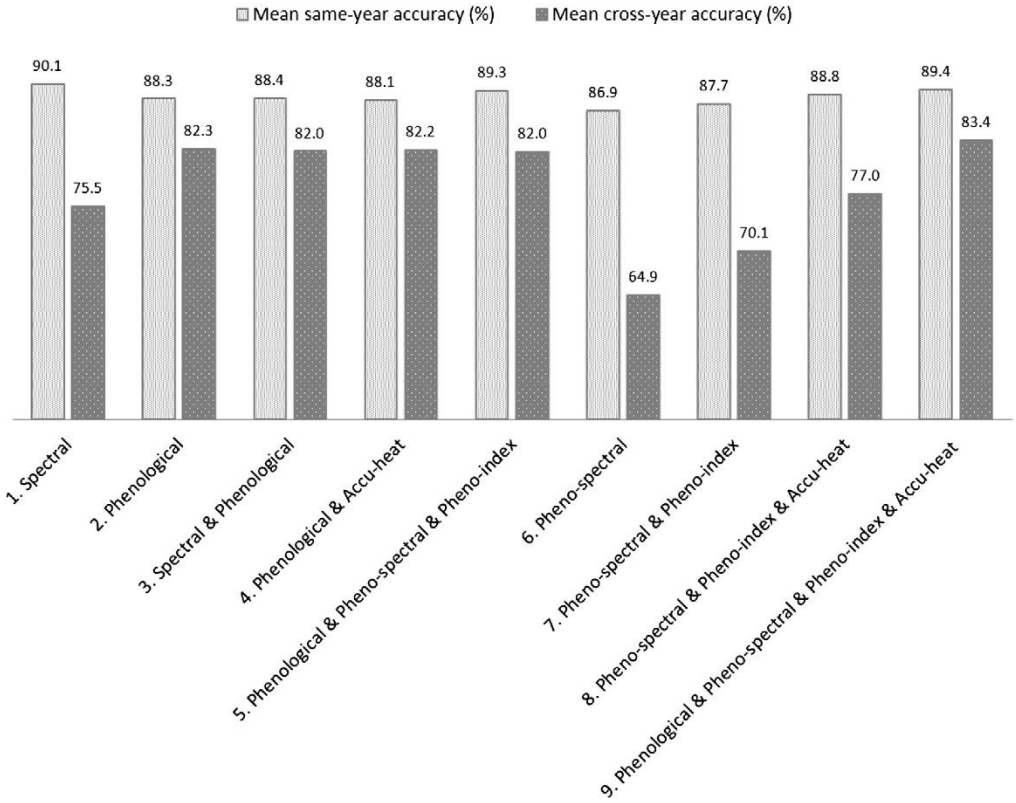

Figure 4: Same Year and Cross Year Accuracies (Zhong et al., 2014)

Geo-parcel based identification of crops using the fusion of high-resolution imagery and time series medium resolution imagery was proposed in (Y. Yang et al., 2017). Parcel boundaries were detected by using high-resolution GF-2 (0.8m) imagery. Time series medium resolution GF-1(16m) and Landsat 8 data were used EVI phenological

feature extraction. Phenological metrics extracted from EVI phenology and geo-parcel information were used as features to Random Forest classifier to obtain 93.72% overall accuracy.

Massey et al. developed a decision tree based crop classification for commonly grown crops in the continental USA with 250m resolution MODIS time-series satellite imagery(Massey et al., 2017). The study was conducted in 12 separate agricultural economic zones (AEZs). Corn-soybean, wheat-barley, potato, alfalfa, cotton, and rice were classified; corn was merged with soybean and wheat was merged with barley. Overall accuracies were higher than 78% for 2001-2014 years.

Thenkabail et al. used spectral matching techniques to AVHRR (Advanced Very High-Resolution Radiometer) time series data for determination of LULC and irrigated area classification (Thenkabail, GangadharaRao, Biggs, Krishna, & Turral, 2007).

Mingwei et al. used the Fourier transform of time series NDVI to classify double cropping in Northern China with MODIS images (Mingwei et al., 2008). Wheat, Wheat-Maize, Maize, and Cotton are classified. FFT is used for feature extraction from 1^{st}, $2^{nd,}$ and 3^{rd} harmonics from 8-day MODIS composite images. R^2 scores for cotton and maize are 0.84 and 0.72, respectively. While the use of FFT produces positively correlated results, the FFT method requires full data to operate, which could be possible for high-temporal resolution satellites such as MODIS.

Time series classification of tobacco fields with CBERS 02B and Landsat TM images are studied in (Peng, Deng, Cui, Ming, & Shen, 2009). SAM and Maximum Likelihood Classifier are compared while time series classification with SAM produced higher classification accuracy: 83.4%.

Time Series RapidEye images are used to classify crops (cotton, rice, corn, winter wheat, alfalfa, and melons) in Mid-Asia (F Löw, Michel, Dech, & Conrad, 2013). Seven images were acquired monthly, and a different number of features were used with the SVM classifier. The use of at least three images was able to produce 85% or higher classification accuracies.

Son et al. developed a phenology-based time series classification method using MODIS EVI for rice classification in Vietnam (Son, Chen, Chen, Duc, & Chang, 2013). MODIS images between December 2000 and December 2012 are used in this study. Empirical Mode Decomposition method is used to extract time-series features. Single, double, and triple cropped areas with/without irrigation were classified using this approach. Accuracies were 81.4% for 2002, 80.6% for 2006 and 85.5% for 2012.

Xue et al. used MODIS time-series imagery for LULC (forests, grasslands, water, etc.) classification (Xue, Du, & Feng, 2014). Phenological features were represented with the BFAST method. TIMESAT is used phenological feature extraction, DTW is used for feature selection (remote outliers and select the finest samples), and finally, ensemble and SVM methods are used for classification to obtain 96.44% overall accuracy.

TIMESPEC – A Software Tool for Analyzing Time-Series of Spectral Data is introduced in (M. Foerster, Welle, Schmidt, Nieland, & Kleinschmit, 2014). TIMESPEC provides a toolkit for analysis of time-series satellite data. This study also summarizes toolkits, which could be used in time series satellite data analysis such as TIMESAT.

Another attempt for time series data processing is SPIRITS (Software for the Processing and Interpretation of Remotely Sensed Image Time Series) software, which was supported by the EU and developed by VITO (Eerens et al., 2014).

Integration of low-resolution time-series MODIS data with higher resolution Landsat TM was used in (Li, Cao, Jia, Zhang, & Dong, 2014). Phenological features were extracted from MODIS images, while ML classifier is used with Landsat data to increase classification accuracy from 92.38% (with Landsat only) to 94.67% (MODIS+Landsat).

Sakamato et al. studied time series corn yield with MODIS data in the U.S. (Sakamoto, Gitelson, & Arkebauer, 2014). Wide Dynamic Ranged Vegetation Index (WDRVI) is used with Shape Model Fitting (SMF) for phenological feature extraction. SMF algorithm is used to detect corn crop for further yield estimation analysis.

Hao et al. compared hybrid classifiers with time-series NDVI for crop classification in North Xinjiang, China (Hao, Wang, & Niu, 2015). Multiple voting (M-voting) and probabilistic fusion (Pfusion) are the hybrid strategies that were used with Landsat 5 and HJ-1 NDVI data. Random Forest (RF), Support Vector Machine (SVM), and See 5 (C 5.0) are used as single classifiers. Cotton, grape, winter wheat, watermelon, maize, wheat-maize are classified. Hybrid strategies produced higher classification rates with low sample size; however, a high number of samples classification results were similar. Also, OBIA (object-based image analysis) did not improve numerical results while obtaining a better visual classification.

Spectro-temporal profiles were utilized with NDVI, EVI, and WDRVI using MODIS imagery to discriminate corn and soybean in Brazil (de Souza, Mercante, Johann, Lamparelli, & Uribe-Opazo, 2015a). Spatiotemporal profiles obtained from EVI and WDRVI performed better than using SAM classifier with 80% accuracy. Corn and soybean have similar phenologies, which make discrimination of these crops difficult.

Landsat-RICE system was developed to identify paddy rice fields by using Landsat imagery in China (Dong et al., 2015). Time series Landsat imagery between 1986 and 2010 is used with developed phenology-based algorithms, which exploit unique characteristics of ice to obtain 84-95% accuracy at separate time windows. The algorithms use rules at certain phenological states.

Pan et al. discussed crop mapping capabilities of China's HJ-1A/B satellites (Z. Pan et al., 2015). In their study, phenological feature extraction, data preprocessing, and data smoothing were applied.

Pena and Brenning used eight Landsat 8 imagery for fruit classification in Chile (M. A. Pena & Brenning, 2015). Time series of NDVI, NDWI, and full band (band values) information is used as features with LDA, RF and SVM classifiers. LDA with full band time-series performed best, while NDVI performed worst with all classifiers considered.

Tatsumi et al. studied the classification of time series Landsat 7 ETM+ images in Peru (Tatsumi, Yamashiki, Torres, & Taipe, 2015). Alfalfa, asparagus, avocado, cotton, grape, maize, mango, and tomato were classified with the RF classifier resulting in 81% overall accuracy.

Yan and Roy developed improved the Laplacian Eigenmaps (LE) nonlinear DR algorithms to overcome missing data in time series crop classification: LE-SAM and LE-SAM-R (Yan & Roy, 2015). Tests were conducted with Landsat WELD data of 3 distinct regions (Texas (cotton, corn, wheat), Kansas (alfalfa, sorghum, wheat, corn), and South Dakota (hay, sorghum, sunflower, winter wheat, spring wheat)) for various crops. The dimension of time series data is reduced to five dimensions. The classification was performed with the Random Forest classifier. While LE-SAM-R increases classification accuracy, results vary for the same crop in different regions: Texas (87.8%), Kansas (78.3%), and South Dakota (77.7%).

Zheng et al. used 24 time-series Landsat 5 TM and 7 ETM+ of 2010 for classification of crops in Phoenix, AZ, U.S. (Zheng, Myint, Thenkabail, & Aggarwal, 2015). The SVM method was selected as the classifier with random and intelligent sample selection. Six single crops (alfalfa, cotton, corn, wheat, barley, and potatoes) and three double crops (barley-cotton, wheat-sorghum, and wheat-cotton) are classified. Overall accuracy was 86%, while wheat and barley are mixed.

16-day MODIS time-series data of 2001 was used for land use classification(urban, forest, agriculture) by using a various number of samples in the USA (Shao & Lunetta, 2012). EVI and band-7 (SWIR) are selected as input features of 23 MODIS images SVM classifier was able to provide higher classification results compared to NN and CART with a lower number of training samples at 91%.

2.1.3. Time Series Fusion and SAR

A study conducted in the Lombardy region, Italy, demonstrated the use of multi-temporal SAR and EO images in corn, rice and wheat classification (Fontanelli et al., 2014). 13 Landsat 8 and 15 Cosmo-SkyMed X-band images of May-December 2013 were used in the study. Time series data stacked together. MLC, EMD and SAM methods are applied to time series of optical, SAR and optical-SAR data. MLC applied to optical-SAR data produced the best results at 94%.

Jiao et al. studied object-oriented mapping of wheat, oat, soybean, and canola and forage using 19 time-series RADARSAT-2 data of 2011 and 2012 in Ontario, Canada (Jiao et al., 2014). Multi-temporal decompositions in a hierarchical, object-oriented classification were able to obtain 95% classification accuracy.

Multi-temporal TerraSAR-X and RADARSAT-2 images were used for early season crop classification in Canada (McNairn, Kross, Lapen, Caves, & Shang, 2014). Accuracies above 90% were able to be obtained with decision tree classifier for corn at the end of the growing season. However, more images were required for soybean classification.

Guarini et al. compared 11 HH and 10 VH polarization time series CosmoSky-Med images of 2014 in Austria to classify carrot, corn, potato, soybean, sugar beet (Guarini, Bruzzone, Santoni, & Dini, 2015). SVM machine classifier is used as a classifier, which resulted in higher accuracy with HH, polarized SAR images: 84.50% vs. 81.63%.

Optical and SAR Time Series images are fused for efficient crop identification (Blaes, Vanhalle, & Defourny, 2005). 15 ERS and RADARSAT and 3 optical images (SPOT & Landsat ETM+) of 2000 in Belgium are used. Grass, wheat, maize, sugar beet, barley, and potato are classified. Hierarchical classification with a fusion of temporal SAR and EO images increased classification performance, a minimum of 5% up to 89%. The hierarchical classification scheme is based on Farmer's declarations in which suspicious declarations are processed by using spectral signatures in the first step. In the second step, MLC is used. The computer-assisted photo interpretation (CAPI) and in-situ field visits performed for suspected fields.

Multi-temporal and multi-sensor classification of crops (forage, soybean, corn, and cereal) was proposed by (Shang, McNairn, Champagne, & Jiao, 2008). Classification of crops in Canada is performed with single Landsat TM optical or SAR images. Use of at least one electro-optical and SAR images increased classification rates while further use of multi-temporal imagery let the classification results to be 85% minimum.

Özdarıcı Ok and Akyürek developed a method for segment-based classification of multitemporal Electro-optic and SAR images in Karacabey, Bursa, Turkey (Ok & Akyurek, 2012). Three Kompsat-2 and three ENVISAT ASAR images acquired in June, July, and August in 2008. Crops that are classified are corn, grass, rice, sugar beet, tomato, wheat. Segment based approach produces higher accuracies about 10% compared to pixel-based approach: 79.18% vs. 88.71%.

Sentinel-1 imagery with phenological sequence patterns was developed for grasslands, maize, canola, sugar beets, and potatoes mapping in Germany (Bargiel, 2017). PSP approach outperformed Random Forest and Maximum Likelihood methods.

Veloso et al. combined time-series Sentinel-1 and Sentinel-2 data to generate crop maps of wheat, rapeseed, maize, soybean, and sunflower in southwest France (Veloso et al., 2017). Their most significant finding was that the use of VH/VV ratio could be used for the analysis of biophysical parameters.

2.1.4. Multi-temporal Crop Classification

Lucas et al. used eCognition Expert software to classify multi-temporal Landsat ETM+ images of 2001-2002 for land use/land classification (grassland, tree types, soil, water bodies etc.) (Lucas, Rowlands, Brown, Keyworth, & Bunting, 2007). Four Landsat images were obtained in March, April, July, and September. Rule-based classification is performed in four stages. Average accuracy using rule-based classification with multi-temporal images was 80%.

George Mason University developed the CropScape system for USDA NASS (Han et al., 2012). Rule-based classification for each region and year from multi-temporal Landsat and other satellites are used. Rules are manually developed for each region using RuleQuest and applied by ERDAS Imagine software.

Hemissi et al. conducted a temporal-spectral-spatial classification of Hyperion images (four 2003, three 2009, two 2010) in Tunisia (Hemissi, Farah, Saheb Ettabaa, & Solaiman, 2013). Classes that are considered in this study are carex, henne, bare soil, water, and palm. Multi-temporal spectral data is constructed as a 3D feature space for spectral signatures. An adopted SOM method is used for classification, which resulted in 89.46% accuracy.

An object-oriented multi-temporal crop classification methods for four Landsat 7 ETM+ SLC-off images of 2012 in Montana, the USA with random forest classifier (Long, Lawrence, Greenwood, Marshall, & Miller, 2013). Multi-temporal data is used to classify cereal, pulse, and other classes. The object-based classification approach produced higher classification accuracies than pixel-based methods with 85.5% accuracy.

Conrad et al. investigated the optimum number of imagery acquisitions using RapidEye imagery in Uzbekistan (Conrad et al., 2014). Crops, which are classified in this study, are cotton, wheat, rice, maize, alfalfa, sunflower, watermelon. Nine RapidEye images were acquired in 2009. Mean, and standard deviation of five bands with NDVI and EVI values of all nine images were used as features. In their study, the optimal number of images required for optimal classification is found to be at least five. The overall accuracy of the Random Forest classifier is 85.7%.

Pena et al. used bi-temporal ASTER images of 2006 in California, the USA, to detect summer crops with machine learning methods (J. M. Pena et al., 2014). The C4.5 decision tree, logistic regression (LR), support vector machine (SVM) and multilayer perceptron (MLP) neural network methods were evaluated as single-level and two-level classifiers: while SVM + SVM classifier performed higher than other classifiers at 89% accuracy.

Çelik et al. used SPOT 6 images of the Harran region from multi-temporal June, July, and September of for corn and cotton crop classification(Celik, Sertel, & Ustundag, 2015). NDVI obtained from multi-temporal images used object-based classification to reach 94% classification accuracy.

CROPCLASS system is a semi-automatic crop classification system, which uses census parcels (Garcia-Torres, Caballero-Novella, Gomez-Candon, & Pena, 2015). Decision trees are used with seven multi-temporal GeoEye imagery between April-October 2010 in Spain. Crops that were considered in the study are broad beans, chickpeas, citrus orchards, cotton, corn, Mediterranean forest, oat, olive orchards, poplars grove, potatoes, sunflower, and winter wheat. CROPCLASS system was able to classify crops at 80.7% accuracy.

Löw et al. developed a decision fusion system to classify multi-temporal RapidEye imagery for crop classification of alfalfa, cotton, fruit trees, rice, wheat, melon (Fabian Löw, Conrad, & Michel, 2015). The decision fusion approach used decision tree (DT), random forest (RF), support vector machine (SVM), and multilayer perceptron (MLP) classifiers to increase accuracy by 6%. Final accuracies changes between 64% and 74% at various sites. The authors claimed that their methodology is applicable to other satellite imagery such as Sentinel-2 and could be used with images acquired at different years.

2.1.5. Temporal Windows for Phenological Changes

Van Niel and McVicar studied the determination of optimal temporal windows for the detection of rice, maize, sorghum, and soybeans by using 17 Landsat 7 ETM images. An iterative multi-temporal classification approach has been developed. The use of multiple images at different temporal windows for each crop increased classification accuracy up to 95.8% compared to 89.4% of single date imagery (Niel & McVicar, 2004).

Wavelet-based filter for determining Crop Phenology (WFCP) for rice paddy fields as proposed by (Sakamoto et al., 2005). EVI time series are obtained from MODIS images. Data is smoothed before being processed. The Coiflet 4 wavelets were found to be better in predicting phenological date then Fourier transform and other wavelet transforms (Daubechies and Symlet)

2.1.6. Spectral Angle Mapper (SAM)

Knight et al. applied the SAM method for LULC classification with MODIS NDVI time series data (Knight, Lunetta, Ediriwickrema, & Khorram, 2006). Major LULC classes are Agriculture, Urban, Water, Deciduous Trees, and Coniferous Trees. Accuracies were between 50-80% with varying ratios of training pixels.

Rembold and Maselli used the SAM method to determine inter-annual crop area variation (Rembold & Maselli, 2006). Winter wheat areas are estimated from time-series NDVI of NOAA-AVHRR images at different years. Time series data is collected in 10-day periods. Data is shifted 1-2 10-day periods. Summer crops, winter crops, forests,

Yang et al. used the SAM method for classification of crop areas using a single SPOT-5 image (C. Yang, Everitt, & Murden, 2011). However, ML and SVM methods

performed better than SAM for crop classification did. Single date imagery could be effective if the imagery is acquired at a date where the discrimination is higher.

SAM is combined with ML classifier in (Yonezawa, 2007) for LULC classification. Feature extraction is performed using SAM scores in 3x3 window: Total SAM score of each pixel's neighboring is computed by using spectral bands. ML-SAM method is applied to QuickBird images.

2.1.7. Dynamic Time Warping (DTW)

Petitjean and Weber used Dynamic Time Warping for land cover classification with 46 time-series FORMOSAT-2 images of 2006 (Petitjean & Weber, 2014). Time-series data were segmented into spatio-temporal regions for optimal classification performance.

2.1.8. Error Metrics

Niet at al studied the required number of samples (n) for given (p) band images in the case of multi-temporal images(Van Niel, McVicar, & Datt, 2005). It is determined 2-4p samples are enough to obtain similar performance of 30p samples using ML classification of 17 Landsat ETM+ images.

2.1.9. Data Smoothing

Arvor et al. compared smoothing algorithms for time-series MODIS-EVI data for classification(Arvor, Jonathan, Meirelles, Dubreuil, & Lecerf, 2008). Savitzky-Golay filtering led to higher classification results to other smoothing methods such as Weighted Least Squares (WLS).

Kim et al. compared the effect of Savitzky-Golay filtering in LULC classification of MODIS data in South Korea (Kim et al., 2014). It was concluded that the use of EVI with SG filtering produced the highest results.

2.1.10. Studies Regarding South Eastern Anatolia Region of Turkey

Aydoğdu et al. studied the aggregation between crop classification and ÇKS records using Landsat image classification results(Aydoğdu, Akçar, & Çullu, 2005). The aggregation between ÇKS and classification results were 85-92%.

Algancı et al. conducted a study in Şanlıurfa for land use classification using SPOT 6 imagery(U Alganci, Sertel, Kaya, & BerkUstundag, 2013). The object-based classification method produced up to 90% classification results for barley, lentil, and wheat.

Algancı et al. studied multi-resolution pixel and object-based classification methods for corn and cotton (Ugur Alganci, Sertel, Ozdogan, & Ormeci, 2013). eCognition software is used for segmentation and segment-based feature extraction. OBC, SVM, ML, and SAM methods are compared. OBC produced the highest accuracy, while SVM results are acceptable; on the other hand, ML and SAM results are worst.

Çelik and Gülersoy studied the development of irrigated areas in Harran Plain. They analyzed crop fields with Landsat imagery between 1984 and 2011(Çelik & Gülersoy, 2013).

2.1.11. Ground Truth Error

Carlotto studied the effect of erroneous training data in remote sensing(Carlotto, 2009). The actual performance of classifiers is observed by increasing the number of samples in the case of erroneous ground truth data. Foody studied the effect of mislabeled training data with the SVM classifier (Foody, 2015). SVM classification accuracy was decreased by 8% when training data with 20% mislabel was given. On the other hand, discriminant analysis was affected by 3.11% by the same amount of mislabeled data. Recent work made a detailed analysis of class label noise by using time series data (Pelletier et al., 2017). RF, SVM-RBF and SVM-Linear classifiers were compared with synthetic and real datasets. The RF classifier is found to be more robust to low class label noise.

2.1.12. Deep Learning

DL has gained popularity in recent years due to its applications in numerous areas (Lecun, Bengio, & Hinton, 2015). Deep convolutional neural networks and recurrent neural nets were applied for crop mapping (Kamilaris & Prenafeta-Boldú, 2018; Liakos, Busato, Moshou, Pearson, & Bochtis, 2018). DL methods achieved higher classification accuracies compared to other classification methods such as SVM and RF (Kussul, Lavreniuk, Skakun, & Shelestov, 2017). However, DL requires a vast amount of training data and an extensive amount of computing power. The crop-mapping studies that used DL, mentioned above, were tested with only same-year data, while the majority of the data were used in training.

2.2. Phenology Feature Extraction

In this section, vegetation indices that are used to extract phenological features are presented. Their formulas are given in the form of band names. Vegetation indices have values in the range of $[-1, 1]$.

2.2.1. Normalized Difference Vegetation Index (NDVI)

NDVI is the most used vegetation index. Chlorophyll pigments in leaves absorb visible light while the cell structure of the leaf reflects the majority of the light in near-infrared (NIR) wavelengths. NDVI is formulated as:

$$NDVI = \frac{NIR - Red}{NIR + Red} \tag{1}$$

Healthy photosynthetically active vegetation generally has higher NDVI values. Vegetation has NDVI values of greater than 0.3.

2.2.2. Enhanced Vegetation Index (EVI)

EVI index is an optimized index for detecting vegetation biomass without affecting canopy (vegetation structure) background noise and atmospheric effects.

The Enhanced Vegetation Index is an improved vegetation index that compensates canopy cover and atmospheric effects. C1 and C2 are atmospheric terms for red and blue bands, while L is the canopy background adjustment factor (A. Huete et al., 2002).

$$EVI = \frac{NIR - Red}{NIR + C1 \times Red - C2 \times Blue + L} \tag{2}$$

L is canopy background adjustment; C1 and C2 are aerosol resistance coefficients. EVI reduces saturation, atmospheric noise, and background noise. *C1 = 7.5, C2 = 6* and L = 1 are used for Landsat 8(*Landsat 8 Surface Reflectance Product Guide v1.2*, 2015). While NDVI is chlorophyll sensitive, EVI is more sensitive to vegetation canopy changes.

2.2.3. Soil Adjusted Vegetation Index (SAVI)

Soil adjusted vegetation index (SAVI) incorporates soil brightness correction factor (L) defined as 0.5 to accommodate most land cover types (Qi, Chehbouni, Huete, Kerr, & Sorooshian, 1994). L = 0.5 is selected for Landsat 8 (U.S. Geological Survey, 2017).

$$SAVI = (1 + L) * \frac{NIR - Red}{NIR + Red + L} \tag{3}$$

2.2.4. Optimized Soil Adjusted Vegetation Index (SAVI)

Optimized Soil adjusted vegetation index (OSAVI) estimates soil line by using simulations and experiments (Rondeaux, Steven, & Baret, 1996). Values of soil variability X was determined experimentally as 0.16.

$$OSAVI = \frac{NIR - Red}{NIR + Red + X} \tag{4}$$

2.2.5. Modified Soil Adjusted Vegetation Index (MSAVI)

Modified Soil Adjusted Vegetation Index replaces L in SAVI with an inductive function(Qi et al., 1994). Instead of computing the soil line experimentally, MSAVI computes L value from NIR and Red bands. Soil adjusted vegetation indices aim to improve the insensitivity of NDVI to canopy cover changes with the addition of soil line parameters. In this text, MSAVI refers to the second version of MSAVI: MSAVI2.

$$MSAVI = \frac{\left(2 \times NIR + 1 - \sqrt{(2 \times NIR + 1)^2 - 8 \times (NIR - Red)}\right)}{2} \tag{5}$$

2.2.6. Enhanced Normalized Difference Vegetation Index (ENDVI)

Healthy vegetation reflects NIR and green spectra, mostly because of photosynthesis.

$$ENDVI = \frac{NIR + Green - 2 \times Blue}{NIR + Green + 2 \times Blue} \tag{6}$$

2.2.7. Green Normalized Difference Vegetation Index (GNDVI)

GNDVI replaces NIR band with Red compared to NDVI (Motohka, Nasahara, Oguma, & Tsuchida, 2010). Healthy vegetation reflects green spectra the most in the visible range. GNDVI is also useful in RGB imagers where NIR band is not available.

$$GNDVI = \frac{Green - Red}{Green + Red} \tag{7}$$

2.2.8. Wide Dynamic Range Vegetation Index (WDRVI)

Wide dynamic range vegetation index was developed to remove the weakness of NDVI when crops reach maturity and excessing LAI values over two NDVI saturates (Gitelson, 2004). WDRVI achieves a more sensitive crop canopy measurement by modifying NIR values. WDRVI is more sensitive to changes to canopy cover, which is useful in precision agriculture applications. WDRVI is defined in equation (8):

$$WDRVI = \frac{\alpha \times NIR - Red}{\alpha \times NIR + Red} \tag{8}$$

Where optimal values of α were measured as between 0.1-0.2

2.3. Summary

A majority of the studies on multi-temporal or time-series satellite imagery crop classification did not take time into account as a feature and focused on mapping crops using same-year data for both training and validation. However, multi-year analysis enables earlier classification of crops based on previous years' data. Only a limited number of studies conducted multi-year comparisons such as Zhong et al. used Landsat TM and ETM+ images of 2006-2010 to classify maize and soybean in central USA (Zhong et al., 2014). These studies presented classification accuracies where cross-year results were considerably lower compared to same-year results, and they required a substantial amount of training samples. Even if cross-year crop mapping eliminated the necessity of yearly training sample collection, these studies still needed considerable training data. Again, most studies did not incorporate annual temporal variations in their studies; one notable exception is the work of (Maus et al., 2016). RF and SVM were the most used classifiers in crop mapping.

Furthermore, deep learning (DL) methods were considered for cross-year crop mapping. DL has gained popularity in recent years due to its applications in numerous areas (Lecun et al., 2015). Deep convolutional neural networks and recurrent neural nets were applied for crop mapping (Kamilaris & Prenafeta-Boldú, 2018; Liakos et al., 2018). DL methods achieved higher classification accuracies compared to other classification methods such as SVM and RF (Kussul et al., 2017). However, DL requires a vast amount of training data and an extensive amount of computing power.

CHAPTER 3

DATA

3.1. Study Areas

In this study, the VDTW method in three different regions: The Harran Plain and The Bismil Plain in Turkey and Kansas, USA. The Harran and The Bismil Plain are located in the South East of Turkey. The locations of the Harran Plain (blue) and the Bismil Plain are shown in Figure 5. The region has a Mediterranean climate with about 400-450mm yearly rainfall, according to the General Directorate of Meteorology of Turkey.

In this study, two separate areas are selected in Southern Anatolia Region of Turkey: The Harran Plain and The Bismil Plain

Bismil County is around the Tigris River. Wheat, corn, and cotton are grown in both regions. In addition to these crops, Soybean is grown after winter wheat in the Bismil Plain.

Figure 5: The Harran and The Bismil Plains are depicted in Turkey.

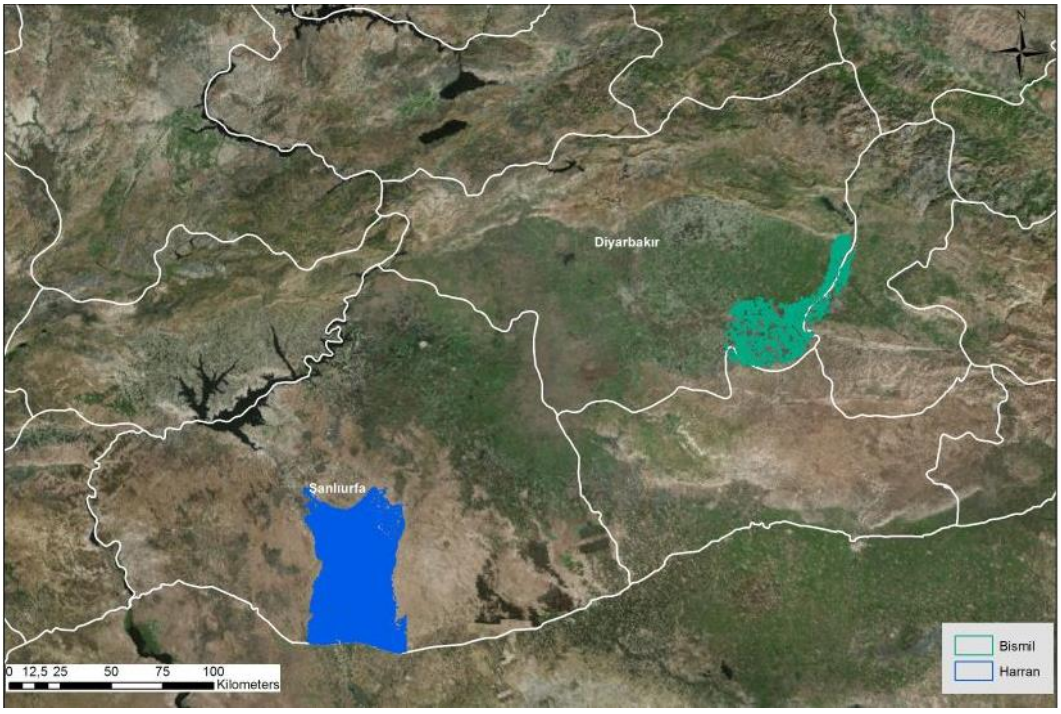

Figure 6: The Harran and The Bismil Plains are shown in detail.

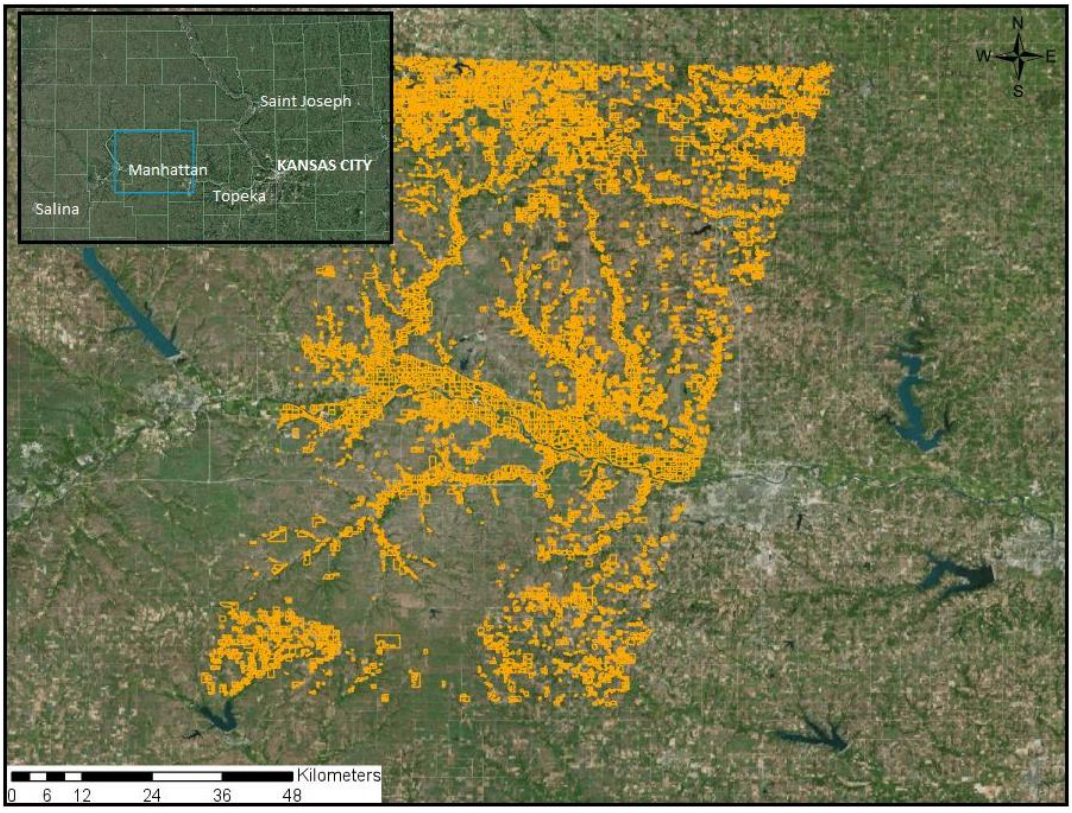

Figure 7: The Kansas dataset is depicted.

3.1.1. The Harran Plain

The Harran Plain is located in the South East of Turkey. The locations of the Harran Plain (blue) and the Bismil Plain are shown in Figure 1. The region has a Mediterranean climate with about 400-450mm yearly rainfall according to the General Directorate of Meteorology of Turkey.

3.1.2. The Bismil Plain

The Bismil dataset covers the Bismil Plain around Bismil city in Diyarbakır County. Bismil city is located along the Tigris River. The area extends next to the border between Batman and Diyarbakır counties. Corn, cotton and soybean are the crops in this dataset.

3.1.3. Kansas

The Kansas dataset covers the North Eastern part of Kansas State. The test area is selected as the overlap of Landsat 8 Path 28/Row 33 and Path 27/Row33 tiles also fully covered by a Sentinel-2 tile. The Kansas data set extends on Brown, Jackson, Nemaha, Shawnee, Pottawatomie, and Wabaunsee counties. Major crops in the region are corn and soybean.

3.2. Satellite Data

3.2.1. Landsat 8

Landsat 8 was launched on February 11, 2013. Landsat 8 has two sensors: the Operational Land Imager (OLI) and Thermal Infrared Sensor (TIRS). The temporal resolution is 15-16 days. Swath width 183 km.

Landsat 8 satellite images are being used as primary test data for the study. Landsat 8 has 8 spectral bands. Launched in February 2013 provides images with 16 days of revisit time.

Landsat 8 data were converted to surface reflectance by the U.S. Geological Survey (USGS)(*Landsat 8 Surface Reflectance Product Guide v1.2*, 2015). Harmonized Landsat Sentinel data were used for the Kansas dataset.

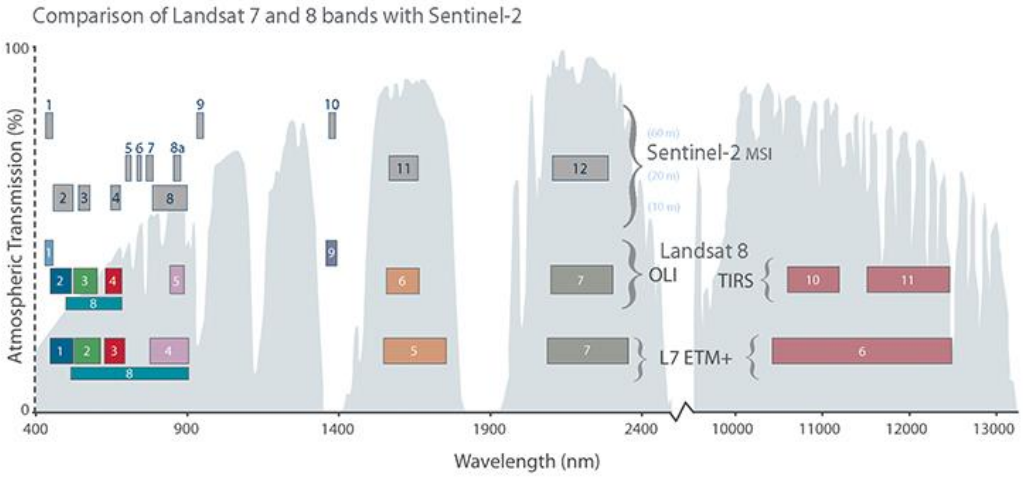

Figure 8: Landsat 7, Landsat 8 and Sentinel-2 Bands Source: http://landsat.usgs.gov/L8_band_combos.php.

Table 1: Landsat 8 satellite spectral information.

Bands	Central wavelength (nm)	Bandwidth (nm)	Spatial resolution (m)
Band 1 - Coastal aerosol	443	20	30
Band 2 - Blue	483	65	30
Band 3 - Green	560	75	30
Band 4 - Red	660	50	30
Band 5 - Near Infrared (NIR)	865	40	30
Band 6 - SWIR 1	1650	100	30
Band 7 - SWIR 2	2220	200	30
Band 8 - Panchromatic	640	180	15
Band 9 - Cirrus	1375	30	30

The imagery of the Harran Plain is from early June to the end of October. Twenty images from 2013, 19 images from 2014 and 20 images from 2015 are used. Imagery acquisition details for the Harran Plain are presented in Figure 9 and Table 2.

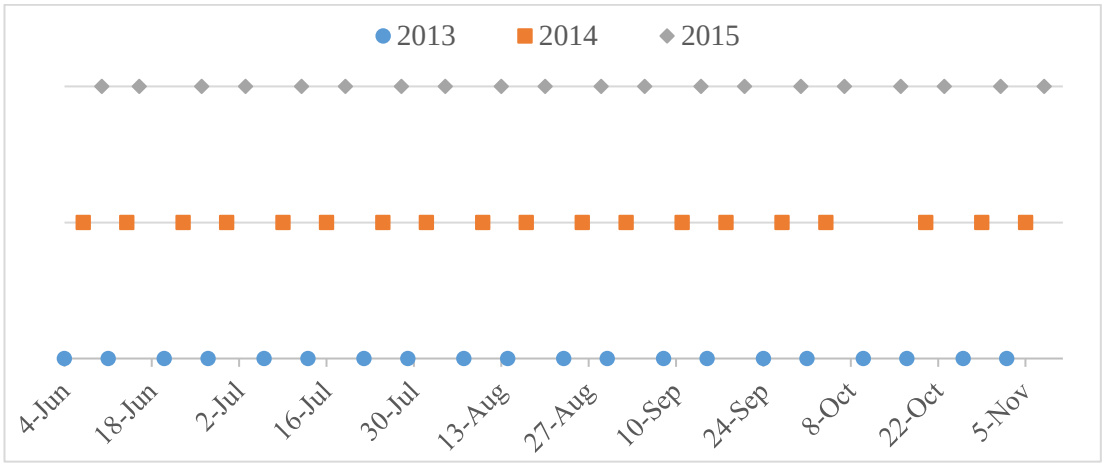

Figure 9: Landsat 8 imagery Harran dataset acquisitions.

Table 2: Landsat 8 imagery Harran dataset acquisitions DoY and date information.

2013		2014		2015	
DoY	Date	DoY	Date	DoY	Date
156	04/06	158	07/06	161	10/06
162	11/06	165	14/06	168	16/06
171	20/06	174	23/06	177	26/06
178	27/06	181	30/06	184	03/07
187	06/07	190	09/07	193	12/07
194	13/07	197	16/07	200	19/07
203	22/07	206	25/07	209	28/07
210	29/07	213	01/08	216	04/08
219	07/08	222	10/08	225	13/08
226	14/08	229	17/08	232	20/08
235	23/08	238	26/08	241	29/08
242	30/08	245	02/09	248	05/09
251	08/09	254	11/09	257	14/09
258	15/09	261	18/09	264	21/09
267	24/09	270	27/09	273	30/09
274	01/10	277	04/10	280	07/10
283	10/10	-	-	289	16/10
290	17/10	293	20/10	296	23/10
299	26/10	302	29/10	305	01/11
306	02/11	309	05/11	312	08/11

Nine of images from the Harran dataset in 2013 are shown in Figure 10 as true-color and in Figure 11 as NIR false-color.

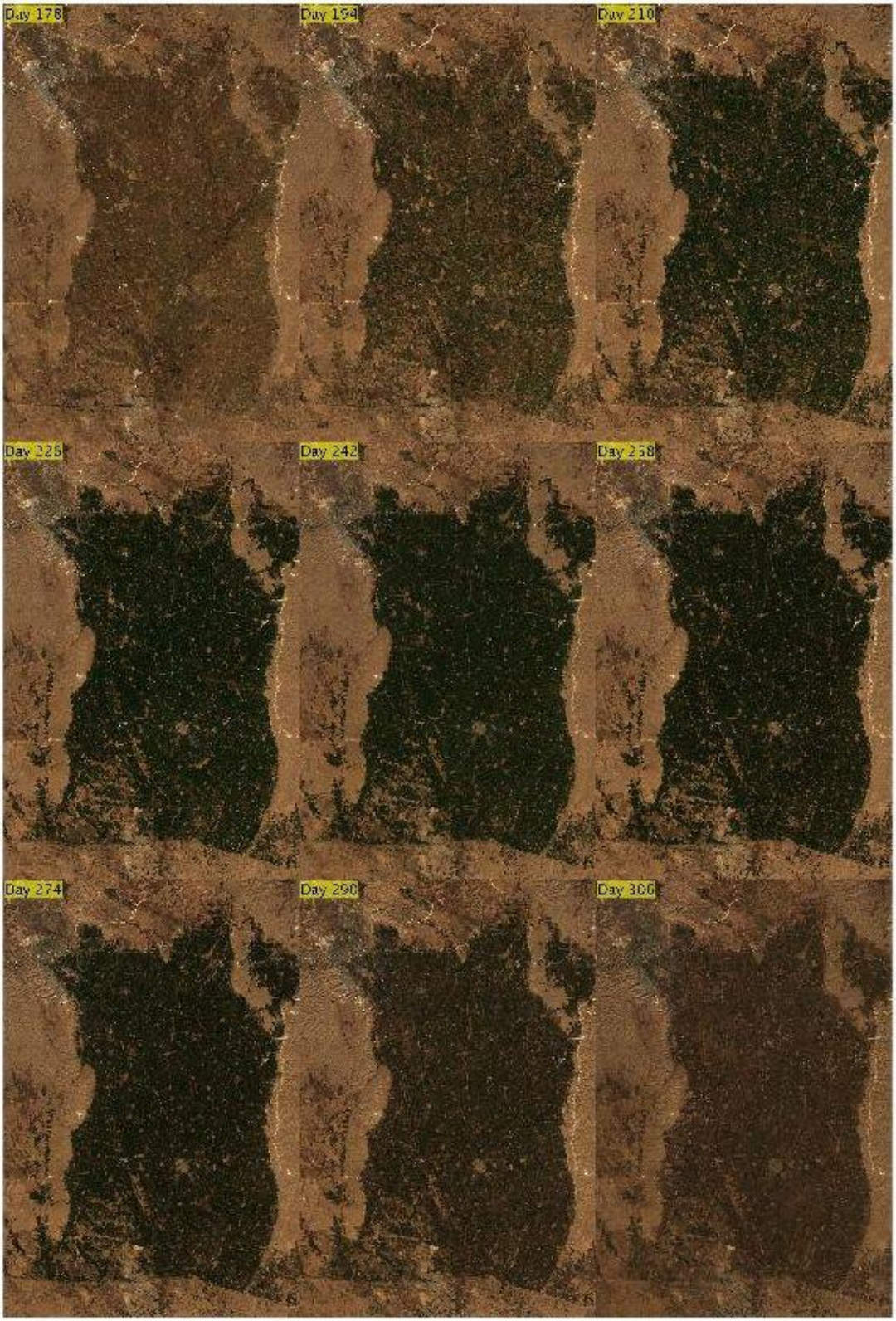

Figure 10: Landsat 8 Harran Images, 2013.

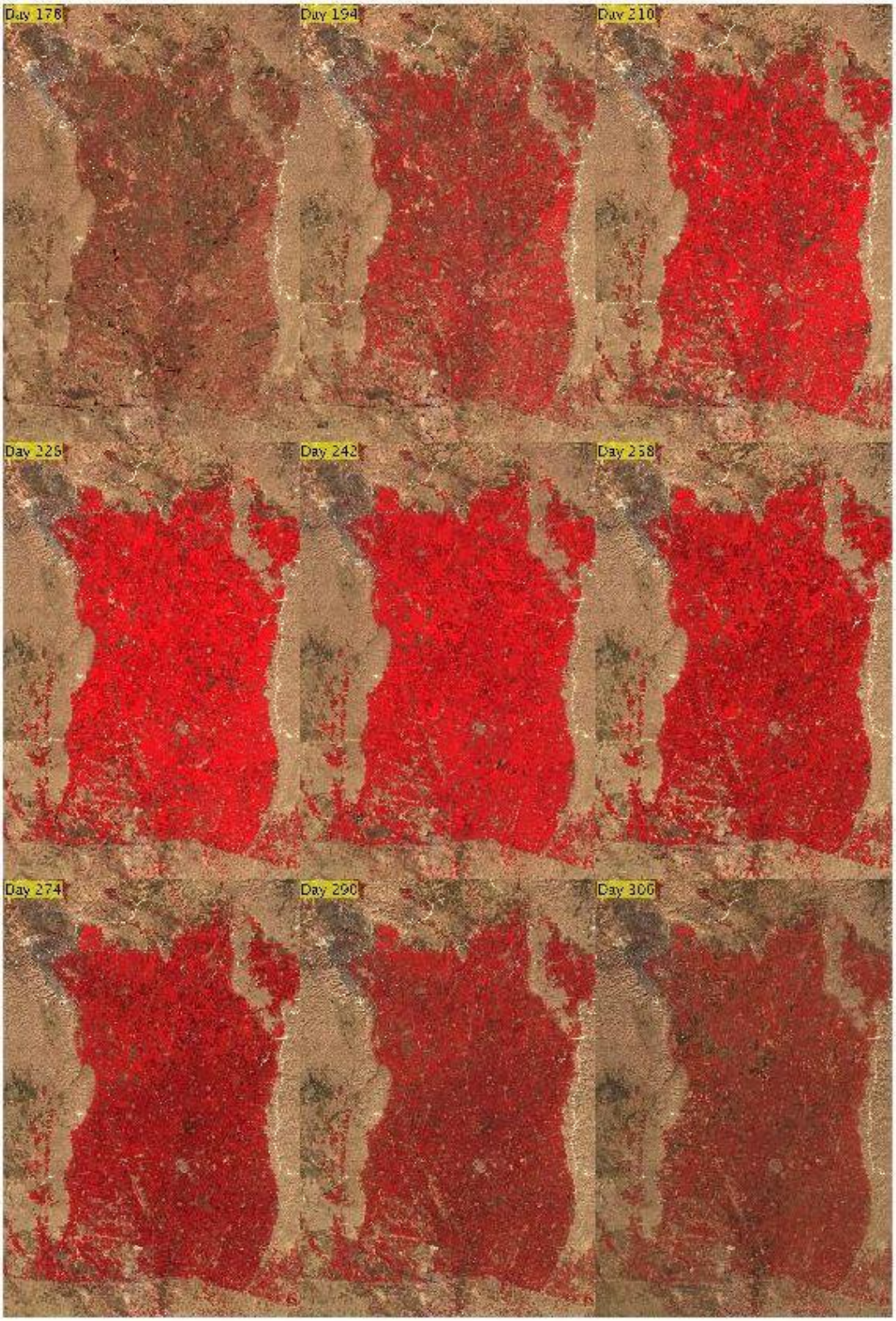

Figure 11: Landsat 8 Harran NIR false-color images, 2013.

The images, which are used for the Bismil Plain, are from April to November. Bismil dataset has 21 images in 2013 and 2014, and 19 images in 2015. The detailed information regarding images of each year is presented in Figure 12 and Table 3.

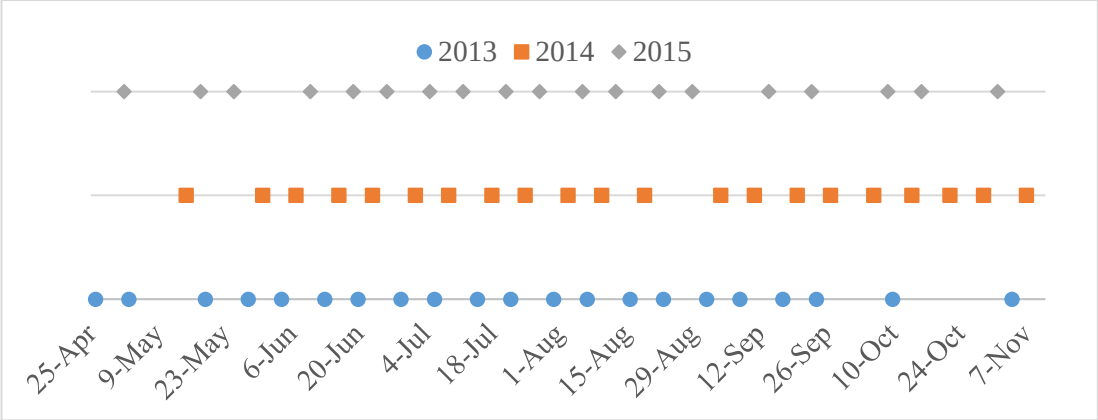

Figure 12: Landsat 8 Bismil dataset imagery acquisitions.

Table 3: Bismil dataset imagery dates DoY and date information .

2013		2014		2015	
DoY	Date	DoY	Date	DoY	Date
116	26/04	-	-	122	02/05
123	03/05	-	-	-	-
-	-	135	15/05	138	18/05
139	19/05	-	-	145	25/05
148	28/05	151	31/05	-	-
155	04/06	158	07/06	161	10/06
164	13/06	167	16/06	170	19/06
171	20/06	174	23/06	177	26/06
180	29/06	183	02/07	186	05/07
187	06/07	190	09/07	193	12/07
196	15/07	199	18/07	202	21/07
203	22/07	206	25/07	209	28/07
212	31/07	215	03/08	218	06/08
219	07/08	221	10/08	225	13/08
228	16/08	231	19/08	234	22/08
235	23/08	-	-	241	29/08
244	01/09	247	04/09	-	-
251	08/09	254	11/09	257	14/09
260	17/09	263	20/09	266	23/09
267	24/09	270	27/09	-	-
-	-	279	06/10	282	09/10
283	10/10	287	14/10	289	16/10
-	-	295	22/10	-	-
		302	29/10	305	01/11
308	04/11	311	07/11	-	-

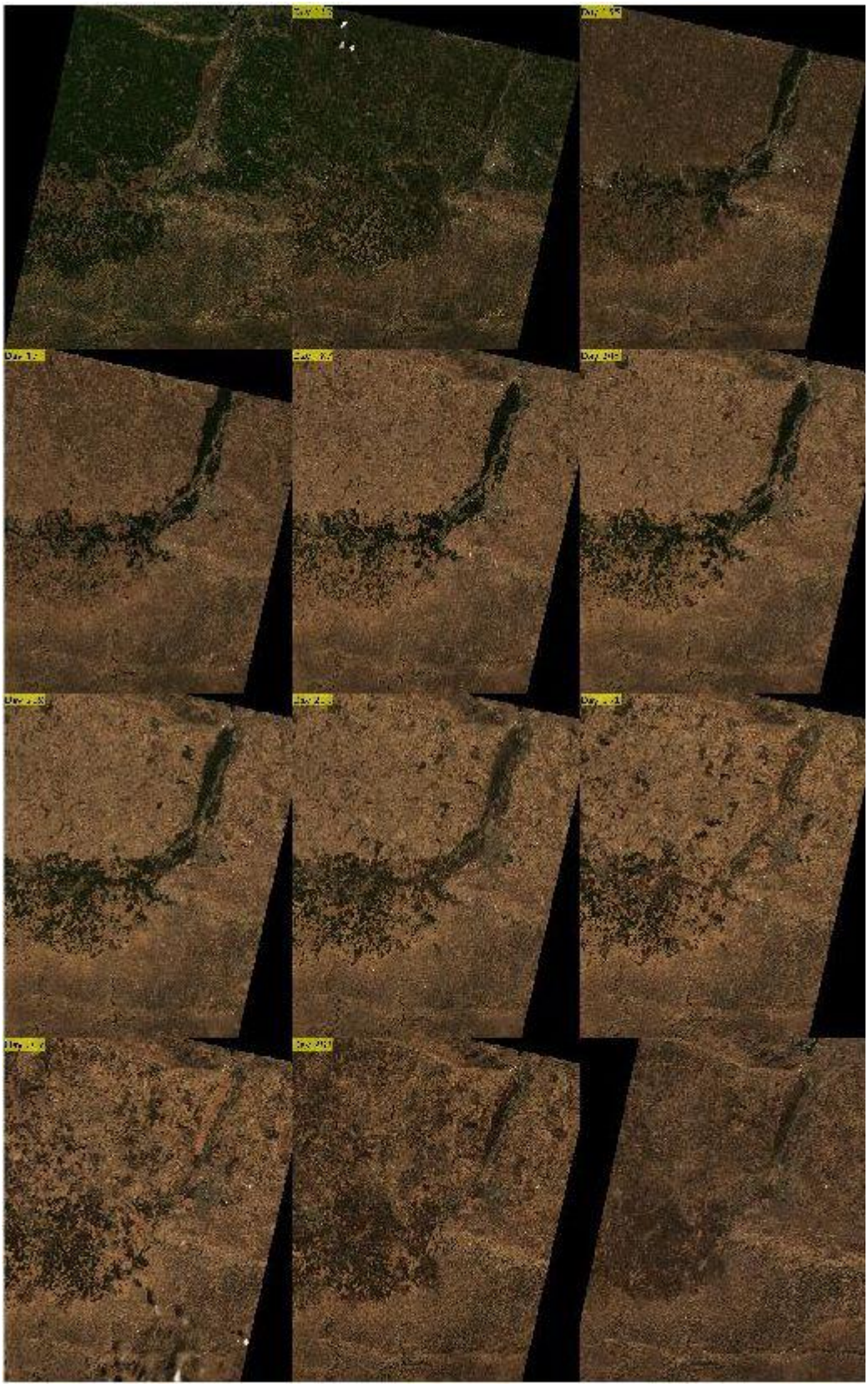

Figure 13: Landsat 8 Bismil true color images, 2013.

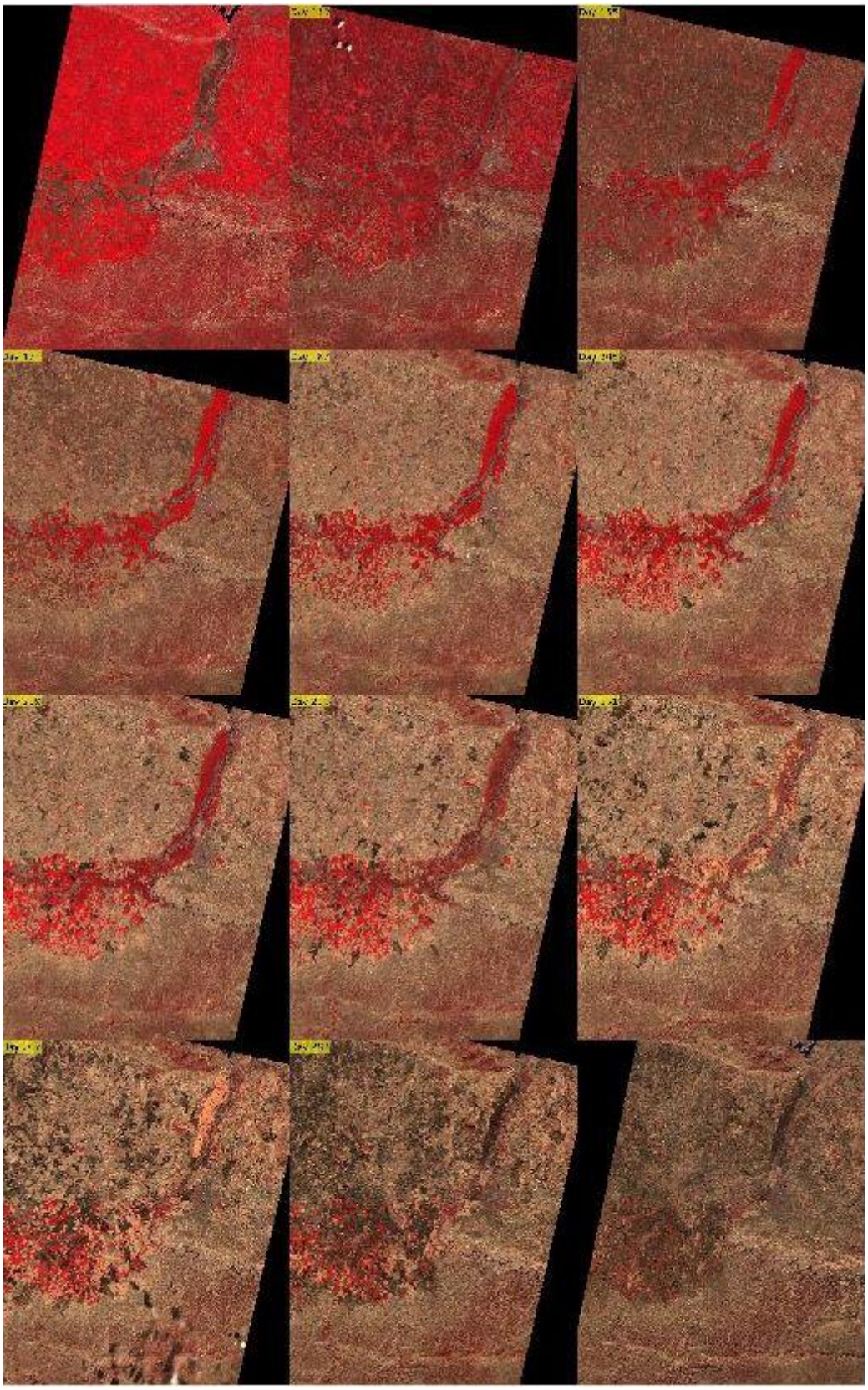

Figure 14: Landsat 8 Bismil NIR false color images, 2013.

3.2.2. Sentinel-2

Sentinel-2A was launched on 23rd June 2015, and Sentinel-2B was launched on 7th March 2015. Both satellites have combined 5-day revisit time. Sentinel-2 satellites also provide higher resolution 10-meter imagery compared to Landsat 8 satellite.

Table 4: Sentinel-2 a/b satellites spectral information.

Sentinel-2 bands	Sentinel-2A		Sentinel-2B		
	Central wavelength (nm)	Bandwidth (nm)	Central wavelength (nm)	Bandwidth (nm)	Spatial resolution (m)
Band 1 - Coastal aerosol	442.7	21	442.2	21	60
Band 2 – Blue	492.4	66	492.1	66	10
Band 3 – Green	559.8	36	559	36	10
Band 4 – Red	664.6	31	664.9	31	10
Band 5 – Vegetation red edge	704.1	15	703.8	16	20
Band 6 – Vegetation red edge	740.5	15	739.1	15	20
Band 7 – Vegetation red edge	782.8	20	779.7	20	20
Band 8 – NIR	832.8	106	832.9	106	10
Band 8A – Narrow NIR	864.7	21	864	22	20
Band 9 – Water vapour	945.1	20	943.2	21	60
Band 10 – SWIR – Cirrus	1373.5	31	1376.9	30	60
Band 11 – SWIR	1613.7	91	1610.4	94	20
Band 12 – SWIR	2202.4	175	2185.7	185	20

Harmonized Landsat 8 and Sentinel-2 (c) data were employed for the Kansas dataset. HLS Project aimed at merging Sentinel-2 data to Landsat 8 data. Thus, Sentinel-2 bands were resampled and radiometrically translated. Processing steps are described in Figure 15.

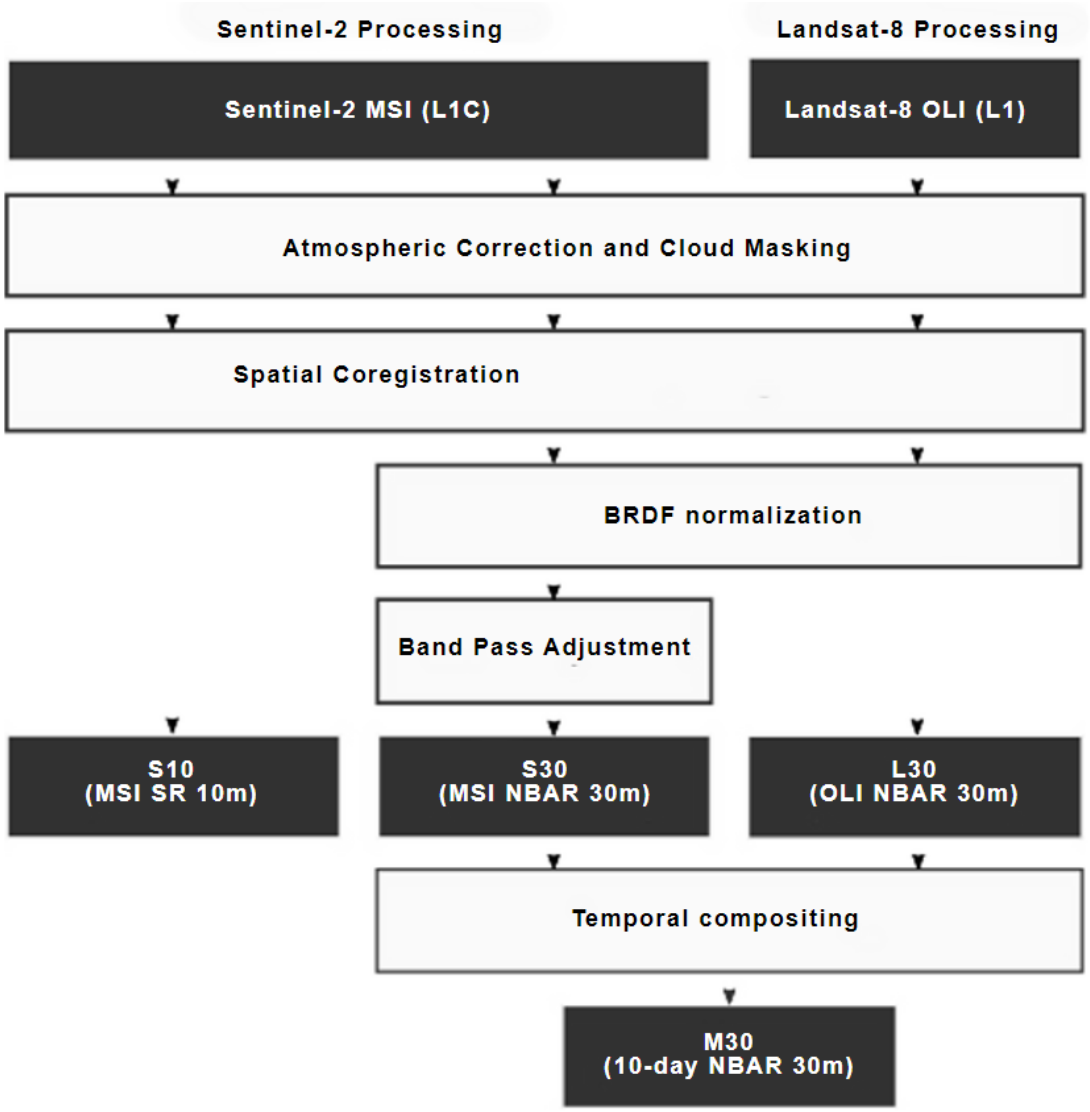

Figure 15: Landsat 8 and Sentinel-2 data harmonization steps.

The HLS data enabled more cloud-free data acquisitions. The Kansas data set has 20 images (15 Landsat 8 and seven Sentinel-2) in 2017 and 22 (five Sentinel-2 and 17 Landsat 8) images in 2018 as shown in Figure 16 and Table 5. Harmonized Landsat Sentinel project resamples Sentinel-2 imagery in to match Landsat 8 in spatial and spectral properties(Claverie et al., 2018).

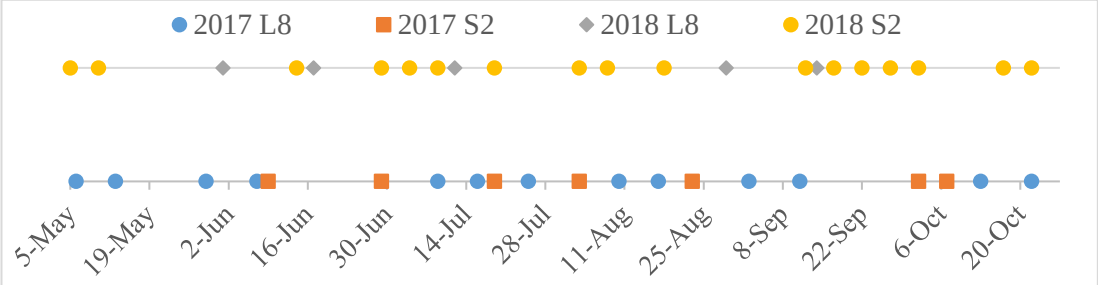

Figure 16: Landsat 8 and Sentinel-2 Kansas dataset imagery acquisition dates in 2017 and 2018.

Table 5: Kansas Imagery Dates with DoY, date and satellite information.

2013			2014		
DoY	Date	Satellite	DoY	Date	Satellite
126	06/05	L8	125	05/05	S2
133	13/05	L8	130	10/05	S2
149	29/05	L8	152	01/06	L8
158	07/06	L8	165	14/06	S2
160	09/06	S2	168	17/06	L8
180	29/06	S2	180	29/06	S2
190	09/07	L8	185	04/07	S2
197	16/07	L8	190	09/07	S2
200	19/07	S2	193	12/07	L8
206	25/07	L8	200	19/07	S2
215	03/08	S2	215	03/08	S2
222	10/08	L8	220	08/08	S2
229	17/08	L8	230	18/08	S2
235	23/08	S2	241	29/08	L8
245	02/09	L8	255	12/09	S2
254	11/09	L8	257	14/09	L8
			260	17/09	S2
			265	2209	S2
			270	27/09	S2
275	02/10	S2	275	02/10	S2
280	07/10	S2			
286	13/10	L8	290	17/10	S2
295	22/10	L8	295	22/10	S2

True-color and false-color HLS data are shown in Figure 17 and Figure 18, respectively. Sentinel-2 frames are full data frames while Landsat 8 frames partially cover the region.

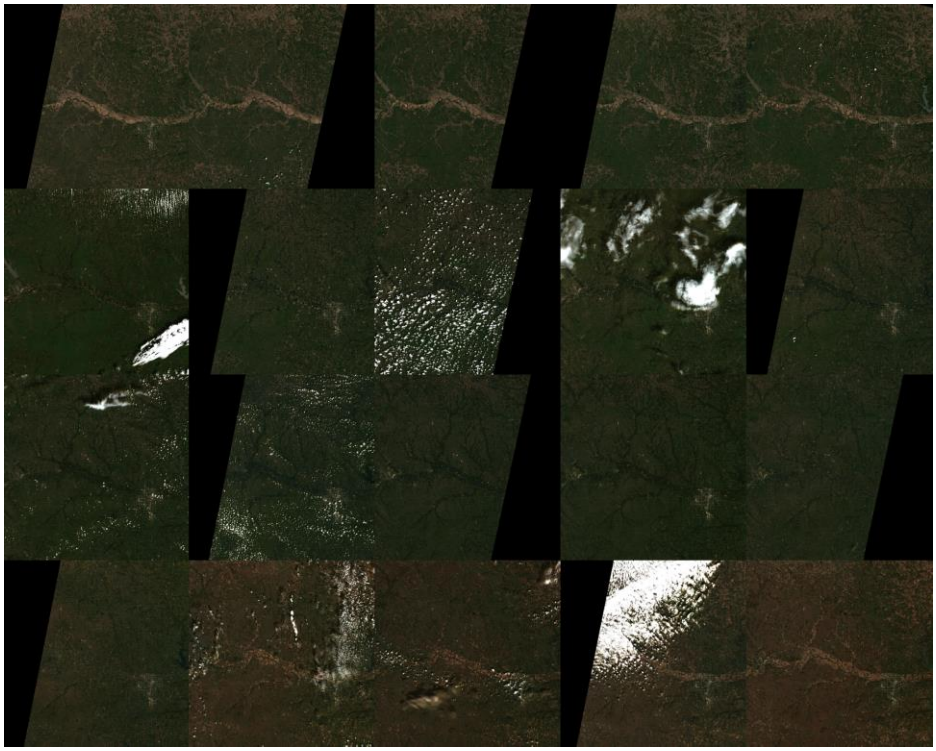

Figure 17: Kansas Dataset 2018 true-color imagery.

Figure 18: Kansas Dataset 2018 false-color imagery.

3.3. Crops of Interest

Major summer crops of the Harran Plain are corn and cotton. Cotton is the first product, and corn is grown as the second product after winter wheat. Corn is grown after winter wheat. Both corn and cotton have similar phenological periods, which makes the classification of these crops challenging.

On the other hand, both Corn and cotton are primary products in Bismil. Both crops have distinct phenological periods. Soybean in the area is grown after winter wheat.

Kansas dataset contains corn and soybean as this region is part of the Corn Belt.

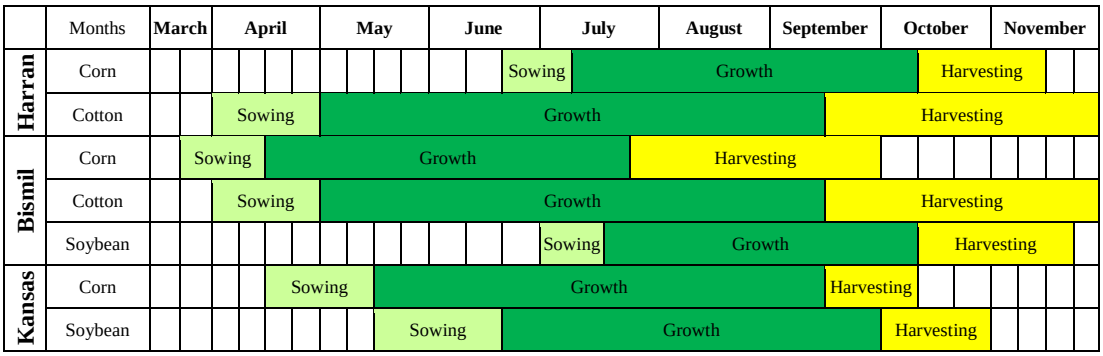

Figure 19: Harran, Bismil, and Kansas crop calendars.

3.4. Ground Truth

Ground truth preparation is crucial and needs utmost care. In this section, details of ground truth preparation will be explained.

The ground truth of the Harran and Bismil datasets are based on the Ministry of Agriculture and Forestry's National Registry of Farmers (NRF, Turkish: Çiftçi Kayıt Sistemi, ÇKS) for Turkey. In the NRF, farmers declare the crops that they will grow in order to apply for government agricultural subsidies (Yomralioglu, Inan, Aydinoglu, & Uzun, 2009). On the other hand, the ground truth of the Kansas dataset is based on USDA NASS's the Cropland Data Layer (CDL). The CDL data was created based on USDA's Farm Services Agency (FSA) Common Land Unit (CLU) data.

The NRF contains vectors of agricultural fields. Regarding the GT, census data was used as the baseline: the declaration from the National Registry of Farmers. In the case of the Kansas dataset, CLU 2008 was used data as field boundaries.

The median vegetation index (VI) time-series vector data of each field is assigned as a sample in the tests. A summary of the characteristics the Harran Dataset is presented in Table 6, The Bismil dataset is presented in Table 7, and the Kansas dataset is depicted in Table 8.

The majority of the crops in the Harran dataset are cotton about 80%. On the other hand, corn is the major crop in the Bismil dataset. The ratio of soybean is very low in the Bismil dataset. Finally, Corn in the Kansas dataset having a 60% ratio against soybean.

Table 6: Number, percentage distribution, and areas of corn and cotton fields in the Harran dataset in 2013, 2014 and 2015.

		#Fields	%Samples	Area (ha)
2013	Corn	1192	21.8	12366
	Cotton	4285	78.2	43968
	Total	5477		**56333**
2014	Corn	692	13.2	7321
	Cotton	4561	86.8	47395
	Total	5253		**54716**
2015	Corn	517	15.4	5863
	Cotton	2849	84.6	31094
	Total	3366		**36957**

Table 7: Number, percentage distribution, and areas of corn, cotton and soybean fields in the Bismil dataset in 2013, 2014 and 2015.

		#Fields	%Samples	Area (ha)
2013	Corn	674	61.38	8887
	Cotton	347	31.60	3991
	Soybean	77	7.02	238
	Total	**1098**		13116
2014	Corn	721	54.91	11606
	Cotton	438	33.36	5115
	Soybean	154	11.73	312
	Total	**1313**		17033
2015	Corn	793	64.37	11842
	Cotton	349	28.33	2580
	Soybean	90	7.30	271
	Total	**1232**		14693

Table 8: Number, percentage distribution, and areas of corn and soybean fields in the Kansas dataset in 2017 and 2018.

		#Fields	%Samples	Area (ha)
2017	Corn	1167	41.66	67952
	Soybean	4083	58.34	89479
	Total	5250		**157431**
2018	Corn	2307	42.99	71714
	Soybean	3059	57.01	86913
	Total	5366		**158627**

CHAPTER 4

METHODOLOGY

4.1. Background

4.1.1. Dynamic Time Warping

Dynamic Time Warping (DTW) is a technique that finds the optimal alignment in translation and scaling between two time-series data sequences (Müller 2007) by using dynamic programming(Bellman, 1966). The sequences are matched in a non-linear way to measure similarities. DTW method outperformed primary time series classification methods (Bagnall, Lines, Bostrom, Large, & Keogh, 2017).

DTW uses the dynamic programming approach to find the optimal distance between two signals, thus determining the similarity between two signals. As the similarity increases, the distance between signals decreases resulting in lower scores.

Figure 20 shows the alignment of corn and cotton crops. The input signals have a size of 20 and resulted in optimal warping is performed over 20 dimensions. The similarity score between these crops is 0.81 by using the Euclidean distance. The optimal warping path of these corn and cotton samples are displayed in Figure 21. The similar parts of these signals warped on the diagonal.

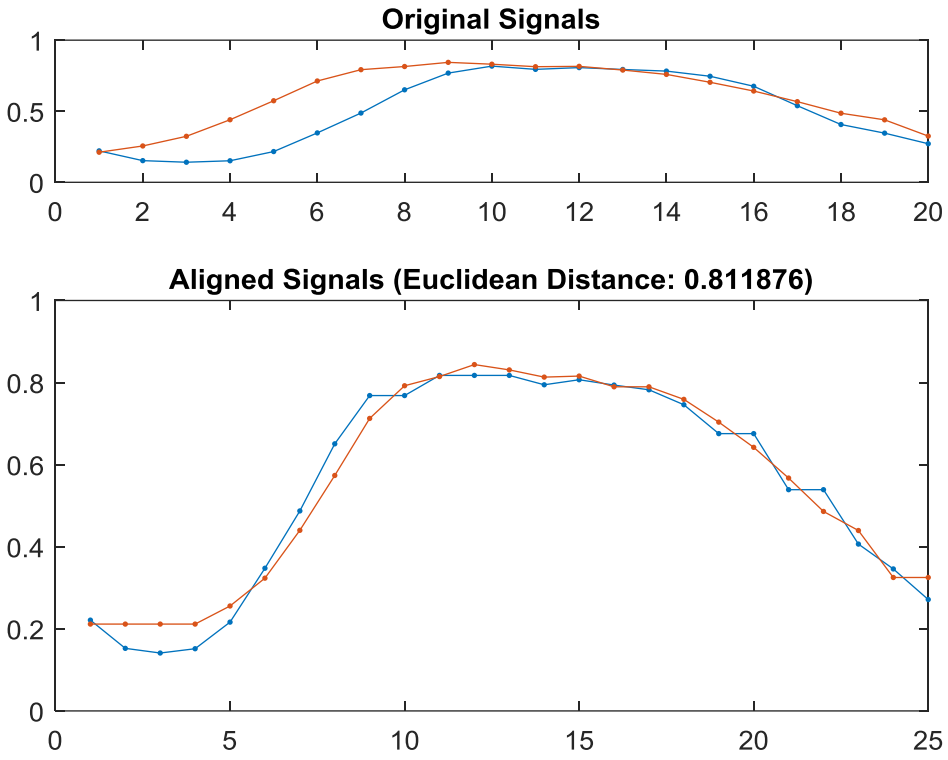

Figure 20: Warping of Two Vegetation Phenologies of corn and cotton having a Euclidean distance of 0.81.

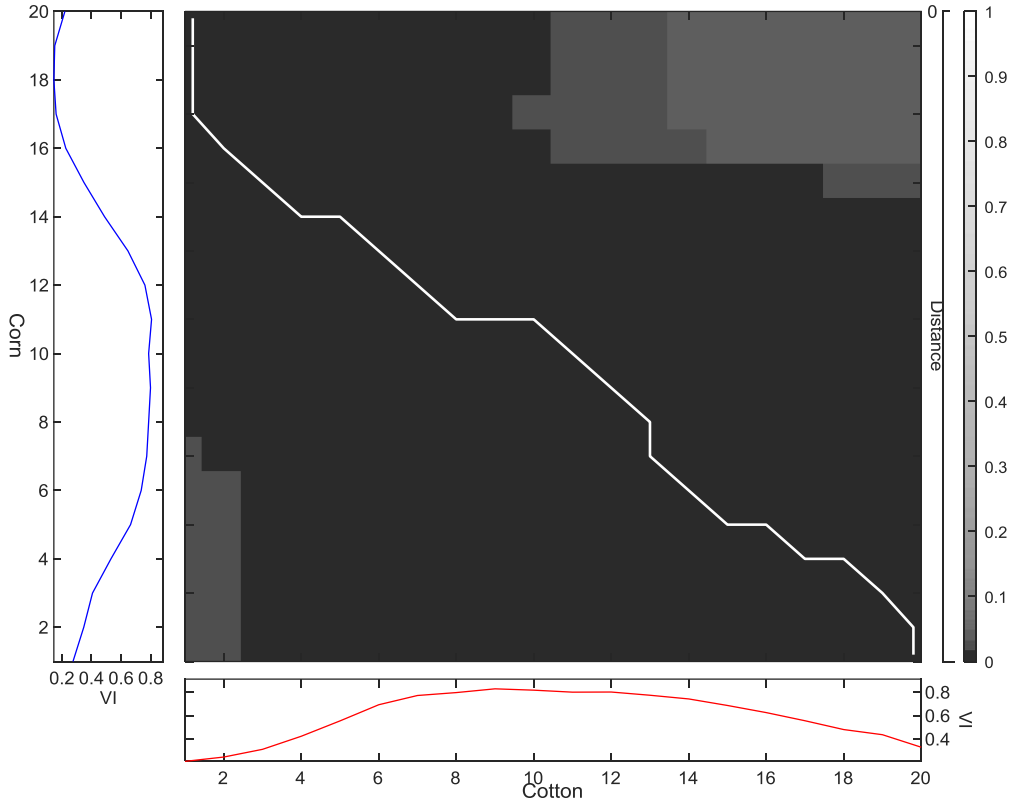

Figure 21: Computation of optimal warping path between corn and cotton samples

4.1.2. Spectral Angle Mapper

Spectral angle mapper is a commonly used measure in hyperspectral image analysis describing the angular distance between two spectra (Kruse et al., 1993). The angle between two vectors, $\vec{\beta}$ and $\vec{\theta}$, is computed in radians as

$$\alpha = \mathbf{cos^{-1}} \frac{\vec{\beta} \cdot \vec{\theta}}{\|\vec{\beta}\| \cdot \|\vec{\boldsymbol{\theta}}\|} \tag{9}$$

SAM is robust to illumination changes so that the effects of yearly climate changes are reduced. VDTW method is based on a vectoral distance between two samples, which is the core of SAM.

4.1.3. Crop Phenology

The phenology of crops is measured by using vegetation indices, which were described in section 0. Phenology information generated by using the ordering of phenological observations in time. Due to differences in growing practices and crop conditions, there were variations in as displayed box plots Figure 22. Variations of different crops in the Harran Plain is depicted in Figure 23 and Figure 24.

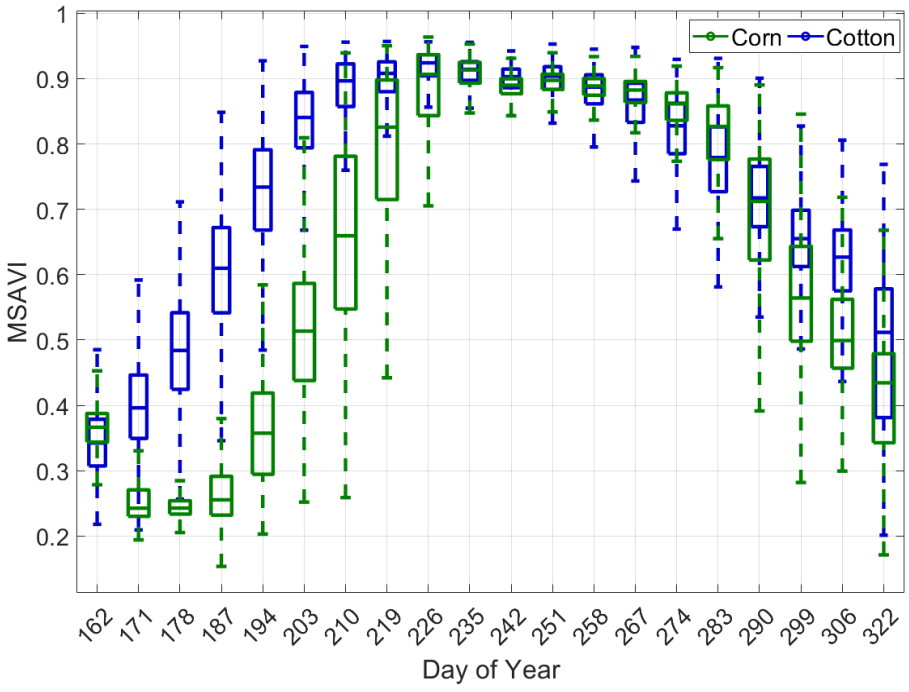

Figure 22: Variations in MSAVI phenologies of corn and cotton samples in the Harran Plain in 2013.

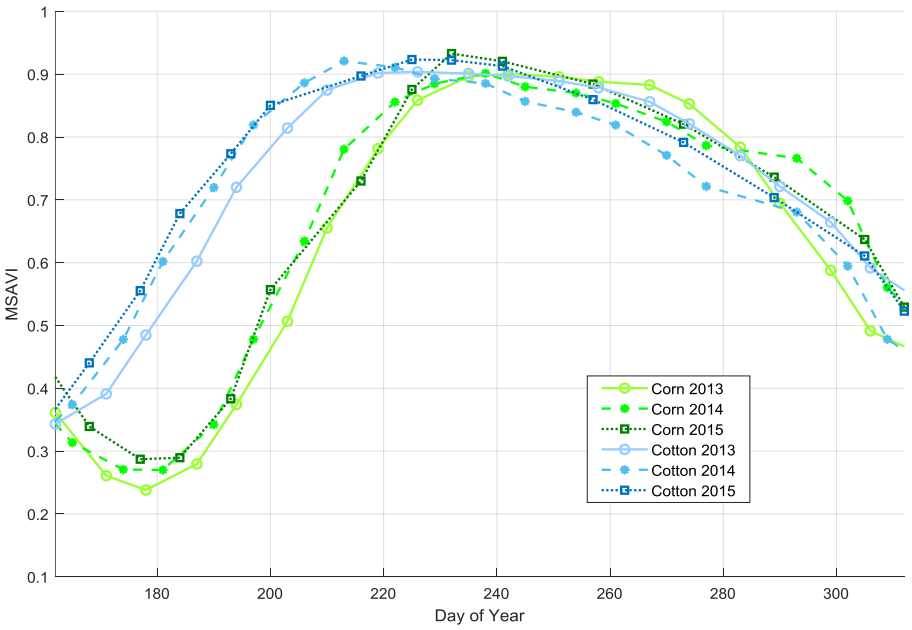

Figure 23: Median values of corn and cotton in the Harran dataset in different years.

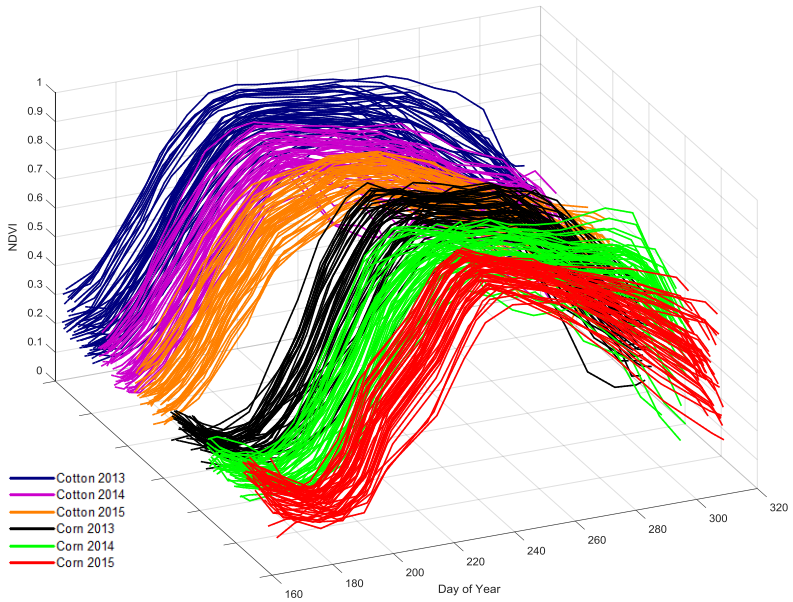

Figure 24: Variations in NDVI values of corn and cotton at different years.

4.1.4. Crop Phenology Indicators

Crop phenology is defined by extracting important transition dates and other critical phenological indicators. Double logistic(double sigmoid) is used as an efficient phenology indicator (Zhong et al., 2014) (Zhang et al., 2003).

Double sigmoid is a combination of two sigmoid signals. Several functions could define a sigmoid. Double hyperbolic function for feature extraction is given below:

$$f(x) = a + 0.5 * b * (tanh(p * (x - Di)) + tanh(q * (x - Dd) \qquad (10)$$

where

- a: minimum NDVI Value
- b: maximum NDVI Value,
- p: the curve of NDVI increase
- Di: center day of increase
- q: the curve of NDVI decrease
- Dd: center day of NDVI decrease

Besides, transition days are used as a function

- D1: Start of NDVI increase
- D2: End of NDVI Increase
- D3: Start of NDVI Decrease
- D4: End of NDVI Decrease

Features in this representation are used in this study (Figure 25).

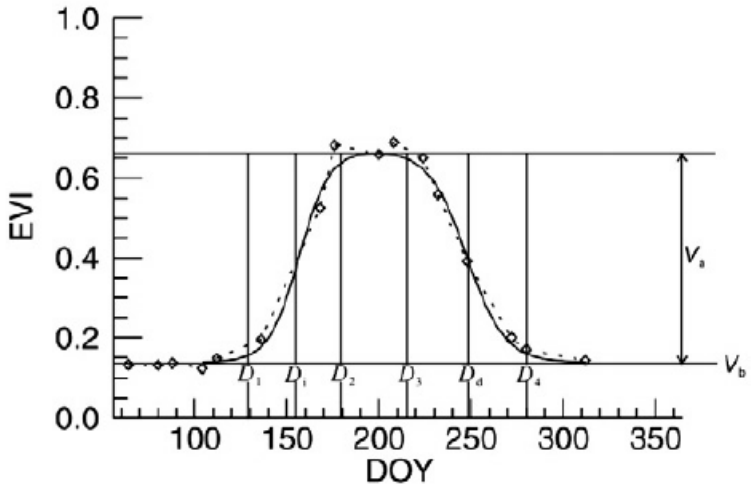

Figure 25: Double sigmoid phenological transition points (Zhong et al., 2014)

4.1.5. Data Smoothing

In this study, time-series data smoothing was applied as a preprocessing step. Savitzky-Golay filtering, spline fitting, and piecewise curve fitting were compared.

Non-static observation conditions (such as atmosphere, weather, and sun position) and changes in crop phenology cause variations in measurements. Comparisons of these methods are presented as NDVI phenologies, which are expected to resemble a smooth double logistics function. SG filtering was performed by a second-order polynomial, and a window size of five samples is presented in Figure 26. The piecewise curve fitting is displayed in Figure 27. Second-order spline fitting results are shown in Figure 28.

Among these methods, Savitzky-Golay filtering produced smoother phenologies while other methods produced data that mostly resembled original forms.

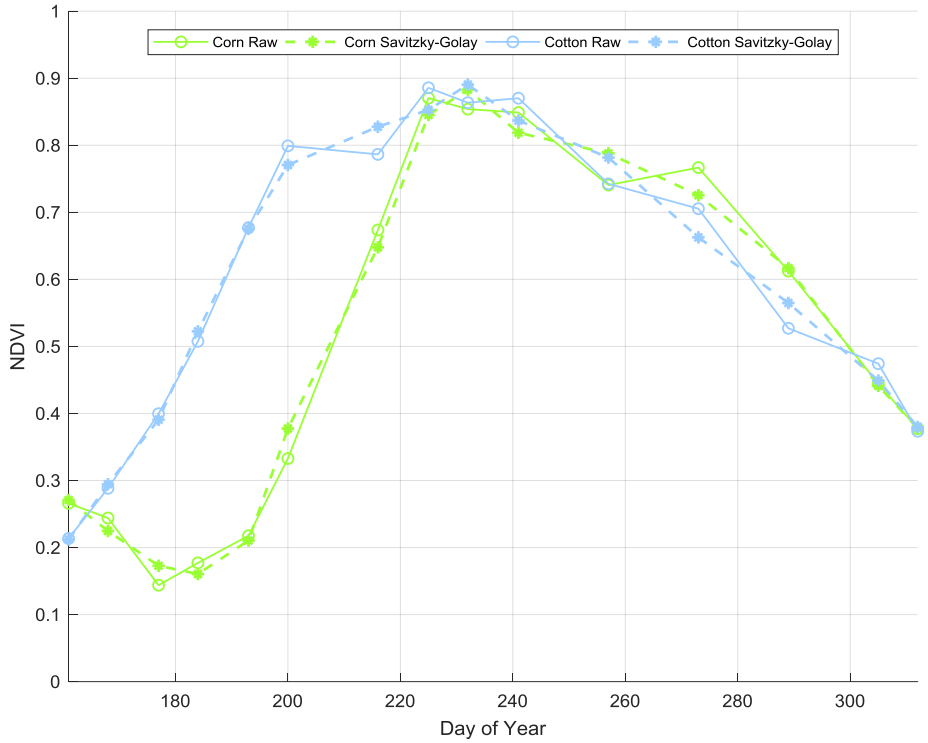

Figure 26: Smoothing of corn and cotton NDVI phenologies by SG filtering.

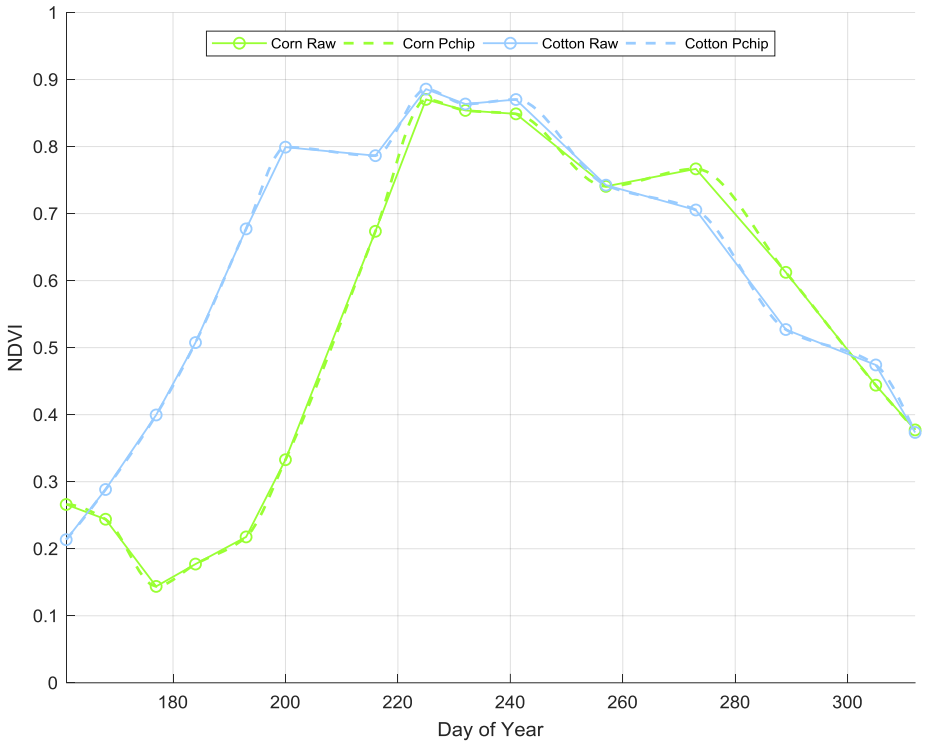

Figure 27: Smoothing of corn and cotton NDVI phenologies by piecewise smoothing.

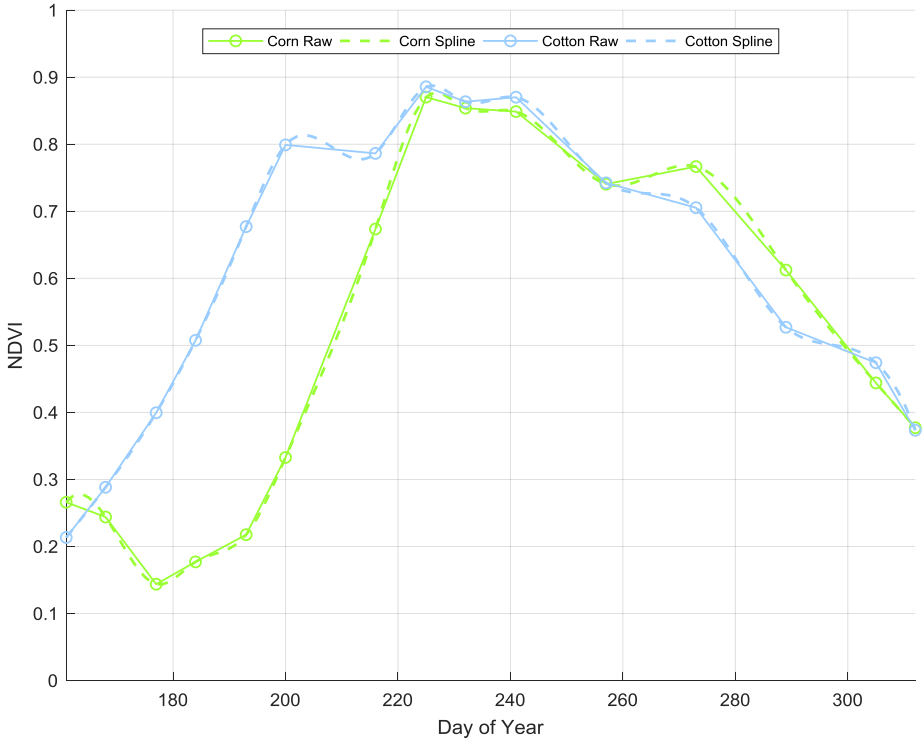

Figure 28: Smoothing of corn and cotton NDVI phenologies by spline smoothing.

4.2. Time Series Simulations

Phenological variations of a crop were studied in various experimental settings within the datasets. For this purpose, crop signatures were simulated to analyze the behavior of VDTW, DTW, and SAM methods, their advantages, and shortcomings in time series crop mapping. Shift and scale are simulated in different scenarios. Figure 29 shows the case if sowing dates vary while harvest dates are the same. Figure 31 shows that crops are sown at the same time, but harvest dates differ. In Figure 33**,** an extreme case is shown, where the crop's both sow and harvest times vary. Figure 35 shows where growth duration of the crop stays the same, but its sow and harvest time shifts in time: this simulation corresponds to some growers sowing earlier or later and yearly climate changes. Both DTW and VDTW similarity scores did not change against varying sowing and harvesting dates(Figure 32, Figure 34, Figure 36). Figure 37 depicts variances in phenological observation in the growing period. These differences may be caused by different atmospheric conditions or variations in fields or farming practices. Finally, an extreme case is displayed in Figure 39**,** where phenological variations are observed globally. It was observed that SAM and VDTW methods obtained similar scores; on the other hand, DTW scores varied based on different values.

These simulations showed that VDTW is invariant to shifts in time as DTW and produced near-valued scores as SAM to shifts in values.

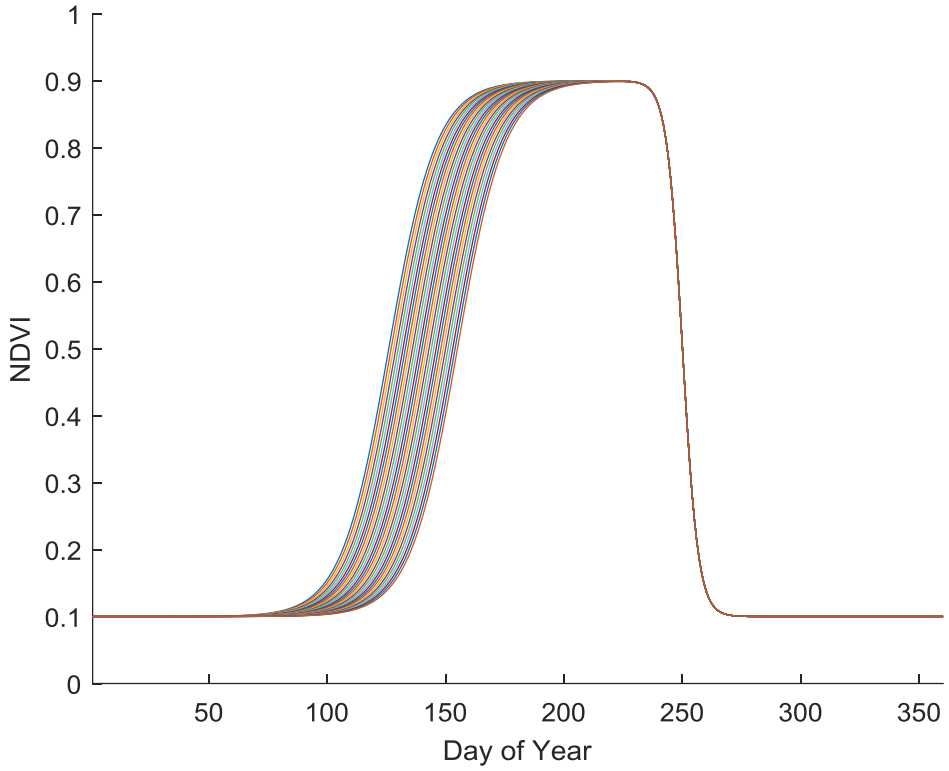

Figure 29: Varying sowing dates simulation.

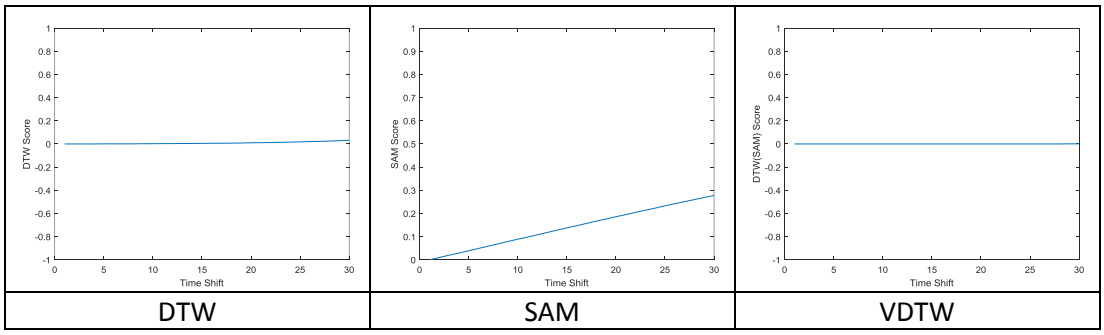

Figure 30: Varying sowing dates simulation similarity scores.

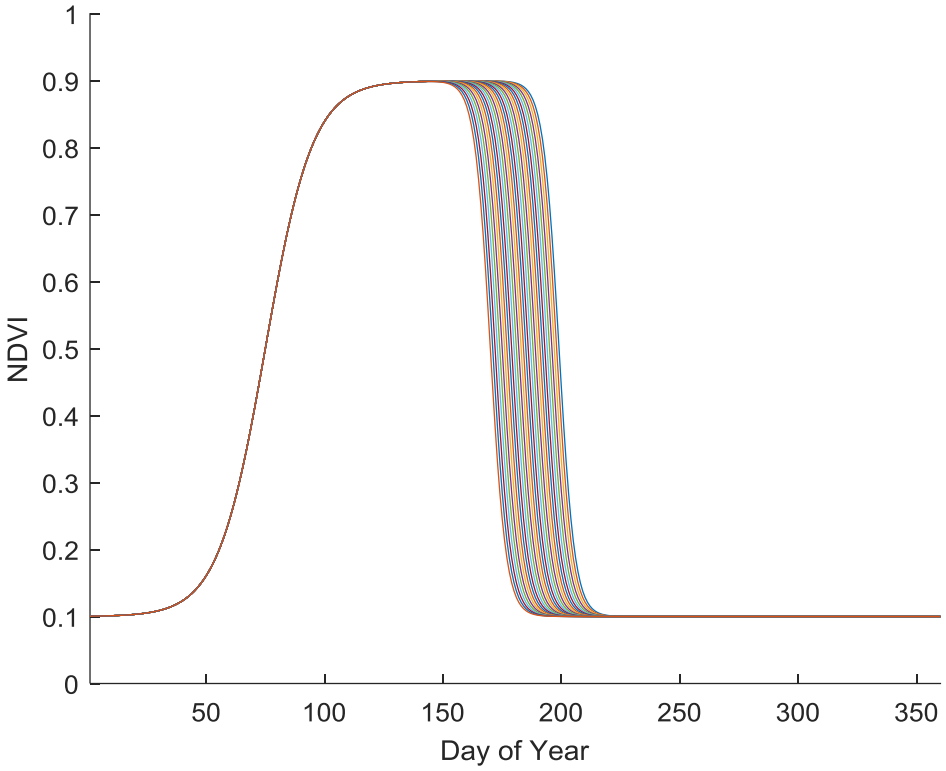

Figure 31: Varying harvest dates simulation.

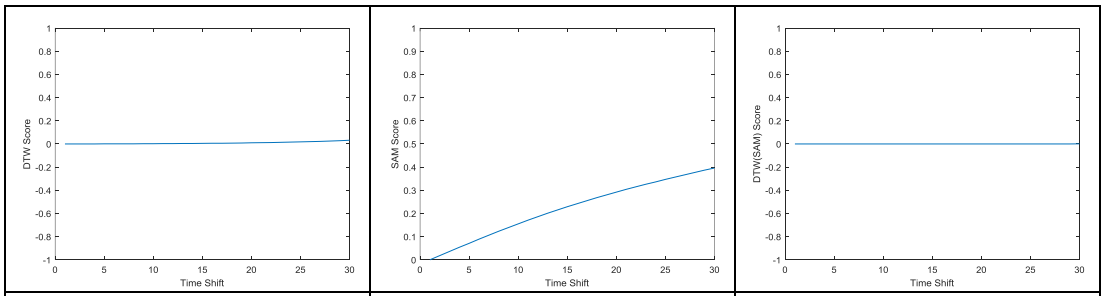

Figure 32: Varying harvest dates similarity scores.

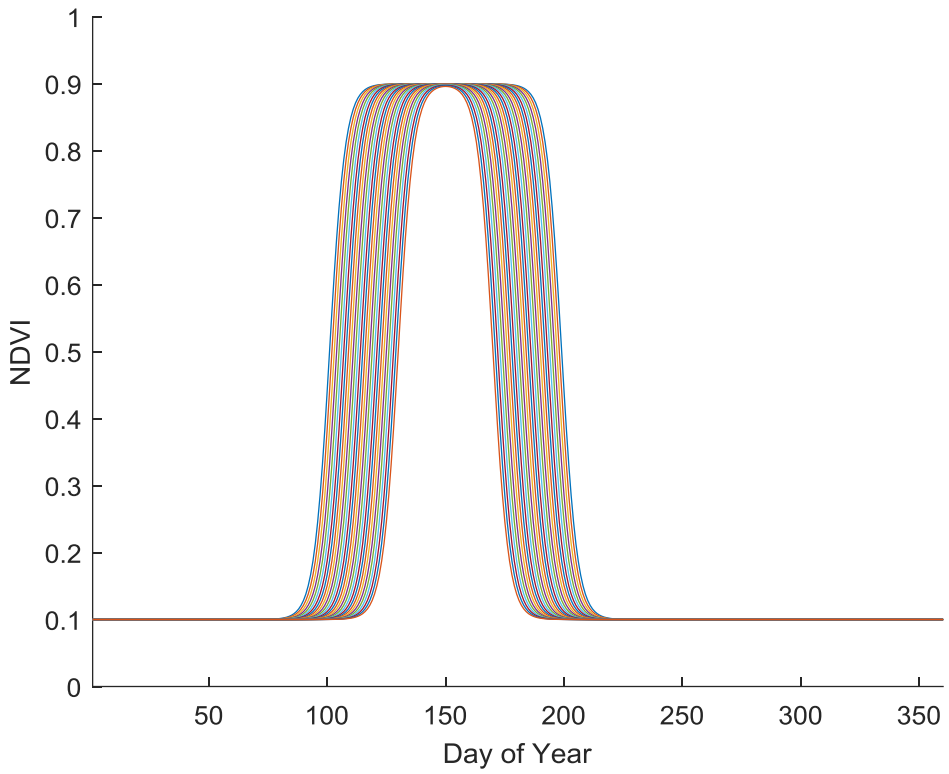

Figure 33: Varying sowing and harvest dates simulation.

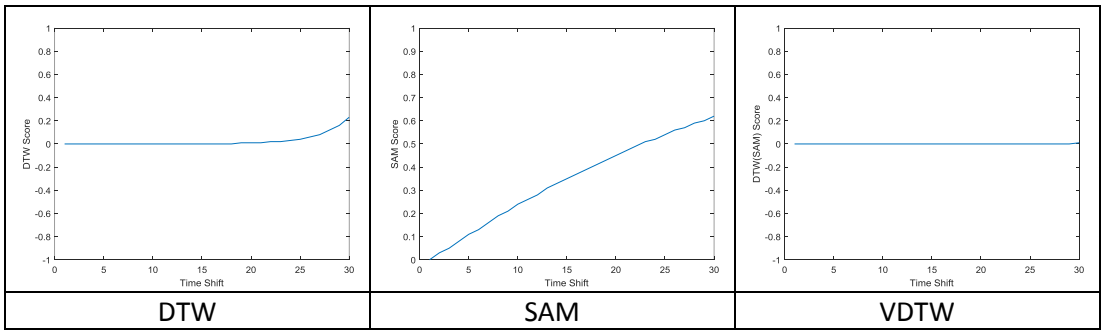

Figure 34: Varying sowing and harvest dates similarity scores.

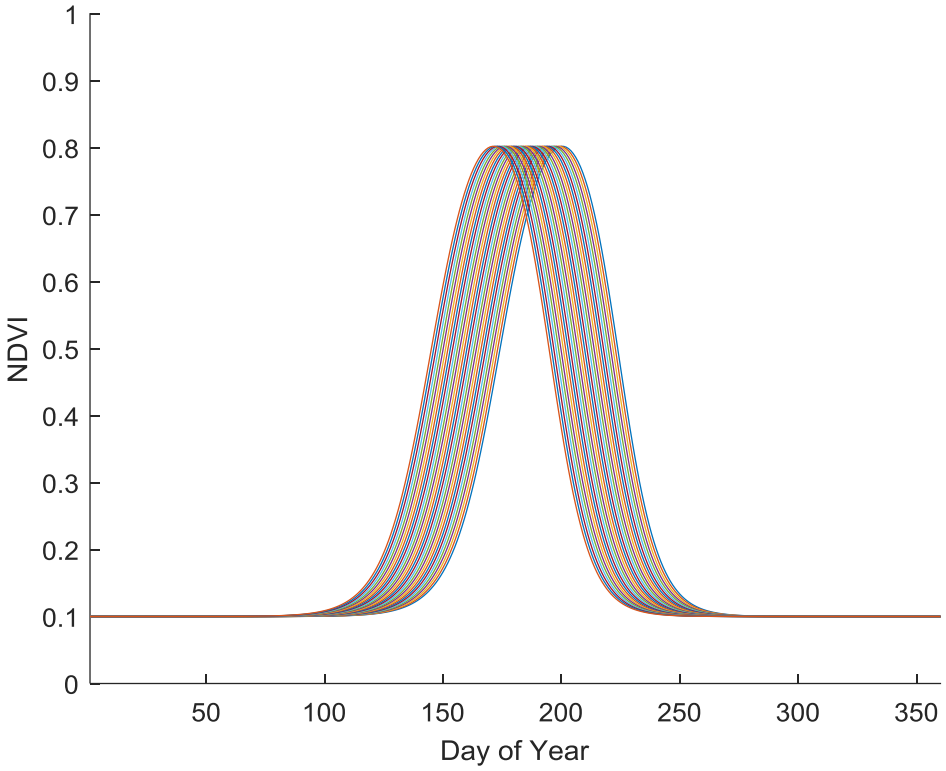

Figure 35: Varying crop growth in time simulation.

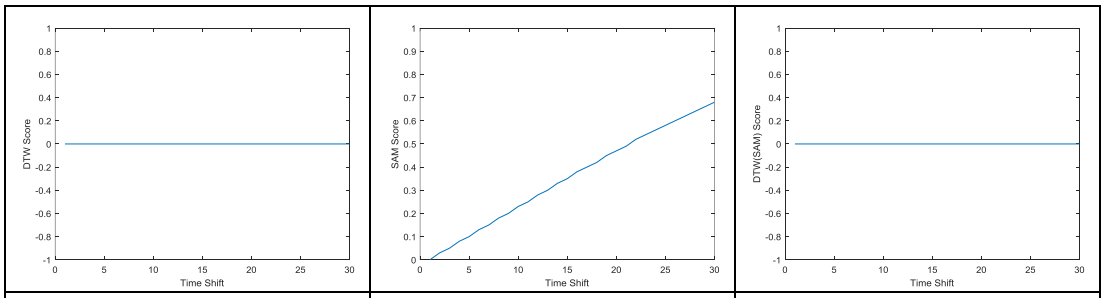

Figure 36: Varying crop growth in time similarity scores.

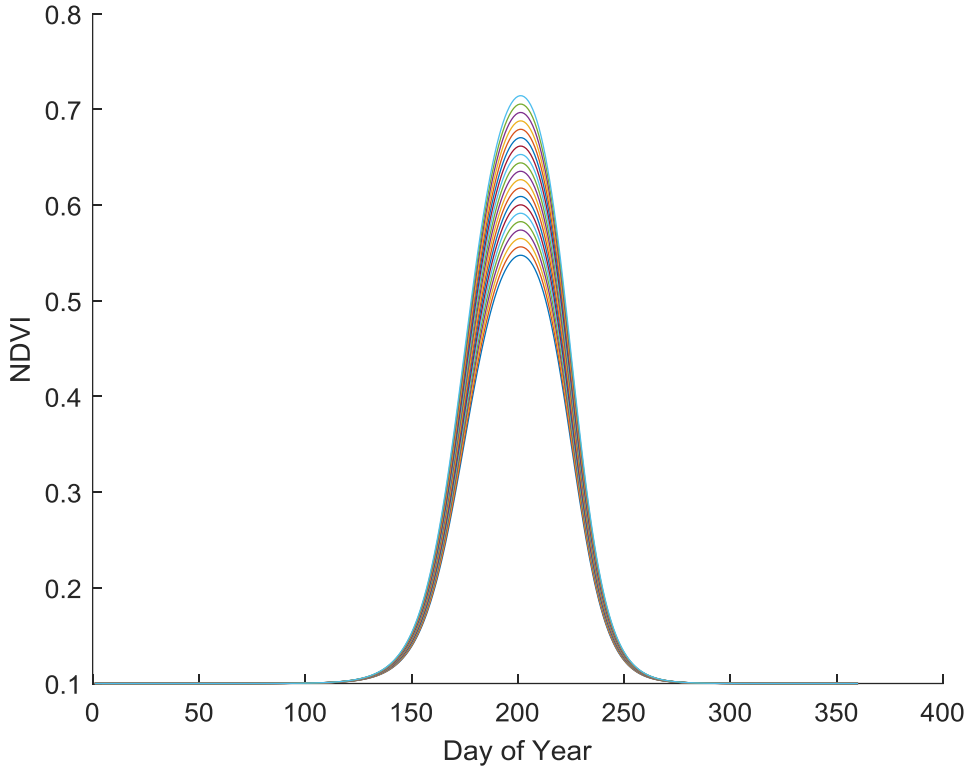

Figure 37: Offsetting crop growth simulation 1.

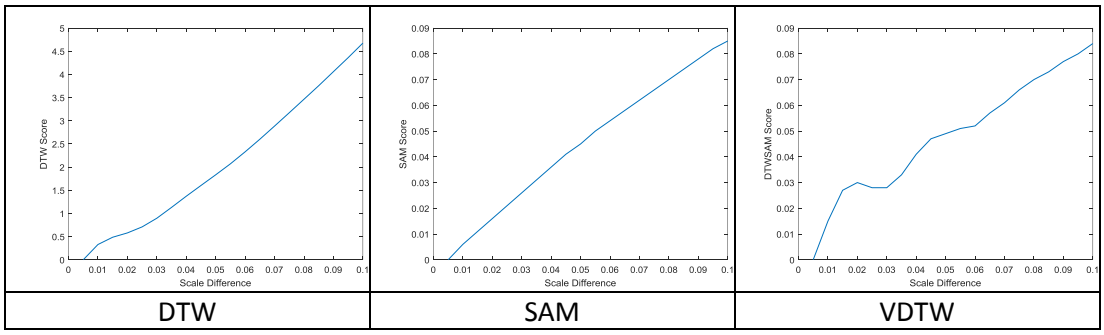

Figure 38: Offsetting crop growth simulation 1 similarity scores

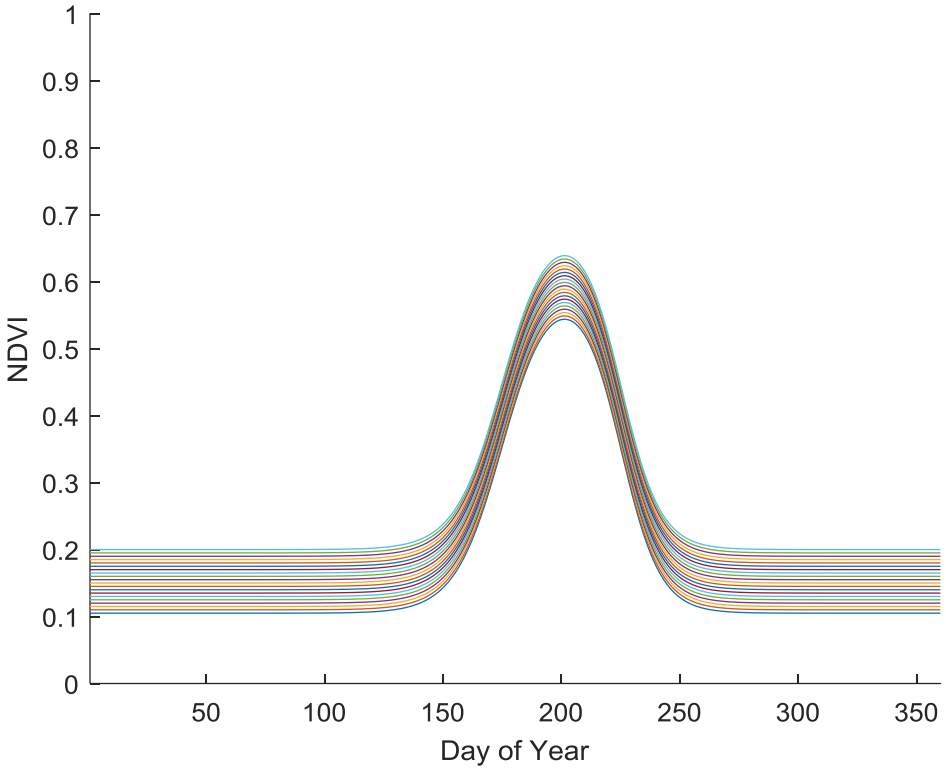

Figure 39: Offsetting crop growth simulation 2

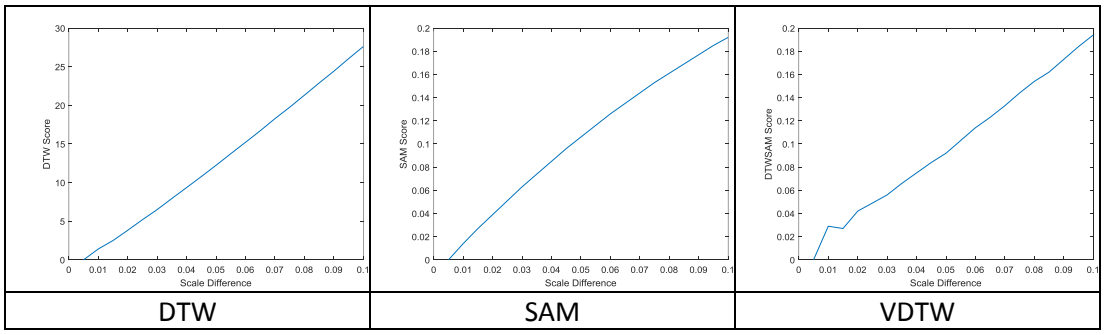

Figure 40: Offsetting crop growth simulation 2 similarity scores

4.3. Vector Dynamic Time Warping Method

Dynamic time warping handles signals, which are shifted or scaled in time. When the original signal shifted in time, DTW handles shifts in time or change in scale. On the other hand, depending on the distance metric such as Euclidian distance, differences in scale or bias of the signal increases scores.

Spectral Angle Mapper (SAM) method was developed to provide robustness w.r.t. illumination changes in hyperspectral data.

There are two significant findings in the simulations:

1. The growth of the crops shifts in time due to climate and other factors.
2. Observations are dependent on illumination and atmospheric conditions.

While DTW is robust to shifts in time, it is not robust to variations in growth and yearly illumination changes. DTW uses Euclidian distance. Instead of using Euclidean distance, it is proposed to utilize spectral angles distances.

Both DTW and SAM have disadvantages while dealing with time series phenological data. Phenological measurements in crops vary in time, and illumination changes at different times cause variations in measurements.

A new method is proposed, which is both robust to shift in crop growth and illumination differences: Vector Dynamic Time Warping (VDTW). While DTW is based on Euclidean distance d, it is proposed to use angular distance a, as shown in Figure 41. VDTW computes the optimal warping path of spectral distances between two phenological observations.

Let c[i] be the corn VI data and d[j] be the cotton VI data, respectively. We generate a vector signal u_i as follows:

$$\overrightarrow{u}_i = \begin{bmatrix} c[i] - c[i-1] \\ t(i) - t(i-1) \end{bmatrix}, \quad i = 1,2, \ldots, n \tag{11}$$

where $t(i)$ represents the time of the i-th measurement. Similarly, a vector time-series v_j is generated from d[i] VI data.

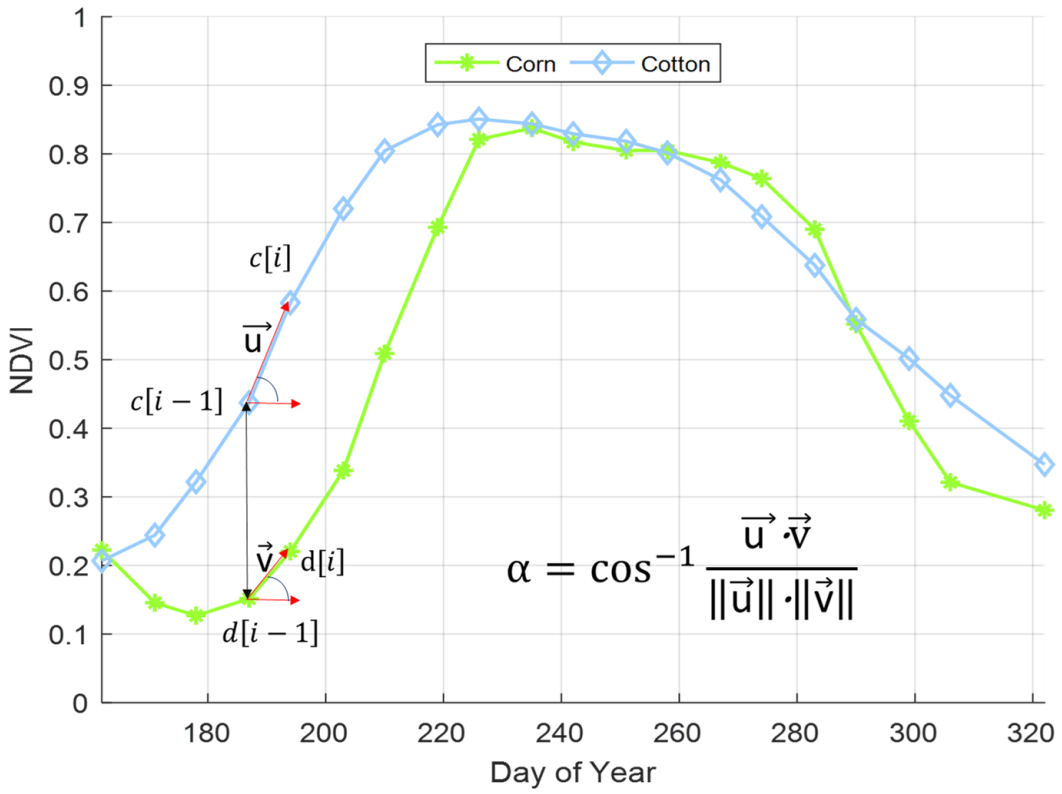

Figure 41: Angular distance metric between phenology of two crops at an observation date

The first step in VDTW algorithm is constructing n-by-m distance matrix Ψ whose elements $\psi_{i,j}$ is computed as the angle α between $\vec{u}_i \in \cup \forall\, i = 2, \dots, n$ and $\vec{v}_i \in \cup \forall\, j = 2, \dots, m$.

$\psi_{i,j}$ is computed as follow:

$$\psi_{i-1,j-1} = cos^{-1} \frac{\vec{u}_i \cdot \vec{v}_j}{\|\vec{u}_i\| \cdot \|\vec{v}_j\|} \tag{12}$$

The accumulated distance matrix is computed from Ψ by computing recursive sum of distances:

$$d_{i,j} = \psi_{i,j} + min\{d_{i-1,j-1}, d_{i-1,j}, d_{i,j-1}\} \tag{13}$$

Computation is subject to following boundary conditions:

$$d_{i,j} = \begin{cases} \psi_{i,j} & i = 1, j = 1 \\ \sum_{k=2}^{i} \psi_{k,j} & 2 < i \leq n-1\,, j = 1 \\ \sum_{k=2}^{j} \psi_{i,k} & i = 1, 2 < j \leq m-1 \end{cases} \tag{14}$$

The pseudocode of VDTW is given in Algorithm 1. VDTW algorithm computes a similarity score between two vectors $\overrightarrow{u}$ and $\overrightarrow{v}$. The same crop type is more likely to have low scores around 0, meaning high similarity.

Algorithm 1: VDTW Algorithm

```
Let u⃗ input vector with size n.
Let v⃗ input vector with size m.
Let D be an mxn matrix initialised to zero.
for i in 2 to m do
    for j in 2 to n do
      ψ(i-1, j-1) ← acos(  ( u(i)*v(i)+u(i-1)*v(i-1) ) / …
                        ( |u(i,i-1)|*|v(j, j-1)|)
D(1,1) ← ψ(1,1)
for i 2 to m do
    d(i, 1) ← ψ(i, 1) + d(i-1, 1)
for j 2 to n do
   d (1, j) ← ψ(1, j) + d(1, j-1)
for i in 2 to m do
   for j in 2 to n do
          d(i, j) ← ψ(i, j)  + min( d(i-1,j-1), d(i-1, j), d(i, j-1))
Score ←d(m,n)
```

DTW algorithm constructs a Euclidean cost matrix between data points of signals. The cost matrix of VDTW is based on vector distances. Another major difference in cost matrix computation is that two data points are needed to compute the angle between these points. For this reason, VDTW starts computing the cost matrix starting from the second data points of signals.

Distance and accumulated distance matrices of DTW and VDTW are compared. Euclidean distances of NDVI values are ranged between the minimum and maximum

values of samples, which are compared. The maximum value in the distance DTW matrix is 0.47 for the crops, which are shown in Figure 42. Regions, where the crops have close vegetation index values, are shown darker. The Accumulated distance matrix of VDTW is shown in Figure 43. On the other hand, the maximum normalized vector distance between two crops, which are shown in Figure 44, is 0.04 radians. The Accumulated distance map of VDTW is displayed in Figure 45.

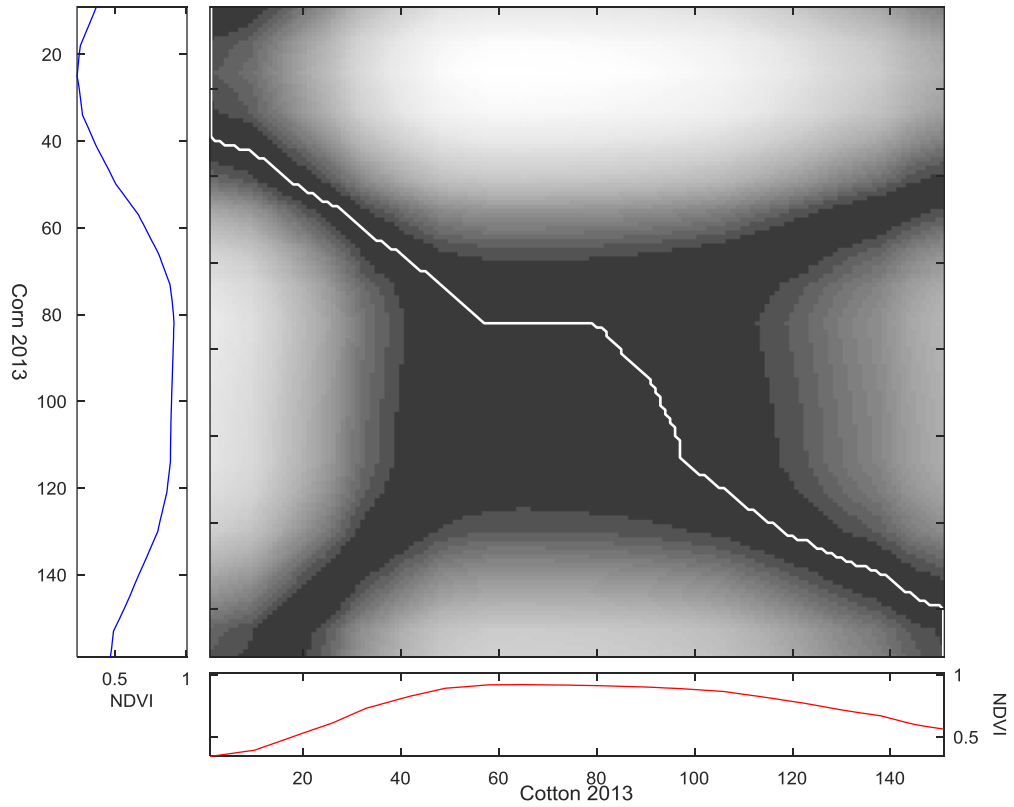

Figure 42: DTW Distance Matrix between corn and cotton in 2013 the Harran Plain.

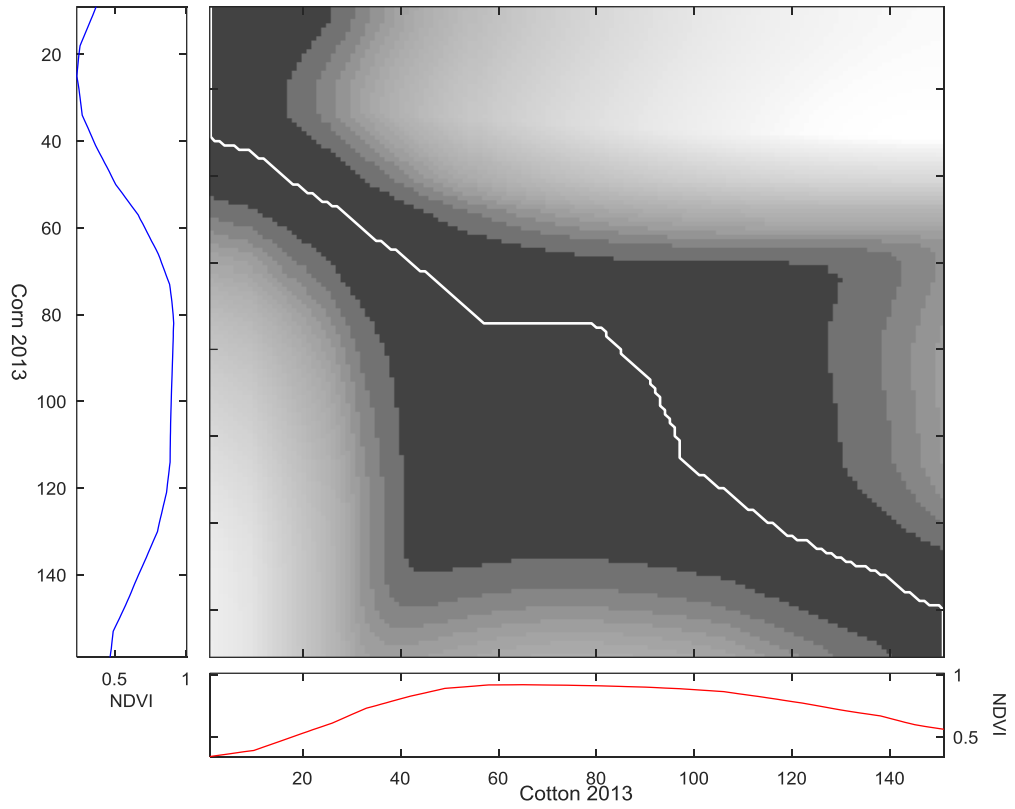

Figure 43: DTW Accumulated Distance Matrix between corn and cotton in 2013 the Harran Plain.

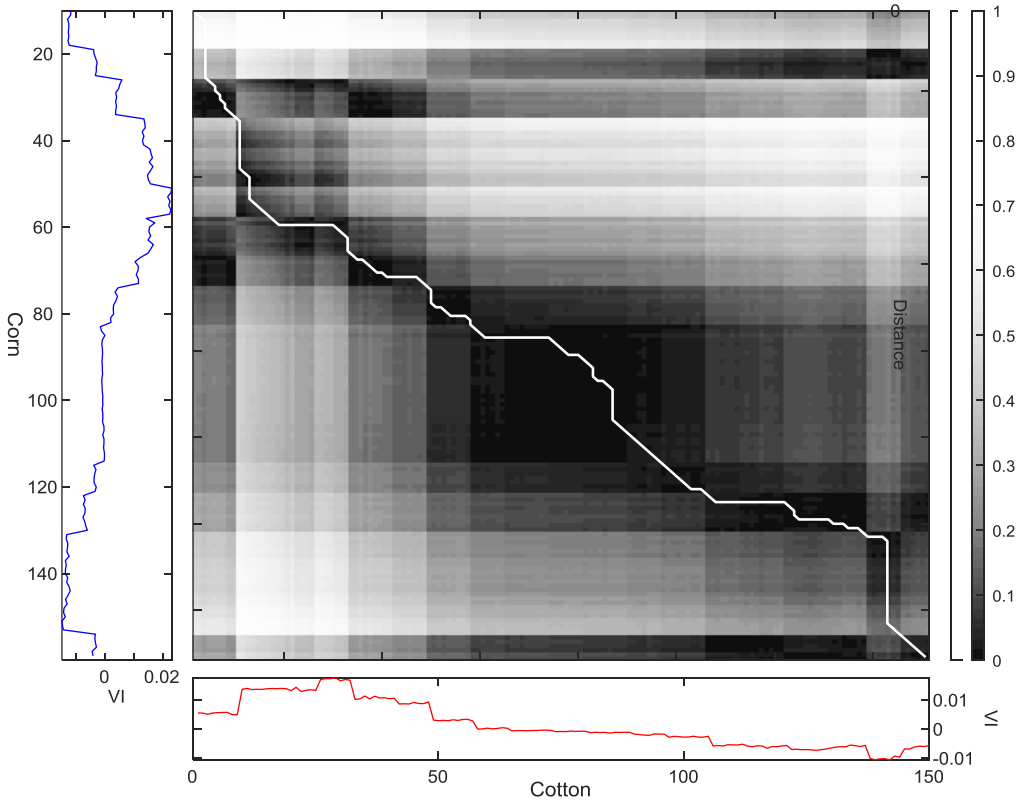

Figure 44: VDTW Distance Matrix between corn and cotton in 2013 the Harran Plain.

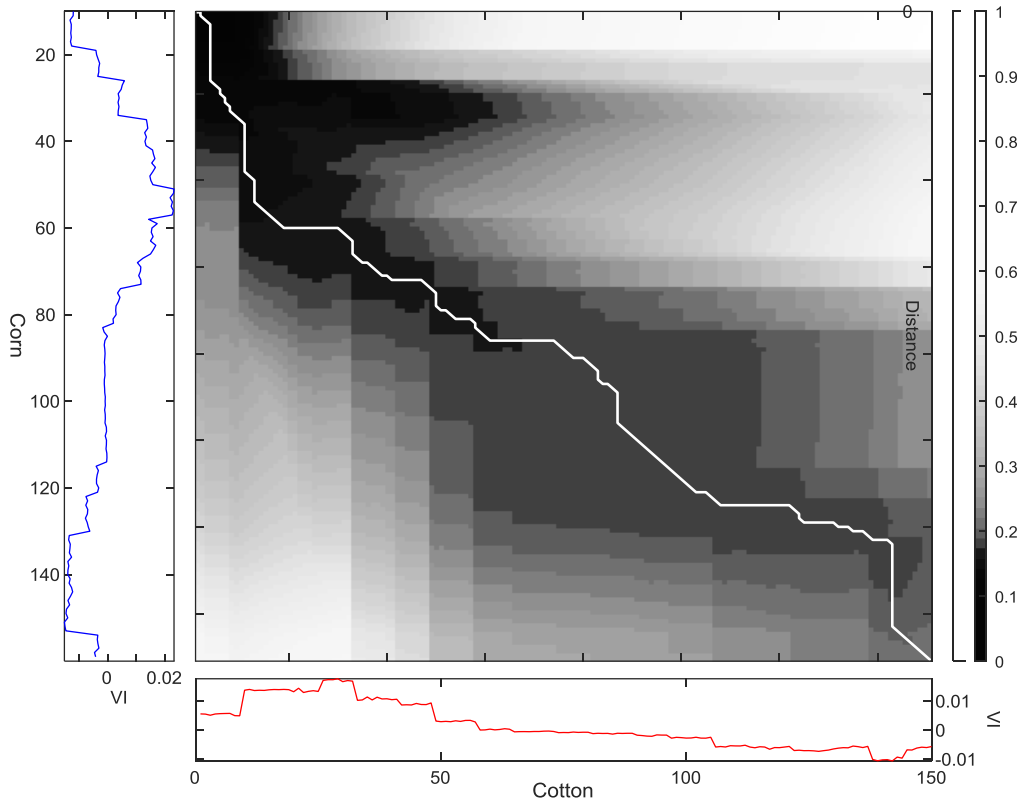

Figure 45: VDTW Accumulated Distance Matrix between corn and cotton in the year 2013 in the Harran Plain.

DTW and VDTW are compared with various settings: same year-different crop and same crop-different year. Warping paths of and warped crops phenologies are shown in Figure 46, Figure 47, and Figure 48. Top graphics show accumulated distance matrices. Bottom graphics show warped signals in Euclidean or vector distances.

Figure 46 presents warping paths of corn and cotton in the year 2013 in the Harran Plain. The warping paths of DTW and VDTW are similar. However, DTW's warping path is smoother compared to VDTW. Accumulated distance matrix between corn and cotton in 2013 is given in Table 9. VDTW determined the vector distance between corn and cotton in 2013 as 0.56 radians.

Figure 47 shows warping paths and warped phenologies of the corn crop in 2013 and 2014 years. VDTW is able to warp the same crop better than different crops, as shown in Figure 46. Accumulated distance matrix between corn in 2013 and 2014 is given in Table 10. VDTW determined the vector distance between corn in 2013 and 2014 as 0.45 radians.

DTW is more robust in warping two signals than VDTW. For this reason, DTW is able to produce lower scores compared to the maximum value of the distance matrix. On the other hand, the accumulated path score of VDTW is greater than the maximum vector distance. VDTW can produce more discriminative scores.

Another same year crop warping performance is shown in Figure 48 for cotton in 2013 and 2014 years. Accumulated distance matrix between corn in 2013 and 2014 is given

in Table 11. VDTW determined the vector distance between cotton in 2013 and 2014 as 0.45 radians.

The vector distance between corn and cotton in the same year is higher than the same crop in the cross-years. Moreover, the corn crop's scores were higher compared to cotton in the cross-years. This is due to the corn's variation between years as it is grown after the winter wheat harvest. On the other hand, the growth of the corn is more stable between years.

VDTW can achieve higher warping performance compared to different crops in the same year, which are shown in Figure 46 and Figure 48 in the year 2013 and 2014, respectively.

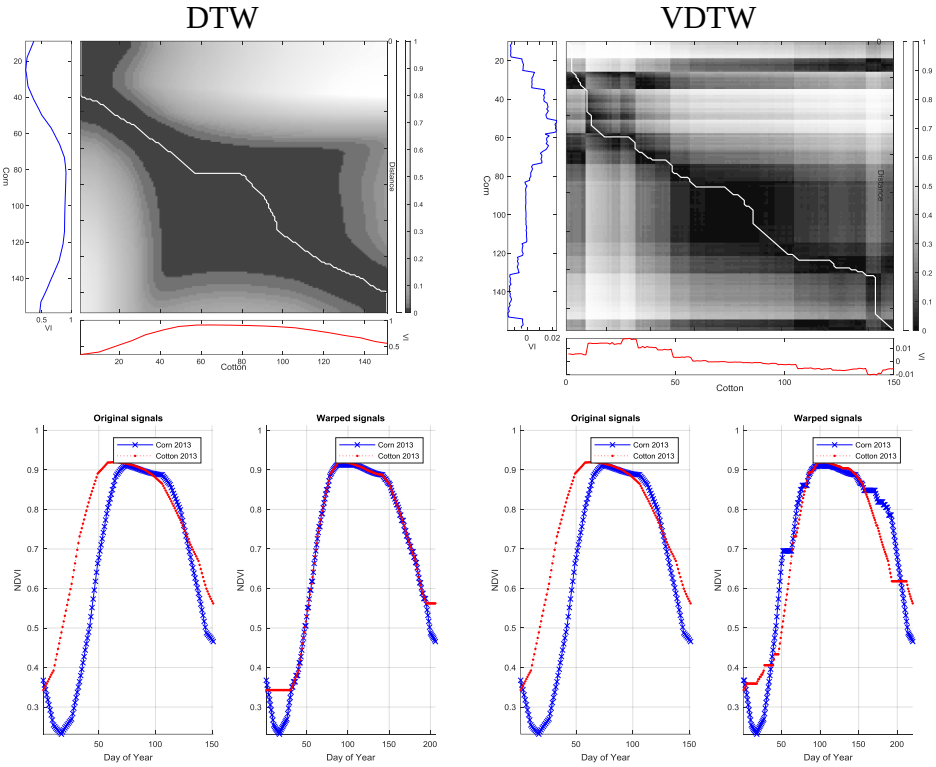

Figure 46: Corn2013-Cotton2013 DTW and VDTW comparison. Top graphics show accumulated distance matrices, and bottom graphics show warped signals.

Table 9: Accumulated distance matrix of VDTW for corn and cotton in 2013

0.00	0.00	0.00	0.00	0.00	0.00	0.00	0.00	0.00	0.00	0.00	0.00	0.00	0.00	0.00	0.00
0.00	0.28	0.50	0.71	0.87	0.99	1.08	1.16	1.24	1.31	1.38	1.44	1.48	1.51	1.54	1.56
0.00	0.37	0.38	0.39	0.39	0.41	0.48	0.55	0.63	0.71	0.80	0.90	1.01	1.13	1.25	1.32
0.00	0.39	0.43	0.44	0.46	0.48	0.54	0.61	0.68	0.76	0.84	0.93	1.03	1.15	1.27	1.40
0.00	0.41	0.41	0.45	0.52	0.60	0.66	0.73	0.80	0.87	0.95	1.05	1.15	1.26	1.39	1.52
0.00	0.43	0.44	0.45	0.49	0.55	0.65	0.75	0.86	0.98	1.06	1.15	1.26	1.37	1.49	1.62
0.00	0.51	0.47	0.47	0.46	0.48	0.53	0.59	0.66	0.73	0.80	0.89	0.99	1.10	1.22	1.34
0.00	0.65	0.55	0.54	0.48	0.47	0.47	0.49	0.51	0.53	0.56	0.60	0.65	0.71	0.78	0.86
0.00	0.76	0.67	0.65	0.55	0.48	0.47	0.47	0.48	0.48	0.48	0.50	0.53	0.57	0.62	0.67
0.00	0.83	0.80	0.76	0.62	0.51	0.48	0.48	0.48	0.48	0.48	0.50	0.53	0.57	0.62	0.67
0.00	0.90	0.93	0.88	0.69	0.53	0.48	0.48	0.48	0.48	0.48	0.50	0.53	0.57	0.62	0.68
0.00	0.97	1.06	1.00	0.76	0.55	0.50	0.49	0.49	0.48	0.49	0.49	0.51	0.53	0.56	0.60
0.00	1.07	1.16	1.15	0.87	0.61	0.53	0.52	0.52	0.51	0.51	0.49	0.50	0.50	0.51	0.53
0.00	1.22	1.31	1.34	1.02	0.71	0.62	0.60	0.60	0.59	0.58	0.55	0.54	0.54	0.51	0.53
0.00	1.40	1.48	1.54	1.19	0.84	0.73	0.71	0.70	0.69	0.67	0.62	0.61	0.60	0.54	0.55
0.00	1.54	1.62	1.68	1.33	0.93	0.81	0.79	0.78	0.76	0.74	0.67	0.65	0.64	0.59	0.56

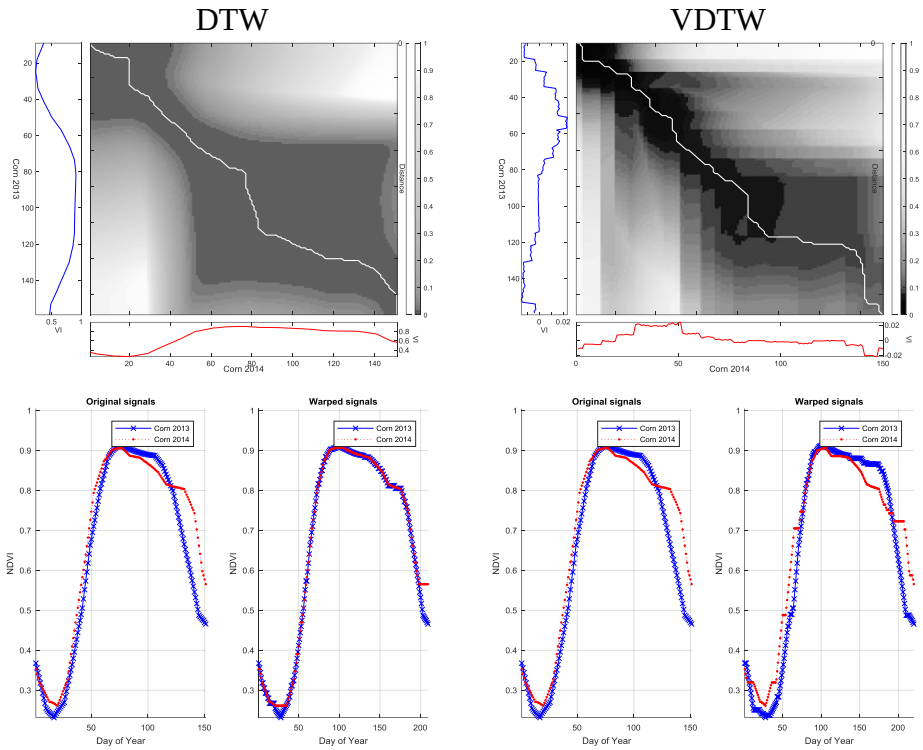

Figure 47: Corn in 2013-Corn in 2014 DTW and VDTW comparison.

Table 10: Accumulated distance matrix of VDTW for corn in 2013 and 2014

0.00	0.00	0.00	0.00	0.00	0.00	0.00	0.00	0.00	0.00	0.00	0.00	0.00	0.00
0.00	0.04	0.10	0.34	0.64	0.87	1.01	1.11	1.19	1.26	1.33	1.39	1.46	1.53
0.00	0.12	0.08	0.12	0.21	0.24	0.26	0.31	0.39	0.47	0.56	0.65	0.74	0.82
0.00	0.35	0.16	0.14	0.13	0.18	0.32	0.38	0.46	0.53	0.61	0.69	0.78	0.85
0.00	0.61	0.21	0.24	0.13	0.13	0.23	0.37	0.53	0.65	0.73	0.81	0.90	0.97
0.00	0.87	0.26	0.29	0.15	0.16	0.21	0.30	0.41	0.52	0.64	0.76	0.88	0.99
0.00	1.04	0.30	0.31	0.23	0.20	0.19	0.24	0.31	0.38	0.45	0.53	0.61	0.67
0.00	1.16	0.39	0.38	0.36	0.30	0.21	0.20	0.22	0.24	0.27	0.30	0.33	0.35
0.00	1.24	0.52	0.49	0.52	0.44	0.25	0.20	0.20	0.21	0.21	0.22	0.23	0.23
0.00	1.32	0.66	0.61	0.70	0.59	0.31	0.21	0.21	0.21	0.21	0.22	0.23	0.23
0.00	1.39	0.78	0.72	0.82	0.73	0.36	0.22	0.22	0.21	0.22	0.23	0.23	0.23
0.00	1.46	0.77	0.84	0.94	0.88	0.42	0.24	0.21	0.22	0.22	0.22	0.23	0.24
0.00	1.50	0.77	0.97	1.09	1.06	0.50	0.28	0.23	0.25	0.24	0.23	0.24	0.26
0.00	1.50	0.82	1.02	1.27	1.28	0.64	0.37	0.30	0.31	0.31	0.29	0.30	0.33
0.00	1.51	0.89	1.09	1.34	1.53	0.79	0.48	0.39	0.40	0.40	0.37	0.38	0.40
0.00	1.57	0.94	1.13	1.37	1.56	0.92	0.57	0.46	0.46	0.47	0.42	0.43	0.45

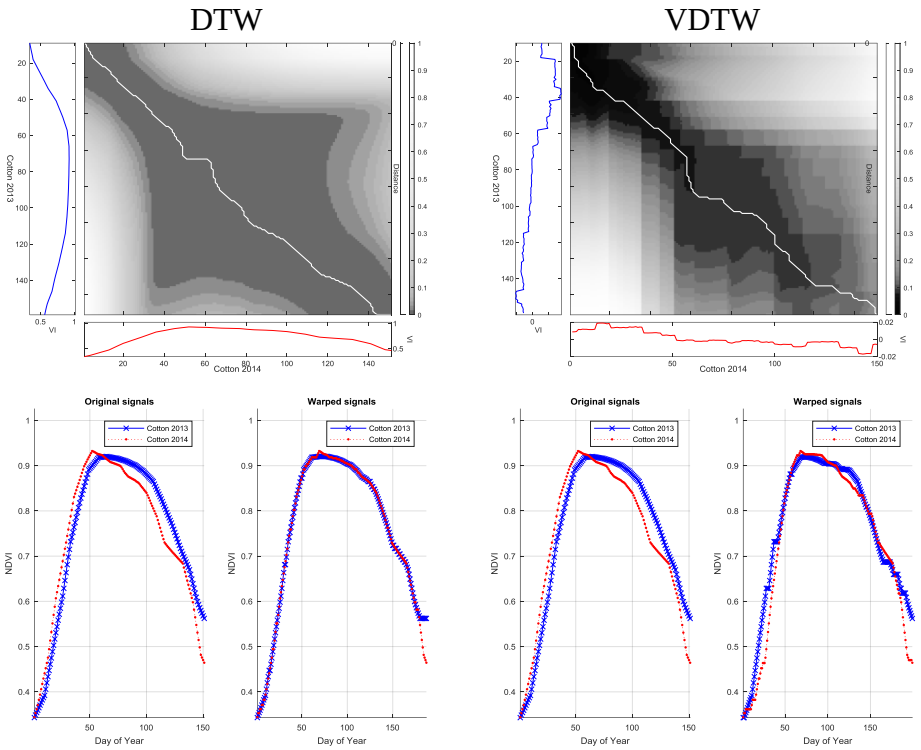

Figure 48: DTW and VDTW comparison of Cotton in 2013-Cotton in 2014.

Table 11: Accumulated distance matrix of VDTW for cotton in 2013 and 2014

0.00	0.00	0.00	0.00	0.00	0.00	0.00	0.00	0.00	0.00	0.00	0.00	0.00	0.00
0.00	0.06	0.09	0.16	0.18	0.21	0.28	0.35	0.43	0.50	0.58	0.68	0.79	0.87
0.00	0.05	0.08	0.10	0.16	0.25	0.36	0.43	0.51	0.58	0.66	0.77	0.87	0.95
0.00	0.06	0.08	0.10	0.15	0.22	0.34	0.45	0.57	0.64	0.73	0.83	0.93	1.01
0.00	0.11	0.12	0.11	0.12	0.15	0.22	0.29	0.37	0.44	0.53	0.63	0.73	0.82
0.00	0.19	0.18	0.16	0.12	0.12	0.14	0.17	0.20	0.23	0.26	0.32	0.37	0.41
0.00	0.31	0.28	0.24	0.15	0.13	0.13	0.14	0.15	0.17	0.18	0.22	0.26	0.28
0.00	0.43	0.39	0.33	0.20	0.16	0.13	0.14	0.15	0.16	0.17	0.21	0.24	0.26
0.00	0.57	0.50	0.43	0.25	0.19	0.13	0.14	0.15	0.15	0.17	0.20	0.23	0.25
0.00	0.70	0.62	0.53	0.30	0.22	0.13	0.14	0.14	0.14	0.15	0.18	0.21	0.22
0.00	0.84	0.74	0.64	0.35	0.25	0.14	0.14	0.14	0.14	0.15	0.17	0.19	0.20
0.00	0.99	0.87	0.76	0.42	0.30	0.16	0.15	0.15	0.15	0.15	0.15	0.17	0.18
0.00	1.15	1.02	0.89	0.50	0.36	0.18	0.17	0.16	0.17	0.15	0.15	0.17	0.18
0.00	1.32	1.17	1.03	0.59	0.43	0.22	0.21	0.18	0.19	0.16	0.15	0.17	0.19
0.00	1.50	1.33	1.18	0.69	0.51	0.27	0.25	0.21	0.22	0.18	0.17	0.18	0.20
0.00	1.69	1.51	1.33	0.80	0.60	0.32	0.30	0.25	0.26	0.22	0.18	0.19	0.22

4.4. Multiyear Crop Mapping Strategy

A summary of the algorithm steps is presented in Figure 50. Atmospheric or illumination effects may degrade the performance of times series classification methods. Data smoothing methods have been used to reduce these effects (Arvor et al., 2008), and in this study, time-series data is smoothed by the Savitzky-Golay (SG) filtering method(Kim et al., 2014).

Landsat 8 cloud and shadow masks are produced by the Fmask algorithm (Zhu & Woodcock, 2012). Cloud information cloning was applied, so that cloudy samples were linearly interpolated with the Inverse Distance Weighting (IDW) method by using the nearest two cloud-free images (Kalkan & Maktav, 2018). Even though the Fmask algorithm could detect clouds successfully, it may not detect cloud shadows as effectively (Figure 49). However, it is found that the Fmask algorithm and SG smoothing, followed by computation of the median of time-series field phenology was adequate for successful classification. Kansas dataset uses the Harmonized Landsat 8 and Sentinel-2 satellite imagery (HLS). However, the Fmask algorithm (Fmask v3), which was used in HLS data, is not optimal with Sentinel-2 data. This resulted in missed shadows and clouds in some cloudy Sentinel-2 scenes. The Fmask. Moreover, Fmask version 4was used, which improved shadow and cloud detection with Sentinel-2 data. The double sigmoid was used fitting instead of SG of crop phenologies to remove the remaining artifacts.

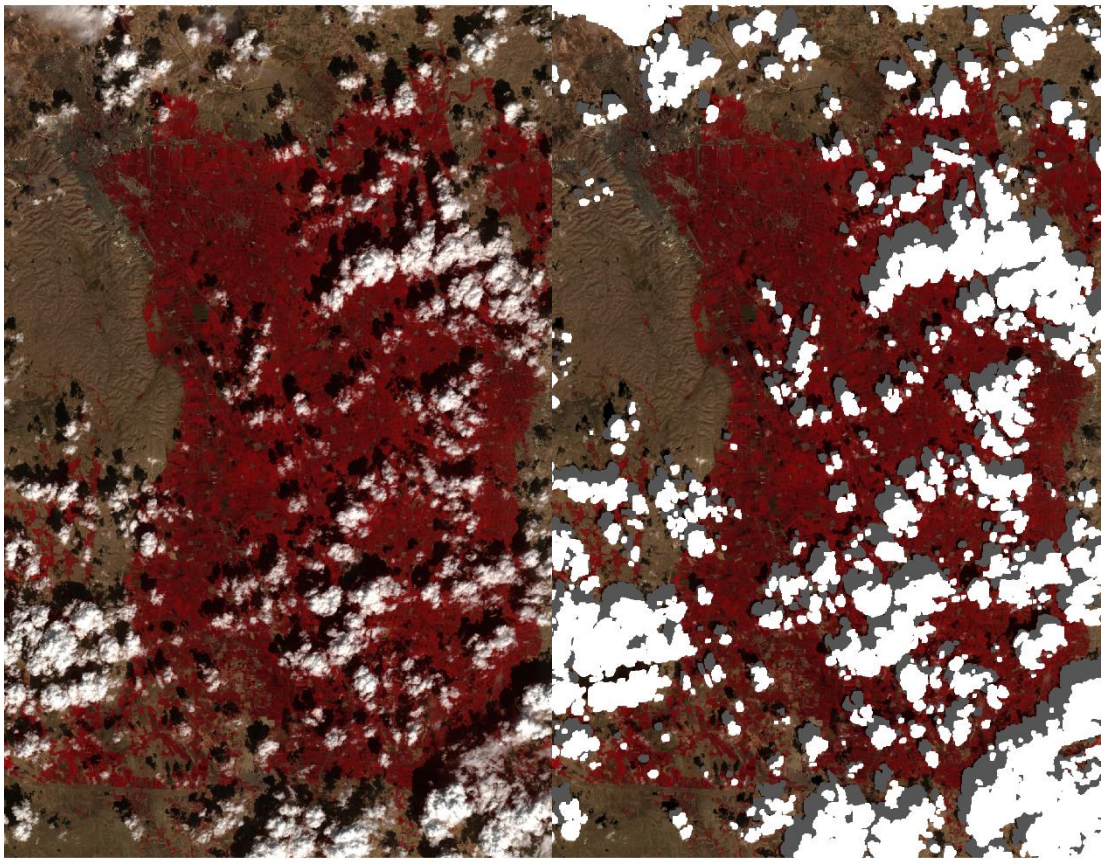

Figure 49: Clouds and their shadows detected by the FMask algorithm.

Data is linearly interpolated between $[t_l, t_u]$ to enable cross-year classification where t_l and t_u be the lower and upper limits of the time window. Time series classification is used to classify with same year or cross year classification. Optionally, data is classified with the partial time series approach. Finally, a cropland layer is produced showing the classification results.

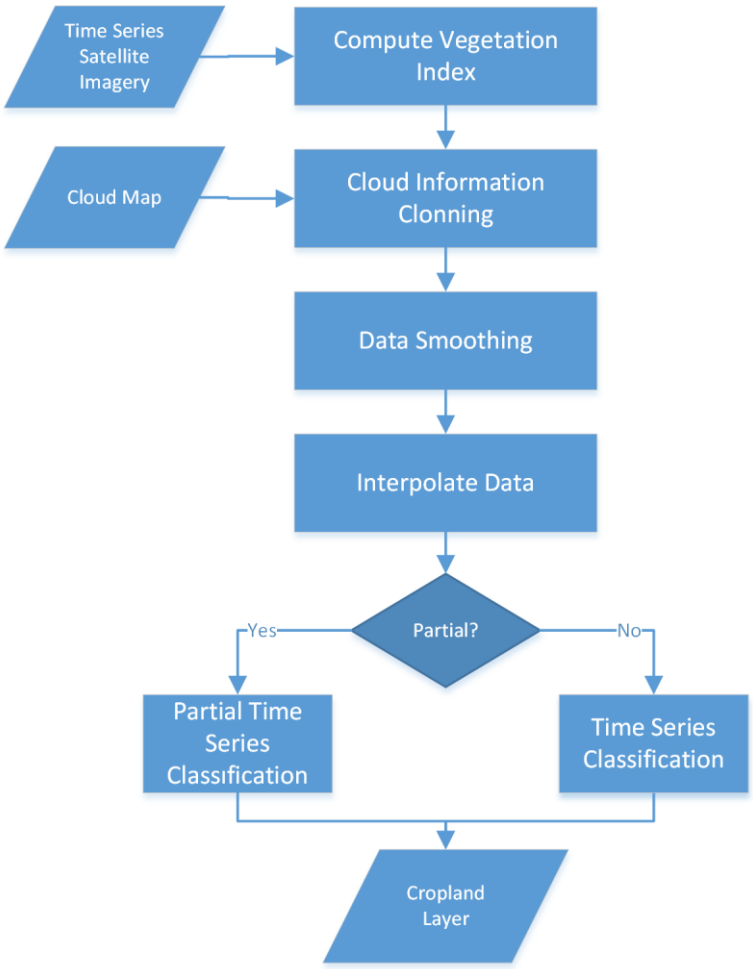

Figure 50: Multi-year time-series classification algorithm steps.

4.5. Partial Time Series Classification

A new method is presented in the previous section. In this study, a partial time series approach is proposed, which achieves high classification accuracies with fewer data using distinct temporal time periods in phenological properties of crops.

For example, corn and cotton in the Harran Plain are sown at specific dates. However, they both start to have the same growth phenological properties starting from mid-August, after which their growths are nearly the same. Figure 51 shows corn and cotton's discriminative regions in their early growth until mid-August. The proposed partial time-series method exploits this phenologically invariant region for improved cross-year crop classification.

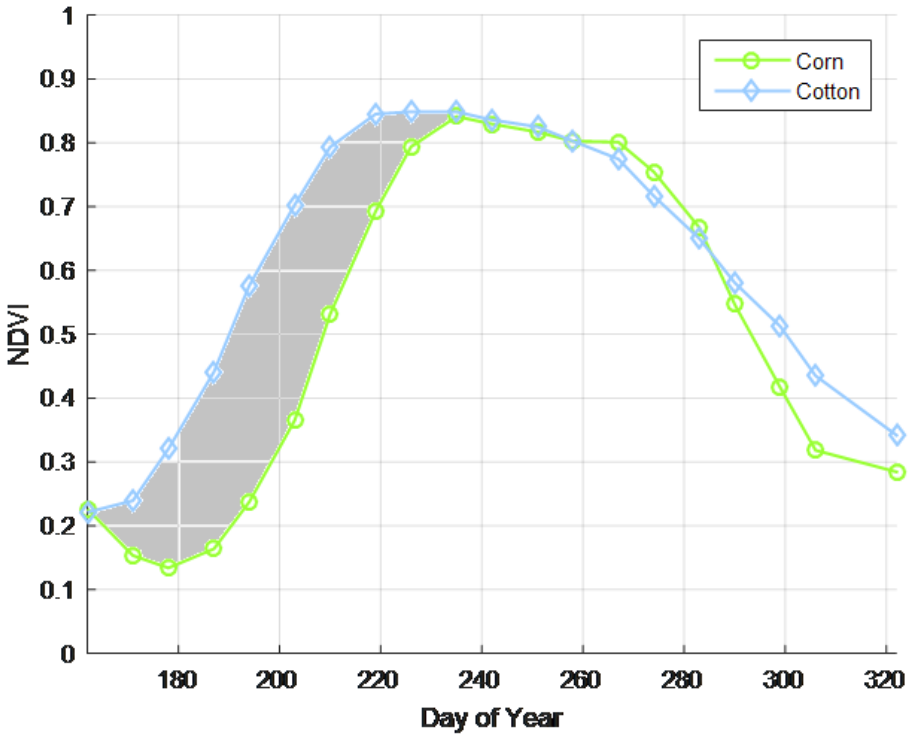

Figure 51: Median phenologies of corn and cotton in 2013.

The partial time series algorithm has three major steps. The algorithm finds the optimal classification window around the pivot day.

Algorithm steps:

First, the pivot day where the difference between the NDVI of crops is maximum is determined (Figure 52 (a)). The median values of all samples from each crop are used in this computation. The pivot day is determined as:

$$J^* = arg \max_{t_l<J<t_u} abs(NDVI_{C_1}(J) - NDVI_{C_2}(J)) \qquad (15)$$

where J^* denotes pivot day, $c_1$and $c_1$are two crops, t_l denotes the minimum common day and, t_u denote the maximum common day shared by time series data of all years.

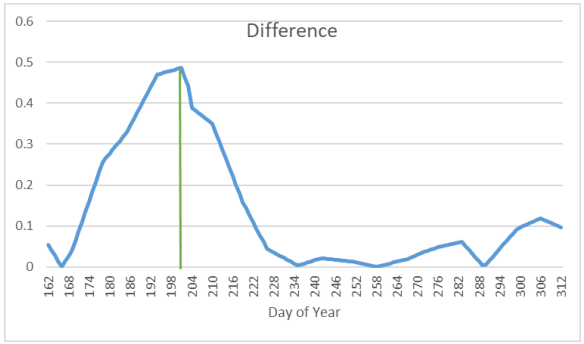

(a)

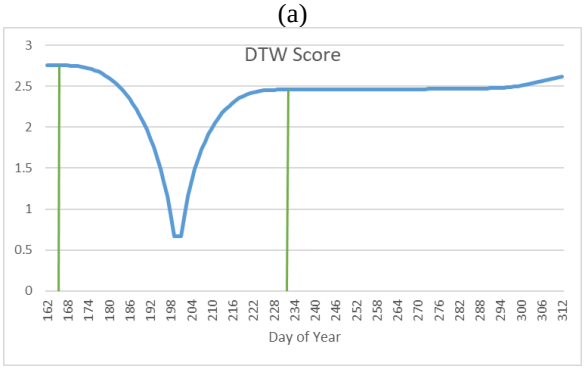

(b)

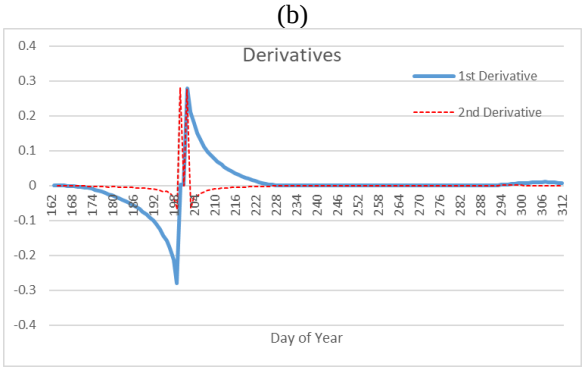

(c)

Figure 52: (a) Maximum difference of VI values between corn and cotton, (b) DTW scores between corn and cotton centered on the pivot day expanding on both sides, (c) First and second derivatives of DTW scores.

Centering the pivot day, DTW scores of vectors extending in both directions are computed (Figure 52(b)). Lower DTW scores represent higher similarity. The increase in DTW scores is steady after certain periods, which coincides with discriminative regions of corn and cotton.

$$Score(J) = DTW(\,NDVI_1([J^*, J]), NDVI_2([J^*, J]), \qquad (16)$$

where $t_l < J < t_u$.

The algorithm finds the first days from the pivot by extending to initial and final dates until first and second derivatives are zero (Figure 52(c)). First and second derivatives

indicate that DTW scores are steady after these days as a result of determining the boundaries of the optimal time window.

$$find\ score(J)' = 0\ AND\ score(J)'' = 0 \quad (17)$$

The optimal time window *[o1, o2]* for classification of corn and cotton are computed as day 170 and day 227, corresponding to mid-June and mid-August.

In the case of three or more crops, each crop is compared to others and a minimum length time window is selected against other crops.

CHAPTER 5

RESULTS & DISCUSSIONS

5.1. Data Representation

The median of each field is used as a sample in the tests. As a result of median field sampling, each field is represented by a single sample, thus decreasing redundancy and equalize the distribution of samples regardless of field sizes. Another advantage is that partly cloudy fields are also represented by their spectral values. The final advantage is the decrease of computation time in tests.

5.2. Performance Metrics

Performance evaluations in this study are based on confusion matrix analysis. The confusion matrix is used to evaluate the performance of a classifier with labeled samples as input and classifier results as outputs.

A sample confusion matrix is presented in Table 12. The sample data contains 17 corn and 13 cotton samples. Assume that a classifier decided 15 of these samples as corn and rest as cotton.

Table 12: Sample confusion matrix.

	Corn	Cotton
Corn	10	7
Cotton	5	8

Overall Accuracy (OA): Overall accuracy is simply the ratio of the sum of diagonal entries in confusion matrix to all samples in the data. In this case, overall accuracy is 18/30 = 0.6. Overall accuracy is itself is necessary as a performance metric but often other statistics such as producer's accuracy, user's accuracy, and Cohen's kappa.

Error of omission: ratio of omitted samples, which are misclassified:

Corn: 7/(5+10) = 7/17.

Cotton: 5/(5+8) = 5/13.

Error of commission: ratio of falsely included samples:

Corn: 5/(5+10) = 5/15 = 33.3%.

Cotton: 7/(7+8) = 7/15 = 38.4%.

Producer's Accuracy (PA): Producer's accuracy is the measurement of how accurate the classifier detects each crop, i.e., how many of the samples are present. The producer's accuracy presents the accuracy of each crop. The producer's accuracy is the complement of omission error: Producer's accuracy = 1 – omission error.

Corn: 10/(10+7) = 10/17 = 58.82%

Cotton: 8/(5+8) = 8/13 = 61.53%.

User's Accuracy (UA): It is determined as the ratio of correctly found crops over the sum of samples which are labeled the same as the crop. User's accuracy is the complement of commission error: Producer's accuracy = 1 – commission error.

Corn: 10/(10+5) = 10/15 = 66.6%.

Cotton: 8/(7+8) = 8/15 = 53.3%.

Cohen's Kappa: Kappa analysis is a statistical method if the classifiers' agreement is by chance. Kappa is measured as the difference between agreement by classifiers and confusion matrix(R. G. Congalton & Green, 2008). Cohen's Kappa was introduced in 1960. It had been commonly used in sociology and psychology fields. It was first used in remote sensing in 1981(R. G. Congalton & Green, 2008).

$$\kappa = \frac{ObservedAccuracy - ExpectedAccuracy}{1 - ExpectedAccuracy} \tag{18}$$

$$ExpectedAccuracy = \frac{ActualFalse \times PredictedFalse + ActualTrue \times PredictedTrue}{Total \times Total} \tag{19}$$

For this sample case *Kappa* values is calculated as follow =

Expected Accuracy: (7×5 + 8×10) / (30×30) = 115/900 = 0.127

κ = (0.6 – 0.127)/(1-0.127) = 0.5418

5.3. Optimal Vegetation Index Selection

The most commonly used spectral indices were compared with the VDTW classifier. NDVI is the most well-known and deployed phenological feature. Other indices such as EVI (Maus et al., 2016). Tests were performed with 50 samples. The stratified random selection was used, and tests were performed 100 times.

NDVI, SAVI, and MSAVI all performed highest in same year crop classification. EVI performed closely. ENDVI and WDRVI performances were considerably lower. Cross-year performances of NDVI and SAVI were similarly higher than other vegetation indices except for MSAVI. MSAVI contributed to a 0.6% increase in the cross-year accuracy. Detailed performance analysis is presented in Table 13.

Table 13: Overall accuracy comparisons of notable vegetation indices.

Vegetation Index	Same Year %	Cross Year
NDVI	99.6	98.0
MSAVI	99.6	98.6
EVI	99.4	96.9
SAVI	99.6	98.0
ENDVI	98.8	93.6
OSAVI	99.6	92.2
WDRVI	97.3	92.1

Soil-vegetation indices such as SAVI, OSAVI, and MSAVI. Soil line values are selected in SAVI and OSAVI by experimentally or experience. On the other, MSAVI incorporates the computation of soil line into its equation (5).

Phenologies of corn and cotton of the Harran Plain between 2013 and 2015 are presented in Figure 53. These phenologies were computed by field medians of all samples for each year. The Harran plain is overlapped by Landsat 8 orbital paths 172 and 173 thus have positive and negative observation angles. These various angles and different observation conditions, such as current weather and sun position, lead to different reflectance values.

Huete et al. compared NDVI and SAVI at various observation angles(A. R. Huete, Hua, Qi, Chehbouni, & van Leeuwen, 1992). In their study, they found out the measurement of NDVI was asymmetric about nadir viewing angles while SAVI was symmetric. On the other hand, MSAVI computes the soil line automatically makes it more resistant to canopy cover estimation.

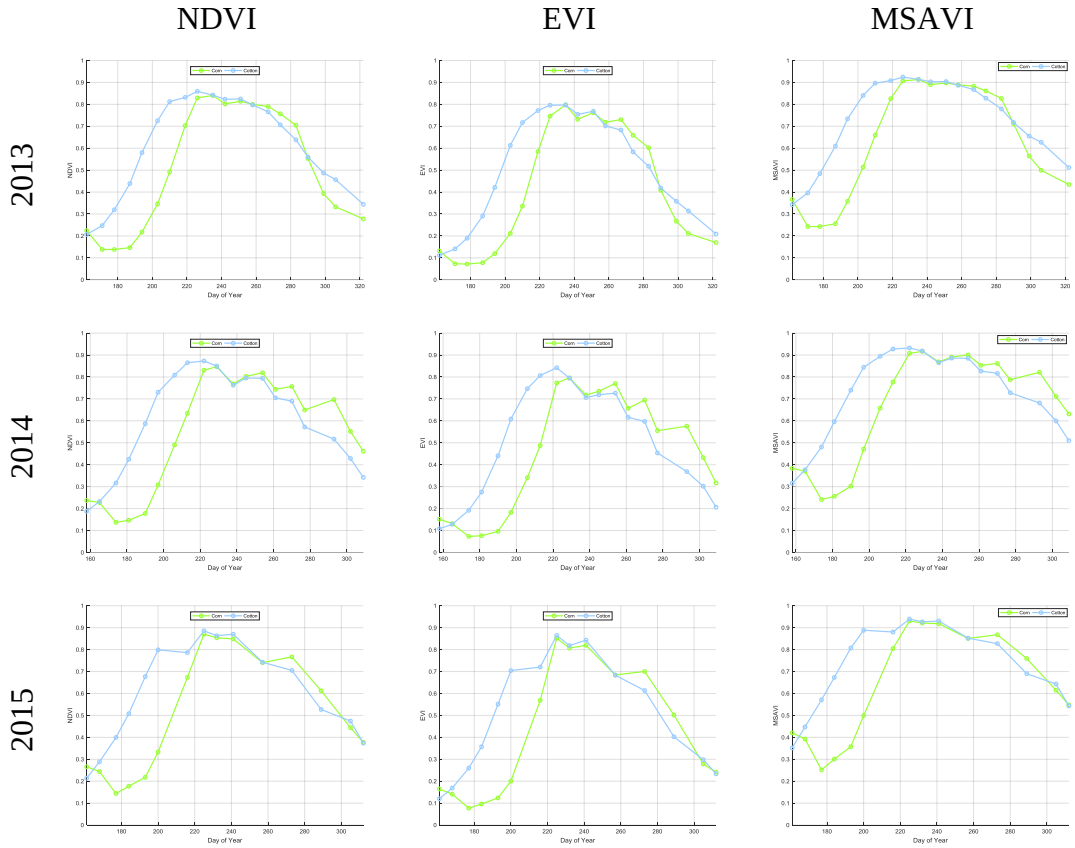

Figure 53: Depiction of corn and cotton phenologies by NDVI, EVI, and MSAVI vegetation indices.

Furthermore, the most common vegetation indices were compared, namely NDVI and EVI with MSAVI in different classifiers. The Kansas dataset contains both Landsat 8 and Sentinel-2 imagery. Even though Sentinel-2 imagery is BRDF matched to Landsat 8, this dataset is more suitable for comparison, especially in cross-year tests. Moreover, each year contains imbalanced combinations of these satellite imagery. The use of MSAVI improved the overall cross-year classification accuracies by 2% compared to NDVI (Table 13). The usage of MSAVI and EVI resulted in the similar the same-year accuracies while MSAVI's the cross-year overall accuracies are higher than EVI.

Table 14: Comparison of MSAVI, NDVI, and EVI vegetation indices in same-year and cross-year tests with the Kansas dataset.

	SY	CY
MSAVI	98.74	**87.31**
NDVI	98.56	85.29
EVI	98.75	85.97

5.4. Analysis of Preprocessing Steps on Classification Performance

In this section, data preprocessing steps are compared. The same-year and the cross-year tests were performed to demonstrate contributions of individual preprocessing steps. The Savitzky-Golay(SG) data smoothing method was selected as the default method.

Time-series satellite data were preprocessed by data smoothing and cloud information cloning. Furthermore, missed cloud detection of Sentinel-2 data reduced the cross-tests. Double Sigmoid curve fitting was employed to correct missing cloud detection where SG filtering could not correct those gaps efficiently.

Figure 54 shows a median crop sample from the Kansas dataset with two cloudy acquisitions. The Fmask algorithm was able to detect only one of them while the first cloudy sample was partially smoothed by the SG filter. Double Sigmoid curve fitting did generate a smoother phenological signature. A missing crop map detection at the end of the crop phenology is displayed in Figure 55. SG filter modified the phenology causing incorrect data.

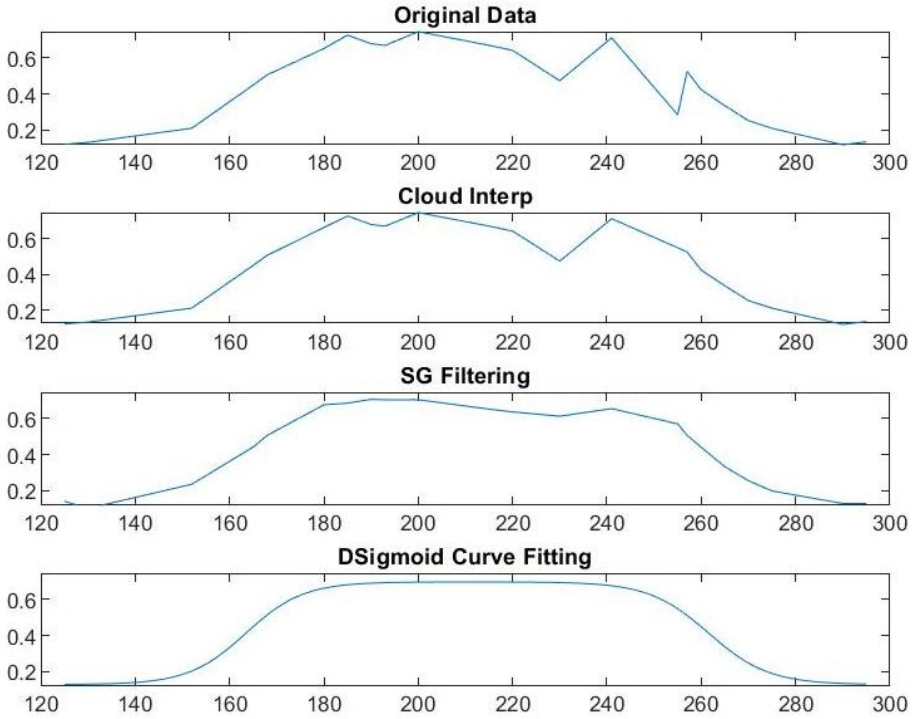

Figure 54: A median crop sample from the Kansas Dataset with two cloudy acquisitions.

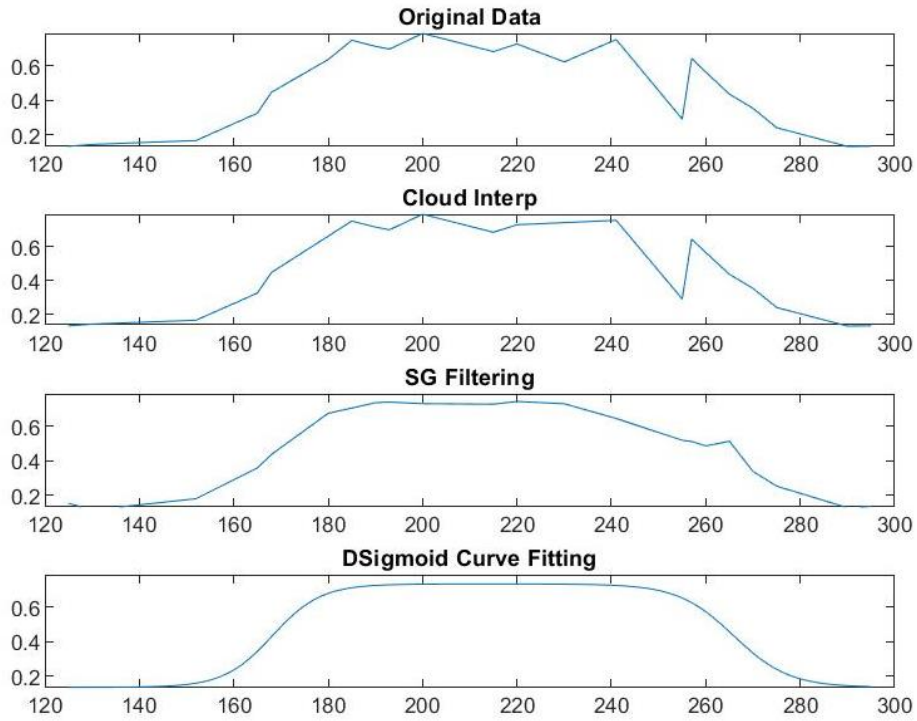

Figure 55: A median crop sample from The Kansas dataset with single cloudy acquisitions

The same-year and cross-year accuracies are described in Table 15. Application of preprocessing has a more significant effect in the same-year than cross-year. The same-year accuracy was increased by 1.24%. The cross-year accuracy was increased by 14.76%. In addition, cloud cover, variations caused by Landsat 8 and Sentinel-2 degrades cross-year accuracies as different years have an unmatched composition of these satellites data as described in 3.2.2.

Table 15: Preprocessing step performance analyses.

	Same-year	Cross-year
No Preprocessing	97.44	72.82
SG	98.19	75.09
SG-Cloud Cloning	98.57	78.73
Dsigmoid-Cloud Cloning	98.64	87.58

5.5. VDTW Search Window Selection

DTW and VDTW methods could be set to work within a specific time window. The length of the DTW search window should consider the possible phenological variation between years.

Tests were run to determine the optimal time window in the same-year and the cross-year settings. Optimal Time Window of the VDTW method is determined experimentally. Computation cost is lowered by limiting the time-window. Search window limitation by window size T is shown in Figure 56.

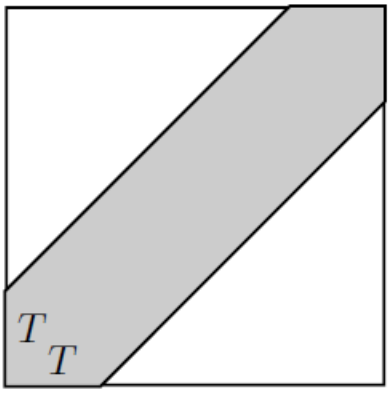

Figure 56: Visualization of DTW warping window limits.

Optimal window sizes were determined experimentally for the datasets. Tests were performed by using median phenology. The same year and cross-year accuracies were computed to determine an optimal time window for different datasets.

Important phenological transition dates were extracted by fitting double sigmoid functions to the median phenology of crops, as described in 0.

Phenologies of corn and cotton in the Harran Plain are similar. They overlap starting around day 200. The maximum difference of corn and cotton phenologies to reach maturity is about twenty days.

Tests showed that same year accuracies reached top accuracy at seven days difference and it is the point where cross-year accuracies start to decrease for VDTW (Figure 57). In a similar trend, the same-year and cross-year overall accuracies of DTW starts to decrease by window size of seven. The seven-day window is due to the phenological differences of the corn and cotton in the Harran Plain.

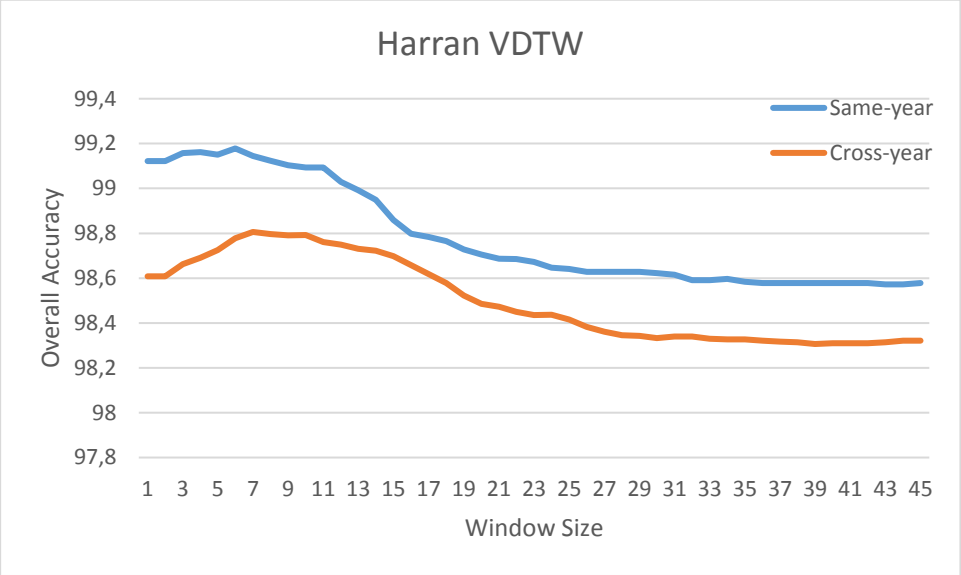

Figure 57: Optimal VDTW window size search for the Harran dataset.

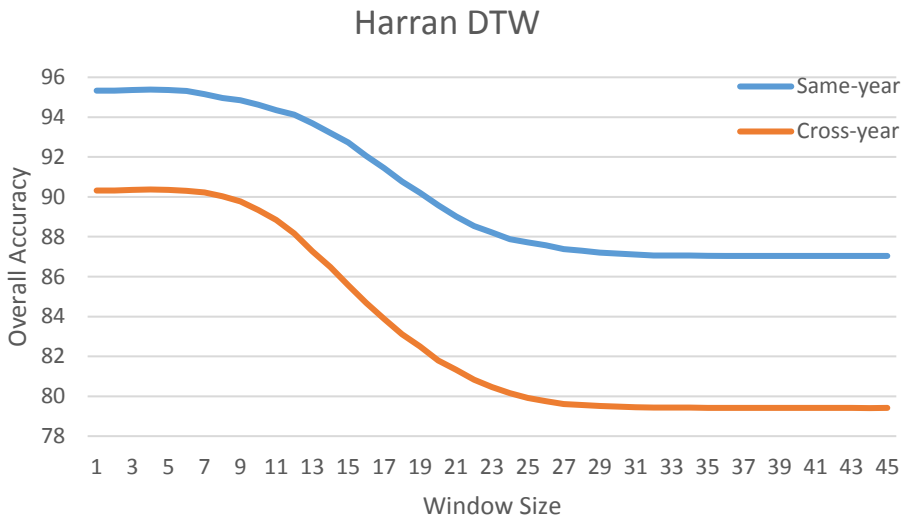

Figure 58: Optimal DTW window size search for the Harran dataset.

An increase in NDVI [D1, D2] and decrease in NDVI [D3, D3] is provided in Table 16 for the crops in the Harran Plain. Same year minimum differences 11 days at D2 (end of NDVI increase) in 2013, 12 days at D2 and D4 in 2014, 11 days at D4 in 2015. Cross year differences have similar values such as difference at D3 between Cotton in 2013 and corn in 2015 is 12 days.

Table 16: Phenological transition dates of corn and cotton in the Harran Plain.

		Di	Dd	D1	D2	D3	D4
2013	Corn	213	289	203	223	270	308
	Cotton	196	286	179	212	252	323
2014	Corn	209	298	200	218	270	327
	Cotton	191	278	175	206	243	315
2015	Corn	211	290	201	220	264	316
	Cotton	190	281	172	208	248	317

Bismil dataset contains three distinct crops. Both the same and cross-year classification accuracies reach the highest accuracies at 21 days differences for VDTW (Figure 59); then, it starts to decrease for the cross-year. Similarly, the DTW method obtains the highest overall accuracies starting from a window size of 21 days (Figure 60).

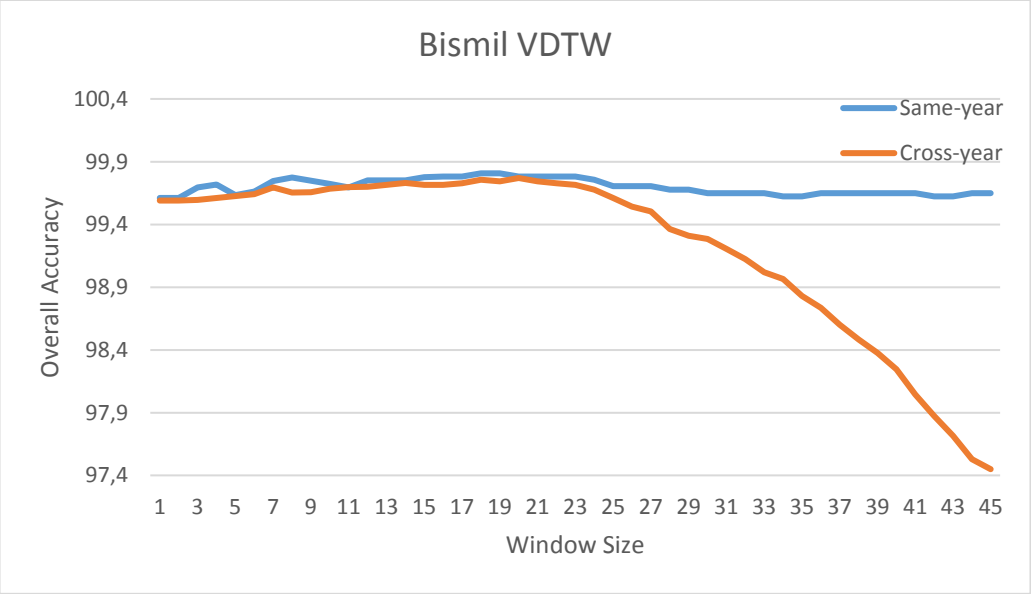

Figure 59: Optimal VDTW window size search for the Bismil dataset.

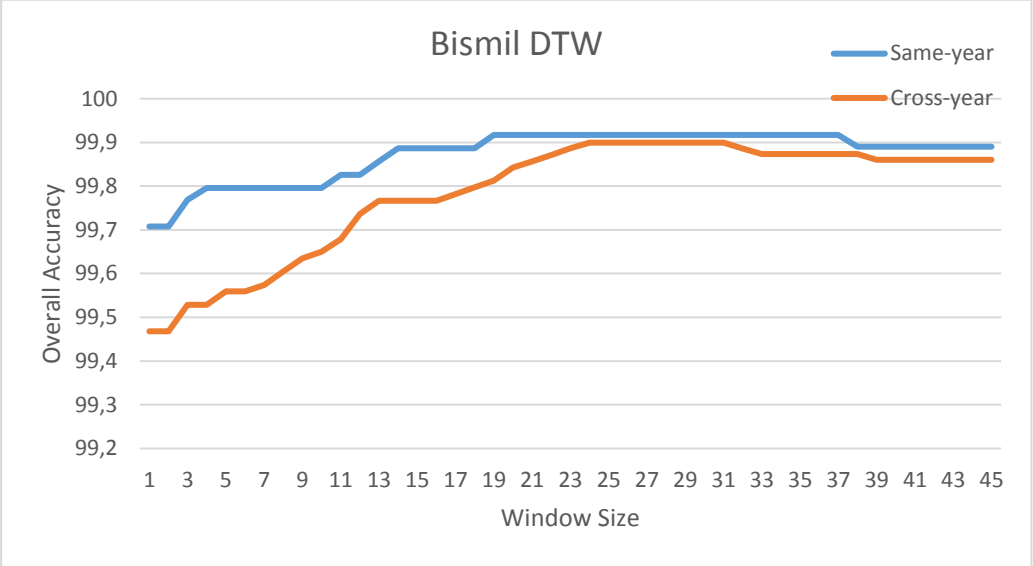

Figure 60: Optimal DTW window size search for the Bismil dataset.

Phenological indicators for the Bismil dataset is provided in Table 17. The time difference is 20 days at D3 between cotton and soybean in 2013. This value increases to 30 days in 2014 while it decreases to 17 days in 2015 — time differences between cotton and soybean change between 30 and 40 days. The time difference between cotton and soybean at D4 was very close as these crops have similar harvest seasons as low as five days in 2014.

Table 17: Phenological transition dates of Corn, Cotton, and Soybean in the Bismil Plain

		Di	**Dd**	**D1**	**D2**	**D3**	**D4**
2013	Corn	132	232	116	148	208	256
	Cotton	186	299	168	204	264	334
	Soybean	214	297	199	229	284	310
2014	Corn	136	232	118	153	212	252
	Cotton	180	290	161	200	255	325
	Soybean	219	308	202	236	285	330
2015	Corn	146	242	131	160	219	264
	Cotton	180	289	162	198	263	314
	Soybean	220	304	210	231	281	326

The overall accuracies of VDTW are stable against varying window sizes (Figure 61). DTW's same year accuracies decreased increasing the window size. On the other hand, VDTW's and DTW's cross-year overall accuracies were similar in shape having different values (Figure 62). VDTW cross-year accuracies have local maxima values

at which the cross-year overall accuracies have a 1.5% difference compared to minimum overall accuracy.

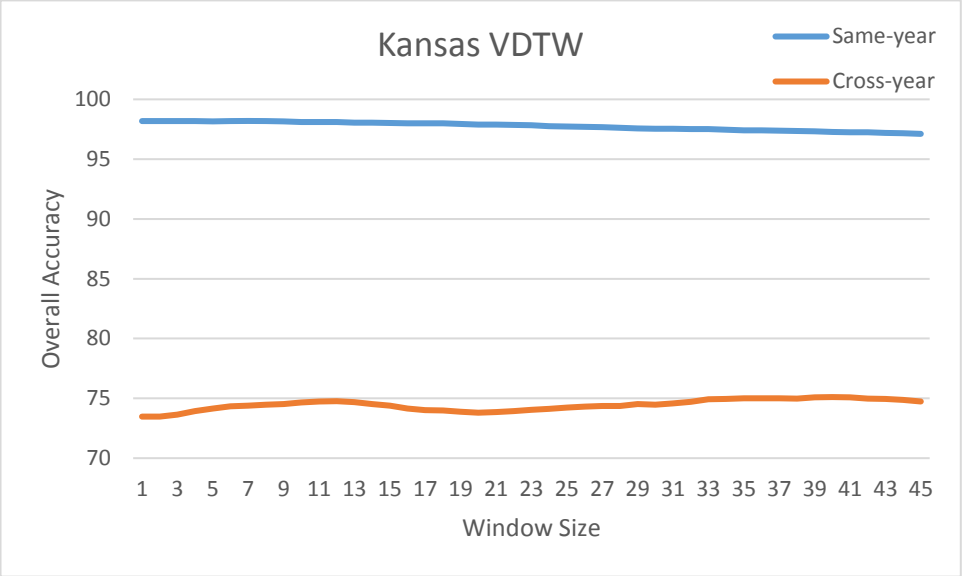

Figure 61: Optimal VDTW window size search for the Kansas dataset.

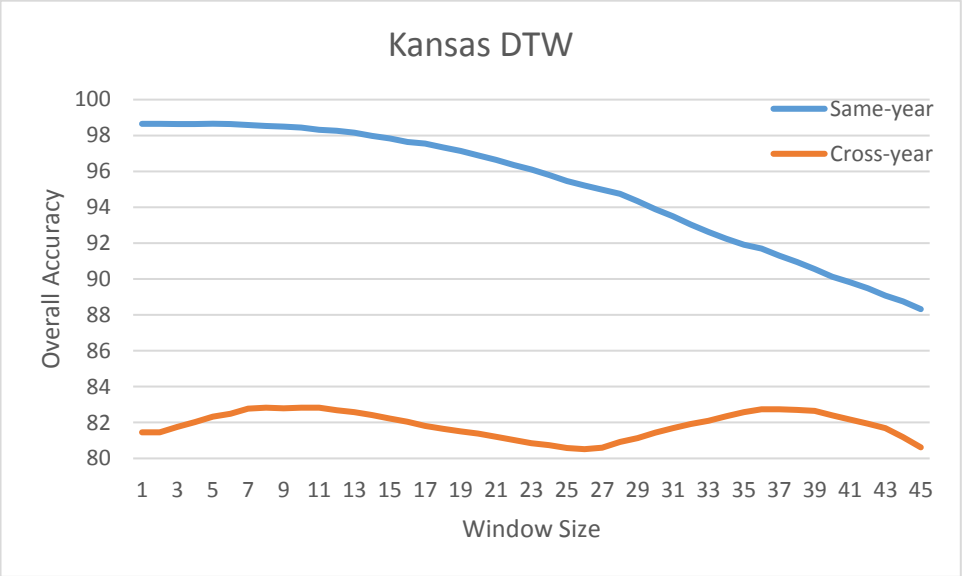

Figure 62: Optimal DTW window size search for the Kansas dataset.

Phenological transition dates of the Kansas dataset are presented in Table 16. The time difference of at D2 between corn and soybean is 44 days in 2017 and 36 in 2018. However, the harvest of corn is closer to the harvest of the soybean in 2017.

Table 18: Phenological transition dates of corn and soybean in the Kansas dataset.

		Di	**Dd**	**D1**	**D2**	**D3**	**D4**
2017	Corn	164	240	151	176	221	262
	Soybean	195	261	168	220	250	273
2018	Corn	157	205	145	168	183	229
	Soybean	178	269	154	204	257	280

The decrease of VDTW performance is related to differences between phenological indicators. Minimum Phenological differences between crops are 11 days in the Harran Plain, 30 days in the Bismil Plain and 36 days in the Kansas dataset. The window sizes are increased as the phenology of crops are distanced. For each dataset, the window sizes are different. Thus, the window sizes were experimentally selected. Moreover, selecting different windows size for each dataset confirmed the most recent literature in which 15 and 30-day time windows were selected for various cropping patterns(Csillik, Belgiu, Asner, & Kelly, 2019).

5.6. Multi-Year Tests

In this study, the median of each field was used as a sample. A stratified random selection strategy was applied to training sample selection (Olofsson et al., 2014), and selected training samples were excluded from the test samples in same-year tests. The same training samples for each test are used in training for all methods. Tests were repeated 100 times to minimize the effect of non-representative outlier samples such as crops grown too early or too late. Different methods were compared against various numbers of training samples to evaluate their performance with a limited number of training samples. Congalton suggested using at least 50 samples from each class when the number of classes is less than 12 (R. G. Congalton, 1988). In the tests, the number of training samples was varied in 5,10,…,50 based on their findings.

Detailed tests were performed for same-year and cross-year classification accuracies. Double sigmoid features with RF classifier and SVM, Time-series (VDTW, SAM, and DTW, TWDTW) and partial time-series (PVDTW) were compared in this study. RF classifier contains 1000 trees. SVM has the RBF kernel, and its parameters are selected after an extensive grid search of cross-validation of training samples. As DL methods gained much attention in classification, two-layer deep long short-term memory (LSTM) was used with 100 units at each layer followed by a softmax layer (Reimers & Gurevych, 2017).

In cross-year tests, the Harran dataset is the most challenging since corn and cotton's phenologies vary each year after peak growth until the harvest. Same-year and cross-year percent overall accuracy scores of tested methods are shown in Table 19. The tests have shown that VDTW provides the highest overall accuracies both in the same year at 99.22% (Figure 63) and cross-year at 98.29% (Figure 64).

SAM and RF methods had similar accuracies in the same year; however, RF was not robust to growth changes in the cross-year as SAM. SAM cross-year scores were below 94.78%. RF was able to reach 94.45% with a maximum number of training samples. VDTW was more robust to the shifts in growth and changes in illumination compared to other methods. The best two performers VDTW and TWDTW achieved the cross-year 50 training sample and 100-replication overall average classification accuracies of 98.29% and 95.29%, respectively. The 95% confidence interval for overall accuracy differences between VDTW and TWDTW methods were between 2.77% and 3.23%. (Table 19). TWDTW's time cost improved DTW's cross-year overall accuracy from 93.31% to 95.29%. The effect of window size of VDTW and DTW was investigated by extensive runs. Even though window size makes a difference in the accuracy, VDTW was always superior. Time series with Deep LSTM initially produced lower accuracies for training sample size < 20 for each class. Deep LSTM obtained similar overall accuracies with DTW and SAM for the training sample size of 50 (~%1 of samples) for each class. Moreover, shallow networks did not produce high accuracies compared to deep networks.

Tests with a varying number of training samples revealed that VDTW maintained high classification accuracies with a fewer number of samples compared to other methods as shown in Figure 63. In other words, the advantage of the proposed approach is its ability to attain high classification accuracy independent of the training set size.

Partial time-series applied to VDTW also achieved similar accuracy values as the core method. Partial time-series, the applied version of VDTW, PVDTW, reduces the amount of data by using fewer data limited by time windows. These time windows are based on phenological differences between crops.

RF and SVM classifiers, which use features extracted from time-series data, have lower performance than other methods in the tests. Performances of RF and SVM are lower since curve fitting is designed for single cropping and may not always fit the optimal curve for double cropping case. Time-series methods such as proposed VDTW, SAM, and DTW are robust to double cropping cases.

Finally, the VDTW method was tested with data from Kansas. Crops in Kansas are distinctly grown. Same year crop mapping accuracies were high for all classifiers, as shown in Table 21. TWDTW method obtained highest the same-year overall accuracy of 99.02%, followed by VDTW and LSTM having overall accuracies of 98.74% and 98.60%. On the other hand, VDTW resulted in higher overall accuracies than TWDTW by 1.72% and other methods in the cross-year tests.

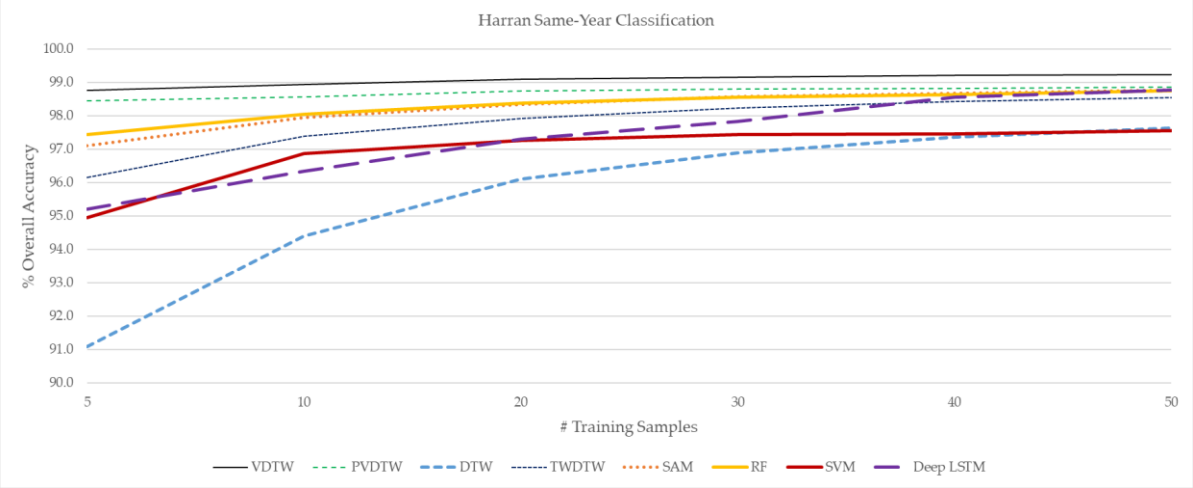

Figure 63: Harran dataset same-year classification results at various training sample sizes.

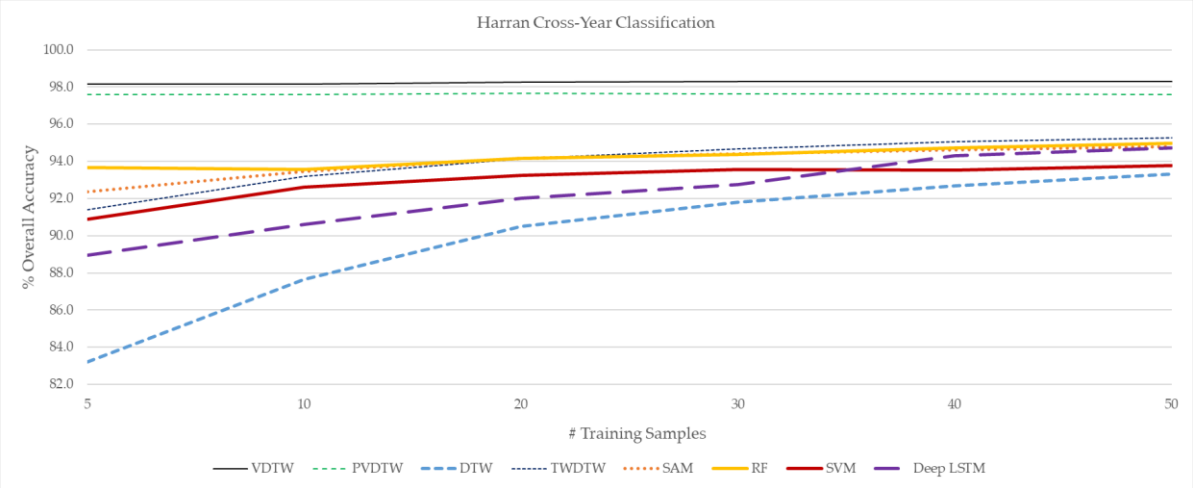

Figure 64: Harran dataset same-year classification results at different training sample sizes.

Table 19: Percent average overall accuracies of proposed and compared methods with 50 samples from each class for the Harran Dataset. Samples are selected with the stratified random selection

	VDTW	PVDTW	DTW	TWDTW	SAM	RF	SVM	Deep LSTM
Same-year	**99.22**	98.86	97.64	98.54	98.77	98.72	98.36	98.76
Cross-year	**98.29**	97.58	93.31	95.29	94.78	94.45	92.40	94.74

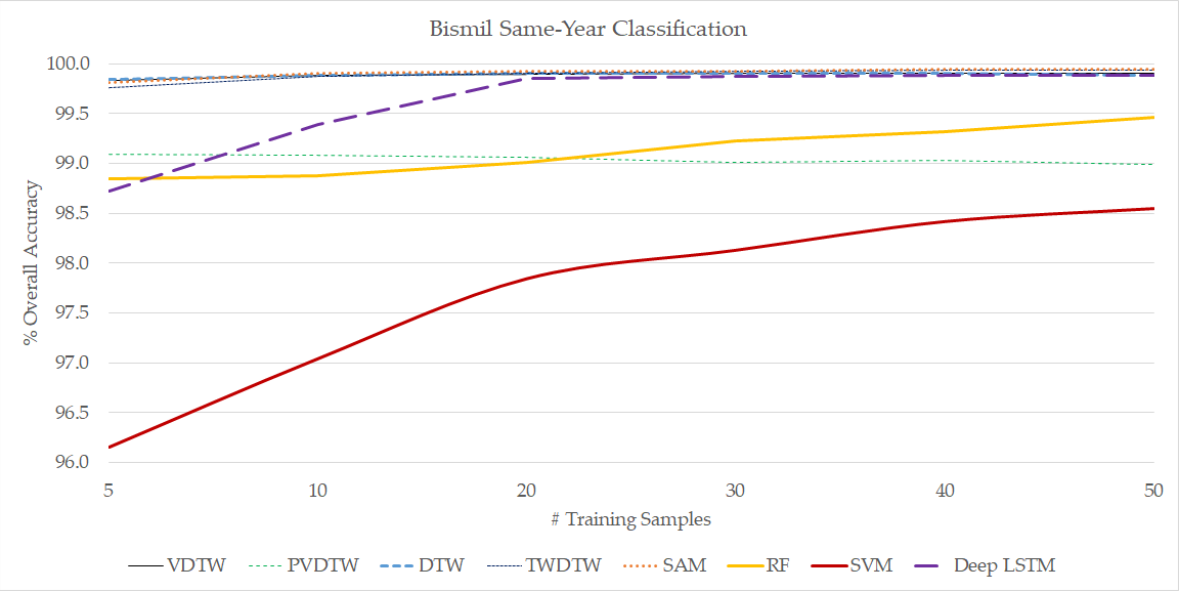

Figure 65: The Bismil dataset same-year classification results at various training sample sizes.

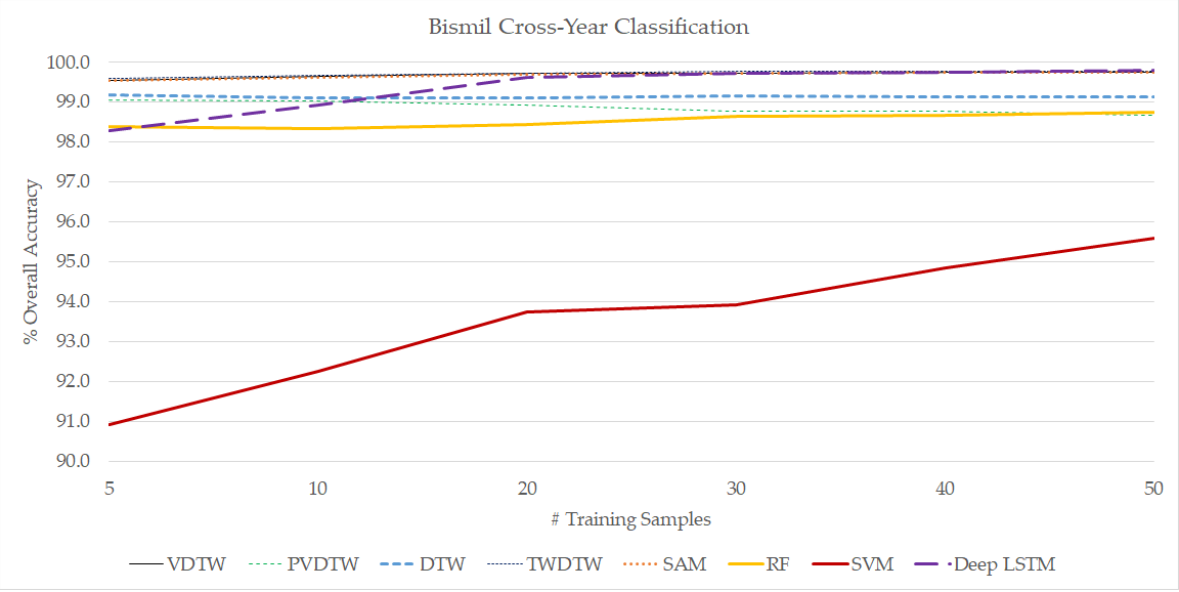

Figure 66: The Bismil dataset cross-year classification results at different training sample sizes.

Table 20: Percent average overall accuracies of proposed and compared methods with 50 samples from each class for the Bismil Dataset. Samples are selected with the stratified random selection.

	VDTW	PVDTW	DTW	TWDTW	SAM	RF	SVM	Deep LSTM
Same-year	99.90	98.99	99.89	99.94	99.94	99.46	98.55	99.88
Cross-year	99.74	98.67	99.13	99.78	99.76	98.75	95.60	99.80

Table 21: Percent average overall accuracies of proposed and compared methods with 50 samples from each class for the Kansas Dataset. Samples are selected with the stratified random selection

	VDTW	PVDTW	DTW	TWDTW	SAM	RF	SVM	Deep LSTM
Same-year	98.38	97.57	78.53	98.63	98.42	98.35	97.91	98.30
Cross-year	89.68	84.89	73.01	88.40	85.55	86.06	86.26	87.10

The user's accuracy and producer's accuracy for the Harran dataset are presented in Table 22. User's accuracies are similar for both crops; however, several mislabeled corns result in lower producer's accuracy for corn. Both user's and producer's accuracies of cotton are over 99% in same-year tests and 98% in cross-year tests.

Table 22: Average User's Accuracy and Producer's Accuracy of VDTW classification results with 50 samples for the same-year and cross-year.

	User's Accuracy		Producer's Accuracy	
	Corn	Cotton	Corn	Cotton
Same-year	97.29	99.57	97.90	99.48
Cross-year	95.28	99.16	95.73	98.72

High user's accuracy both in the same and cross-year tests show that misclassification percentage of corn and cotton is low. However, low user's accuracy of corn indicates that 4.72% of corn is labeled as cotton in cross-year tests. Misclassification error is 2.71% in the same-year tests. Kappa values were 0.97 for the same-year tests and 0.94 for the cross-year tests.

A detailed view of VDTW classification is provided in the form of confusion tables. The confusion matrix in Table 23 shows the number of fields that were correctly classified as corn and cotton with training data from the same or other years. Cotton was correctly classified while some percent of corn is misclassified as cotton.

Table 23: Average Confusion Matrix of 100 tests for VDTW Classification with 50 samples in the Harran Plain. Columns are observations, while rows are predictions. Years in rows are training and years in rows are test years.

		2013		2014		2015	
		Corn	Cotton	Corn	Cotton	Corn	Cotton
2013	Corn	1108	34	619	13	513	4
	Cotton	34	4201	73	4548	4	2845
2014	Corn	1158	231	622	30	514	19
	Cotton	34	4054	20	4481	3	2830
2015	Corn	1123	39	656	13	466	3
	Cotton	69	4246	36	4548	1	2796

Table 24: Average Percent Confusion Matrix of 100 tests for VDTW Classification with 50 samples in the Harran Plain. Columns are observations while rows are predictions. Years in rows are training, and years in rows are test years.

		2013		2014		2015	
		Corn	Cotton	Corn	Cotton	Corn	Cotton
2013	Corn	97.11	2.89	97.96	2.04	99.22	0.78
	Cotton	0.79	99.21	1.57	98.43	0.15	99.85
2014	Corn	85.04	14.96	95.61	4.39	96.82	3.18
	Cotton	0.82	99.18	0.45	99.55	0.09	99.91
2015	Corn	96.67	3.33	98.06	1.94	99.45	0.55
	Cotton	1.61	98.39	0.78	99.22	0.04	99.96

Table 25: Average percent overall accuracy results for the VDTW classification with 100 samples in the Harran Plain.

	2013	2014	2015
2013	99.39	97.96	96.47
2014	97.84	99.54	99.10
2015	98.64	98.43	99.56
Same Year	99.5	Cross Year	98.1

Classification accuracy of cotton was above 99.81% in the same-year tests and 99.64% in cross-year tests. The accuracy of corn was as low as 91.81% in cross-year tests in 2016. The difference in classification accuracies was partly due to how corn is sown after the harvest of wheat, so a late harvest of wheat may shift the growth of corn in different years. On the other hand, the plantation of cotton is not dependent on other agricultural activities.

As the distinct growth times of crops in the Bismil dataset allow classifiers to reach high classification results, VDTW has high same and cross-year accuracies.

Both user's and producer's accuracies are close to 100% (Table 26). The Cross-year producer's accuracy of cotton shows that 1% of cotton classified incorrectly and labeled as corn. Kappa values were 0.99 for the same-year and the cross-year tests.

Table 26: Average User's Accuracy and Producer's Accuracy of VDTW classification results with 50 samples in the Bismil Plain for the same-year and cross-year.

	User's Accuracy			Producer's Accuracy		
	Corn	Cotton	Soybean	Corn	Cotton	Soybean
Same-year	99.87	99.96	100	99.98	99.70	100
Cross-year	99.57	99.98	99.99	99.99	99.06	100

The confusion matrix of the Kansas dataset is depicted in Table 27. The same year user's and producer's accuracies of corn and soybean are above 98%. However, cross-year accuracies are lower (Table 28). VDTW mislabel 22.84% of the corn fields trained with 2018 data and tested with 2017 and 13.98% of soybean fields trained with 2018 data and tested with 2017 data. Crops in 2018 were sown eight days earlier on average compared to 2017. This caused lower accuracies in the cross-year tests.

Table 27: Average Confusion Matrix of 100 tests for VDTW Classification with 50 samples in the Kansas dataset. Columns are observations, while rows are predictions. Years in rows are training and years in rows are test years.

		2017		2018	
		Corn	Soybean	Corn	Soybean
2017	Corn	2048	142	2283	429
	Soybean	78	2855	24	2630
2018	Corn	1679	31	2224	76
	Soybean	497	3016	33	2933

Table 28: Average User's Accuracy and Producer's Accuracy of VDTW classification results with 50 samples for the same-year and cross-year for the Kansas Dataset.

	User's Accuracy		Producer's Accuracy	
	Corn	Soybean	Corn	Soybean
Same-year	98.33	99.04	98.67	98.79
Cross-year	91.17	92.48	88.06	92.47

Same year user's and producer's accuracies are between 98.33-99.04% (Table 28). However, the cross-year user's and producer's accuracies are up to 10% lower. Kappa values were 0.97 for the same-year and 0.81 for the cross-year tests.

5.7. Discussions

Test results show that the proposed approach improved overall accuracy results in both the same-year and cross-year tests. VDTW fuses advantages of both DTW and SAM methods; thus, it provides flexibility in time and measurement variations: DTW can be flexible in time; SAM is robust to illumination changes and measurement differences.

Previous work had an overall accuracy difference of 10% between same-year and cross-year Zhong et al. used Landsat TM and ETM+ images of 2006-2010 to classify maize and soybean in central USA (Zhong et al., 2014). The proposed approach also improved same-year crop mapping accuracies in the Harran Plain compared to previous object-based (Ugur Alganci, Ozdogan, Sertel, & Ormeci, 2014) and multi-temporal (Celik et al., 2015) studies. The results with the Kansas dataset was also in conjunction with the previous work Zhong et al. used Landsat TM and ETM+ images of 2006-2010 to classify maize and soybean in the central USA (Zhong et al., 2014). having 9-10% accuracy difference between the same-year and the cross-year tests. Yearly change of cropping practices decreased the accuracy of all classification methods in the Kansas dataset.

On the other hand, the VDTW method was more robust compared to other methods in the cross-year tests. TWDTW approach was proposed to improve DTW performance (Maus et al., 2016). However, it did not include changes in illumination and variations in measurements as in SAM or VDTW approach. Deep LSTM's accuracy was improved as the number of training samples were increased. This result was expected as DL requires a large amount of data and fine-tuning of parameters. RF with a double-sigmoid features approach has similar results compared to SAM and DTW methods.

Our multiyear crop mapping approach overcame difficulties in cross-year classification. In addition to SG data smoothing, vegetation index values of cloudy data samples were interpolated. This cloud information cloning approach improved cross-year overall accuracies.

NDVI and EVI were commonly used in phenological feature extraction (de Souza et al., 2015a) (Z. Pan et al., 2015). However, the use of MSAVI was proposed since it was obtained higher the cross-year overall accuracies with the use of the MSAVI. Soil adjusted vegetation indices, such as SAVI, include the effect of the soil line as a parameter; on the other hand, MSAVI computes the soil line parameter automatically. For this reason, the use of MSAVI further reduced variations in observation angles.

A limited time window version of VDTW, PVDTW, achieved similar overall accuracies with fewer data. PVDTW enables mid-season crop classification and has efficient computation requirements. The partial time window method may be applied to other classification algorithms, such as DTW and SAM under the proposed multi-year crop mapping approach.

VDTW and PVDTW methods are not as vulnerable as the other methods to the paucity of available training data. This property is useful since an operational system can use

pure phenologies (as low as a single time-series signature), or it can still operate sufficiently with fewer temporal data samples.

The proposed methods can also be extended to the classification of other crops, such as discrimination of wheat-barley, corn-soybean (Massey et al., 2017), and rice-corn (Tang, Zhu, Zhan, & Ding, 2018), which have overlapped phenological phases.

The difference of the first derivative of vegetation index (VI) was evaluated as an alternative to angles between VI time-vectors (Górecki & Łuczak, 2014). The correlation between two distinct vectors, which have different values and the same slopes, were different. VDTW incorporates Euclidean similarity implicitly, thus resulting in better discrimination.

Missing data acquisitions in large time windows may lower multi-year crop mapping performances. These time windows are growth and harvest, where the changes are exponential rather than linear. The use of the curve fitting with the double logistic function or other non-linear methods may eliminate this problem.

According to the investigations in the Harran Plain, farmers may re-sow cotton if the seedlings did not emerge due to drought or heavy rains. In this case, the growth of the cotton crop was delayed, and its phenology resembled that of corn. Another issue is the growing of cotton as the second crop. However, this practice is not common and may produce low crop yields (Çopur & Yuka, 2016).

One last challenge for the VDTW method is that it requires more computation power than both DTW and SAM methods. Compared to the DTW, vector dot products are computed at each point instead of a simple absolute distance operation. However, VDTW achieved high performance with fewer training samples. It is also suggested using the median of training samples to generate crop mapping from training data for time-sensitive or large-scale applications.

CHAPTER 6

CONCLUSIONS

In this study, vector dynamic time warping (VDTW), a modified version of DTW, was developed and presented in a multi-year crop mapping approach for efficiently classifying crops with similar phenologies, such as corn and cotton, and other crops with distinct phenologies. The proposed method is based on the optimal time vector alignment of crop phenologies for overcoming the difficulties experienced in previous efforts. VDTW for crop mapping is robust against spectral and temporal shifts in yearly crop growths. Simulations were conducted to analyze weaknesses of both DTW and SAM. VDTW is developed to overcome their weaknesses and render it to both variations in time and illumination changes.

VDTW method was tested with multiple crops and in separate regions yielding high classification accuracies. Classification of corn and cotton, which are investigated in this study is challenging due to the overlaps in their phenological characteristics. On the other hand, the crops in the Bismil Plain have distinct phenologies. Corn and Soybean in Kansas have partially overlapping phenologies; however, phenology of crops in 2018 shifted considerably compared to 2017. The proposed VDTW method provided the highest same-year and cross-year overall classification accuracies. The tests with the Kansas dataset showed that there is still room for improvement in cross-year crop mapping. Agro-meteorological information including temperature (such as growing degree days) and rainfall may be employed to improve the cross-year accuracies.

Another improvement of this study is employing discriminative regions for efficient crop classification PVDTW method uses optimal time window selection to achieve comparable accuracies of its base method, with less temporal data. Optimal time-periods to discriminate against these crops are determined by the PVDTW algorithm.

Both VDTW and PVDTW methods achieved higher classification accuracy compared to other methods with a limited number of training samples, thus reducing the repeated effort of collecting ground samples. Time constraints were analyzed DTW and VDTW: it is suggested to determine optimal time windows for each dataset in consideration.

Various vegetation indices including, EVI, NDVI and MSAVI were compared. MSAVI was robust against variations in the cross-year tests. The use of MSAVI

contributed the cross-year accuracy in Kansas dataset since it included both Landsat 8 and Sentinel-2 imagery as they have different BRDF attributes.

Data smoothing improved the cross-year crop mapping performance. In addition, effective cloud detection is required to ensure optimal performance of VDTW in the cross-year setting.

The proposed methods can also be expanded to classify other types of crops. Besides, the VDTW method may also be adapted to different research areas (e.g., data mining and speech recognition) where DTW is commonly preferred.

The approach developed is highly suitable for crop mapping at regional scales. However, further additional datasets are required to expand the VDTW to countrywide levels. In the meantime, the proposed approach may be used to improve the accuracy of the Ministry of Agriculture and Forestry's National Registry of Farmers in the near future for the crop types taken into consideration in this study.

REFERENCES

Alganci, U, Sertel, E., Kaya, S., & BerkUstundag, B. (2013). A research on agricultural mapping capabilities of the SPOT 6 satellite images. In *Agro-Geoinformatics (Agro-Geoinformatics), 2013 Second International Conference on* (pp. 93–96). https://doi.org/10.1109/Argo-Geoinformatics.2013.6621886

Alganci, Ugur, Ozdogan, M., Sertel, E., & Ormeci, C. (2014). Estimating maize and cotton yield in southeastern Turkey with integrated use of satellite images, meteorological data and digital photographs. *Field Crops Research*, *157*, 8–19. https://doi.org/10.1016/j.fcr.2013.12.006

Alganci, Ugur, Sertel, E., Ozdogan, M., & Ormeci, C. (2013). Parcel-Level Identification of Crop Types Using Different Classification Algorithms and Multi-Resolution Imagery in Southeastern Turkey. *Photogrammetric Engineering & Remote Sensing*, *79*(11), 1053–1065. https://doi.org/10.14358/PERS.79.11.1053

Arvor, D., Jonathan, M., Meirelles, M. S. P., Dubreuil, V., & Lecerf, R. (2008). Comparison of Multitemporal MODIS-EVI Smoothing Algorithms and its Contribution to Crop Monitoring. In *Geoscience and Remote Sensing Symposium, 2008. IGARSS 2008. IEEE International* (Vol. 2, pp. II-958-II–961). https://doi.org/10.1109/IGARSS.2008.4779155

Aydoğdu, M., Akçar, H. T., & Çullu, M. A. (2005). Coğrafi Bilgi Sistemleri (CBS) Ve Uzaktan Algılama (UA) Kullanılarak Çiftçi Kayıt Sistemi (ÇKS) Verilerinin Analizi İle Pamuk Ve Mısır Primlerinin Ödenmesi (Şanlıurfa - Harran İlçesi Örneği), 2–7.

Bagnall, A., Lines, J., Bostrom, A., Large, J., & Keogh, E. (2017). The great time series classification bake off: a review and experimental evaluation of recent algorithmic advances. *Data Mining and Knowledge Discovery*, *31*(3), 606–660. https://doi.org/10.1007/s10618-016-0483-9

Bargiel, D. (2017). A new method for crop classification combining time series of radar images and crop phenology information. *Remote Sensing of Environment*, *198*, 369–383. https://doi.org/10.1016/j.rse.2017.06.022

Belgiu, M., & Csillik, O. (2018). Sentinel-2 cropland mapping using pixel-based and object-based time-weighted dynamic time warping analysis. *Remote Sensing of Environment*, *204*(January 2017), 509–523. https://doi.org/10.1016/j.rse.2017.10.005

Bellman, R. (1966). Dynamic programming. *Science*, *153*(3731), 34–37. https://doi.org/10.1126/science.153.3731.34

Blaes, X., Vanhalle, L., & Defourny, P. (2005). Efficiency of crop identification based on optical and {SAR} image time series. *Remote Sensing of Environment*, *96*(3–4), 352–365. https://doi.org/http://dx.doi.org/10.1016/j.rse.2005.03.010

Carlotto, M. J. (2009). Effect of errors in ground truth on classification accuracy. *International Journal of Remote Sensing*, *30*(18), 4831–4849. https://doi.org/10.1080/01431160802672864

Çelik, M. A., & Gülersoy, A. E. (2013). Güneydoğu Anadolu Projesi'nin (GAP) Harran Ovası Tarımsal Yapısında Meydana Getirdiği Değişimlerin Uzaktan Algılama ile İncelenmesi. *Journal of International Social Research*, *6*(28).

Celik, Y. B., Sertel, E., & Ustundag, B. B. (2015). Identification of corn and cotton fields using multi-temporal Spot6 {NDVI} data. In *2015 Fourth International Conference on Agro-Geoinformatics (Agro-geoinformatics)*. IEEE. https://doi.org/10.1109/agro-geoinformatics.2015.7248136

Claverie, M., Ju, J., Masek, J. G., Dungan, J. L., Vermote, E. F., Roger, J.-C., … Justice, C. (2018). The Harmonized Landsat and Sentinel-2 surface reflectance data set. *Remote Sensing of Environment*, *219*, 145–161. https://doi.org/10.1016/J.RSE.2018.09.002

Congalton, R. G. (1988). A comparison of sampling schemes used in generating error matrices for assessing the accuracy of maps generated from remotely sensed data. *Photogrammetric Engineering and Remote Sensing (USA)*.

Congalton, R. G., & Green, K. (2008). *Assessing the accuracy of remotely sensed data: principles and practices*. CRC press.

Congalton, R., Gu, J., Yadav, K., Thenkabail, P., Ozdogan, M., Congalton, R. G., … Ozdogan, M. (2014). Global Land Cover Mapping: A Review and Uncertainty Analysis. *Remote Sensing*, *6*(12), 12070–12093. https://doi.org/10.3390/rs61212070

Conrad, C., Dech, S., Dubovyk, O., Fritsch, S., Klein, D., Löw, F., … Zeidler, J. (2014). Derivation of temporal windows for accurate crop discrimination in heterogeneous croplands of Uzbekistan using multitemporal {RapidEye} images. *Computers and Electronics in Agriculture*, *103*, 63–74. https://doi.org/10.1016/j.compag.2014.02.003

Çopur, O., & Yuka, A. (2016). Buğday Sonrası İkinci Ürün Olarak Yetiştirilen Pamuk (Gossypium hirsutum L.) Çeşitlerinde Verim ve Verim Unsurlarının Belirlenmesi. *Yüzüncü Yıl Üniversitesi Tarım Bilimleri Dergisi*, *26*(2), 245–253. Retrieved from http://dergipark.gov.tr/yyutbd/issue/24190/256545

Csillik, O., Belgiu, M., Asner, G. P., & Kelly, M. (2019). Object-Based Time-Constrained Dynamic Time Warping Classification of Crops Using Sentinel-2. *Remote Sensing*, *11*(10), 1257. https://doi.org/10.3390/rs11101257

Davranche, A., Lefebvre, G., & Poulin, B. (2010). Wetland monitoring using classification trees and {SPOT}-5 seasonal time series. *Remote Sensing of Environment*, *114*(3), 552–562. https://doi.org/10.1016/j.rse.2009.10.009

de Souza, C. H. W., Mercante, E., Johann, J. A., Lamparelli, R. A. C., & Uribe-Opazo, M. A. (2015a). Mapping and discrimination of soya bean and corn crops using spectro-temporal profiles of vegetation indices. *International Journal of Remote Sensing*, *36*(7), 1809–1824. https://doi.org/10.1080/01431161.2015.1026956

de Souza, C. H. W., Mercante, E., Johann, J. A., Lamparelli, R. A. C., & Uribe-Opazo, M. A. (2015b). Mapping and discrimination of soya bean and corn crops using spectro-temporal profiles of vegetation indices. *International Journal of Remote Sensing*, *36*(7), 1809–1824. https://doi.org/10.1080/01431161.2015.1026956

Dennison, P. E., & Roberts, D. A. (2003). The effects of vegetation phenology on endmember selection and species mapping in southern California chaparral. *Remote Sensing of Environment*, *87*(2–3), 295–309. https://doi.org/10.1016/j.rse.2003.07.001

Dong, J., Xiao, X., Kou, W., Qin, Y., Zhang, G., Li, L., … III, B. M. (2015). Tracking the dynamics of paddy rice planting area in 1986–2010 through time series Landsat images and phenology-based algorithms. *Remote Sensing of Environment*, *160*, 99–113. https://doi.org/http://dx.doi.org/10.1016/j.rse.2015.01.004

Eerens, H., Haesen, D., Rembold, F., Urbano, F., Tote, C., & Bydekerke, L. (2014). Image time series processing for agriculture monitoring. *Environmental Modelling & Software*, *53*, 154–162. https://doi.org/http://dx.doi.org/10.1016/j.envsoft.2013.10.021

Esetlili, M. T., Bektas Balcik, F., Balik Sanli, F., Ustuner, M., Kalkan, K., Goksel, C., … Kurucu, Y. (2018). Comparison of Object and Pixel-Based Classifications For Mapping Crops Using Rapideye Imagery: A Case Study Of Menemen Plain, Turkey. *International Journal of Environment and Geoinformatics*, *5*(2), 231–243. https://doi.org/10.30897/ijegeo.442002

Foerster, M., Welle, B. A., Schmidt, T., Nieland, S., & Kleinschmit, B. (2014). TimeSpec — A software tool for analyzing time-series of spectral data. *Geoscience and Remote Sensing Symposium (IGARSS), 2014 IEEE International*, 3941–3944. https://doi.org/10.1109/IGARSS.2014.6947347

Foerster, S., Kaden, K., Foerster, M., & Itzerott, S. (2012). Crop type mapping using spectral-temporal profiles and phenological information. *Computers and Electronics in Agriculture*, *89*, 30–40. https://doi.org/http://dx.doi.org/10.1016/j.compag.2012.07.015

Fontanelli, G., Crema, A., Azar, R., Stroppiana, D., Villa, P., & Boschetti, M. (2014). Agricultural crop mapping using optical and SAR multi-temporal seasonal data: A case study in Lombardy region, Italy. In *Geoscience and Remote Sensing Symposium (IGARSS), 2014 IEEE International* (pp. 1489–1492). https://doi.org/10.1109/IGARSS.2014.6946719

Foody, G. M. (2015). The effect of mis-labeled training data on the accuracy of supervised image classification by SVM. *IEEE Geoscience and Remote Sensing Letters, IGARSS 201*, 4987–4990.

García-Mora, T. J., Mas, J.-F., & Hinkley, E. A. (2012). Land cover mapping applications with MODIS: a literature review. *International Journal of Digital Earth*, *5*(1), 63–87. https://doi.org/10.1080/17538947.2011.565080

Garcia-Torres, L., Caballero-Novella, J. J., Gomez-Candon, D., & Pena, J. M. (2015). Census Parcels Cropping System Classification from Multitemporal Remote Imagery: A Proposed Universal Methodology. *PloS One*, *10*(2).

Gitelson, A. A. (2004). Wide Dynamic Range Vegetation Index for Remote Quantification of Biophysical Characteristics of Vegetation. *Journal of Plant Physiology*, *161*(2), 165–173. https://doi.org/https://doi.org/10.1078/0176-1617-01176

Gómez, C., White, J. C., & Wulder, M. A. (2016). Optical remotely sensed time series data for land cover classification: A review. *ISPRS Journal of Photogrammetry and Remote Sensing*, *116*, 55–72. https://doi.org/10.1016/J.ISPRSJPRS.2016.03.008

Górecki, T., & Łuczak, M. (2014). First and Second Derivatives in Time Series Classification Using DTW. *Communications in Statistics - Simulation and Computation*, *43*(9), 2081–2092. https://doi.org/10.1080/03610918.2013.775296

Guarini, R., Bruzzone, L., Santoni, M., & Dini, L. (2015). Analysis on the effectiveness of multitemporal COSMO-SkyMed images for crop classification. *Proc. SPIE*. https://doi.org/10.1117/12.2193757

Han, W., Yang, Z., Di, L., & Mueller, R. (2012). CropScape: A Web service based application for exploring and disseminating {US} conterminous geospatial cropland data products for decision support. *Computers and Electronics in Agriculture*, *84*, 111–123. https://doi.org/http://dx.doi.org/10.1016/j.compag.2012.03.005

Hao, P., Wang, L., & Niu, Z. (2015). Comparison of Hybrid Classifiers for Crop Classification Using Normalized Difference Vegetation Index Time Series: A Case Study for Major Crops in North Xinjiang, China. *PLoS ONE*, *10*(9), e0137748. https://doi.org/10.1371/journal.pone.0137748

Hemissi, S., Farah, I. R., Saheb Ettabaa, K., & Solaiman, B. (2013). Multi-Spectro-Temporal Analysis of Hyperspectral Imagery Based on 3-D Spectral Modeling and Multilinear Algebra. *Geoscience and Remote Sensing, IEEE Transactions On*, *51*(1), 199–216. https://doi.org/10.1109/TGRS.2012.2200486

Huete, A., Didan, K., Miura, T., Rodriguez, E. P., Gao, X., & Ferreira, L. G. (2002). Overview of the radiometric and biophysical performance of the MODIS vegetation indices. *Remote Sensing of Environment*, *83*(1), 195–213.

Huete, A. R., Hua, G., Qi, J., Chehbouni, A., & van Leeuwen, W. J. D. (1992). Normalization of multidirectional red and NIR reflectances with the SAVI. *Remote Sensing of Environment*, *41*(2–3), 143–154. https://doi.org/10.1016/0034-4257(92)90074-T

Jakubauskas, M. E., Legates, D. R., & Kastens, J. H. (2002). Crop identification using harmonic analysis of time-series {AVHRR} {NDVI} data. *Computers and Electronics in Agriculture*, *37*(1–3), 127–139. https://doi.org/http://dx.doi.org/10.1016/S0168-1699(02)00116-3

Jansen, L. J. M., Badea, A., Milenov, P., & Moise, C. (2014). Land Use and Land Cover Mapping in Europe, *18*. https://doi.org/10.1007/978-94-007-7969-3

Jiao, X., Kovacs, J. M., Shang, J., McNairn, H., Walters, D., Ma, B., & Geng, X. (2014). Object-oriented crop mapping and monitoring using multi-temporal polarimetric RADARSAT-2 data. *ISPRS Journal of Photogrammetry and Remote Sensing*, *96*, 38–46. https://doi.org/http://dx.doi.org/10.1016/j.isprsjprs.2014.06.014

Kalkan, K., & Maktav, M. D. (2018). A Cloud Removal Algorithm to Generate Cloud and Cloud Shadow Free Images Using Information Cloning. *Journal of the Indian Society of Remote Sensing*, *46*(8), 1255–1264. https://doi.org/10.1007/s12524-018-0806-y

Kamilaris, A., & Prenafeta-Boldú, F. X. (2018). Deep learning in agriculture: A survey. *Computers and Electronics in Agriculture*, *147*(July 2017), 70–90. https://doi.org/10.1016/j.compag.2018.02.016

Kim, S.-R., Prasad, A. K., El-Askary, H., Lee, W.-K., Kwak, D.-A., Lee, S.-H., & Kafatos, M. (2014). Application of the Savitzky-Golay Filter to Land Cover Classification Using Temporal MODIS Vegetation Indices. *Photogrammetric Engineering & Remote Sensing*, *80*(7), 675–685.

Knight, J. F., Lunetta, R. S., Ediriwickrema, J., & Khorram, S. (2006). Regional Scale Land Cover Characterization Using MODIS-NDVI 250 m Multi-Temporal Imagery: A Phenology-Based Approach. *GIScience & Remote Sensing*, *43*(1), 1–23. https://doi.org/10.2747/1548-1603.43.1.1

Kotera, A., Berberoglu, S., Nagano, T., & Cullu, M. A. (2015). A global dataset of noiseless time-series vegetation and water indices for farmland analysis. In *Agro-Geoinformatics (Agro-geoinformatics), 2015 Fourth International Conference on* (pp. 173–177).

Kruse, F. A., Lefkoff, A. B., Boardman, J. W., Heidebrecht, K. B., Shapiro, A. T., Barloon, P. J., & Goetz, A. F. H. (1993). The spectral image processing system (SIPS) interactive visualization and analysis of imaging spectrometer data. *Remote Sensing of Environment*, *44*(2–3), 145–163. https://doi.org/http://dx.doi.org/10.1016/0034-4257(93)90013-N

Kussul, N., Lavreniuk, M., Skakun, S., & Shelestov, A. (2017). Deep Learning Classification of Land Cover and Crop Types Using Remote Sensing Data. *IEEE Geoscience and Remote Sensing Letters*, *14*(5), 778–782. https://doi.org/10.1109/LGRS.2017.2681128

Landsat 8 Surface Reflectance Product Guide v1.2. (2015). Retrieved from

https://landsat.usgs.gov/sites/default/files/documents/lasrc_product_guide.pdf

Lecun, Y., Bengio, Y., & Hinton, G. (2015). Deep learning. *Nature*, *521*(7553), 436–444. https://doi.org/10.1038/nature14539

Leite, P. B. C., Feitosa, R. Q., Formaggio, A. R., Da Costa, G. A. O. P., Pakzad, K., & Sanches, I. D. A. (2011). Hidden Markov Models for crop recognition in remote sensing image sequences. In *Pattern Recognition Letters* (Vol. 32, pp. 19–26). https://doi.org/10.1016/j.patrec.2010.02.008

Li, Q., Cao, X., Jia, K., Zhang, M., & Dong, Q. (2014). Crop type identification by integration of high-spatial resolution multispectral data with features extracted from coarse-resolution time-series vegetation index data. *International Journal of Remote Sensing*, *35*(16), 6076–6088. https://doi.org/10.1080/01431161.2014.943325

Liakos, K., Busato, P., Moshou, D., Pearson, S., & Bochtis, D. (2018). Machine Learning in Agriculture: A Review. *Sensors*, *18*(8), 2674. https://doi.org/10.3390/s18082674

Long, J. A., Lawrence, R. L., Greenwood, M. C., Marshall, L., & Miller, P. R. (2013). Object-oriented crop classification using multitemporal ETM+ SLC-off imagery and random forest. *GIScience & Remote Sensing*, *50*(4), 418–436. https://doi.org/10.1080/15481603.2013.817150

Löw, F, Michel, U., Dech, S., & Conrad, C. (2013). Impact of feature selection on the accuracy and spatial uncertainty of per-field crop classification using Support Vector Machines. *ISPRS Journal of Photogrammetry and Remote Sensing*, *85*, 102–119. https://doi.org/http://dx.doi.org/10.1016/j.isprsjprs.2013.08.007

Löw, Fabian, Conrad, C., & Michel, U. (2015). Decision fusion and non-parametric classifiers for land use mapping using multi-temporal RapidEye data. *ISPRS Journal of Photogrammetry and Remote Sensing*, *108*, 191–204. https://doi.org/http://dx.doi.org/10.1016/j.isprsjprs.2015.07.001

Lucas, R., Rowlands, A., Brown, A., Keyworth, S., & Bunting, P. (2007). Rule-based classification of multi-temporal satellite imagery for habitat and agricultural land cover mapping. *ISPRS Journal of Photogrammetry and Remote Sensing*, *62*(3), 165–185. https://doi.org/http://dx.doi.org/10.1016/j.isprsjprs.2007.03.003

Massey, R., Sankey, T. T., Congalton, R. G., Yadav, K., Thenkabail, P. S., Ozdogan, M., & Sánchez Meador, A. J. (2017). MODIS phenology-derived, multi-year distribution of conterminous U.S. crop types. *Remote Sensing of Environment*, *198*, 490–503. https://doi.org/10.1016/j.rse.2017.06.033

Maus, V., Câmara, G., Cartaxo, R., Sanchez, A., Ramos, F. M., & de Queiroz, G. R. (2016). A time-weighted dynamic time warping method for land-use and land-cover mapping. *IEEE Journal of Selected Topics in Applied Earth Observations and Remote Sensing*, *9*(8), 3729–3739.

McNairn, H., Kross, A., Lapen, D., Caves, R., & Shang, J. (2014). Early season monitoring of corn and soybeans with TerraSAR-X and RADARSAT-2. *International Journal of Applied Earth Observation and Geoinformation*, *28*, 252–259. https://doi.org/http://dx.doi.org/10.1016/j.jag.2013.12.015

Mingwei, Z., Qingbo, Z., Zhongxin, C., Jia, L., Yong, Z., & Chongfa, C. (2008). Crop discrimination in Northern China with double cropping systems using Fourier analysis of time-series {MODIS} data. *International Journal of Applied Earth Observation and Geoinformation*, *10*(4), 476–485. https://doi.org/http://dx.doi.org/10.1016/j.jag.2007.11.002

Motohka, T., Nasahara, K. N., Oguma, H., & Tsuchida, S. (2010). Applicability of green-red vegetation index for remote sensing of vegetation phenology. *Remote Sensing*, *2*(10), 2369–2387.

Nidamanuri, R. R., & Zbell, B. (2011). Use of field reflectance data for crop mapping using airborne hyperspectral image. *{ISPRS} Journal of Photogrammetry and Remote Sensing*, *66*(5), 683–691. https://doi.org/http://dx.doi.org/10.1016/j.isprsjprs.2011.05.001

Niel, T. G. Van, & McVicar, T. R. (2004). Determining temporal windows for crop discrimination with remote sensing: a case study in south-eastern Australia. *Computers and Electronics in Agriculture*, *45*(1–3), 91–108. https://doi.org/http://dx.doi.org/10.1016/j.compag.2004.06.003

Ok, A. O., & Akyurek, Z. (2012). A segment-based approach to classify agricultural lands by using multi-temporal optical and microwave data. *International Journal of Remote Sensing*, *33*(22), 7184–7204. https://doi.org/10.1080/01431161.2012.700423

Olofsson, P., Foody, G. M., Herold, M., Stehman, S. V, Woodcock, C. E., & Wulder, M. A. (2014). Good practices for estimating area and assessing accuracy of land change. *Remote Sensing of Environment*, *148*, 42–57. https://doi.org/10.1016/j.rse.2014.02.015

Pan, Y., Li, L., Zhang, J., Liang, S., Zhu, X., & Sulla-Menashe, D. (2012). Winter wheat area estimation from MODIS-EVI time

series data using the Crop Proportion Phenology Index. *Remote Sensing of Environment*, *119*, 232–242. https://doi.org/10.1016/j.rse.2011.10.011

Pan, Z., Huang, J., Zhou, Q., Wang, L., Cheng, Y., Zhang, H., … Liu, J. (2015). Mapping crop phenology using NDVI time-series derived from HJ-1 A/B data. *International Journal of Applied Earth Observation and Geoinformation*, *34*, 188–197. https://doi.org/http://dx.doi.org/10.1016/j.jag.2014.08.011

Pelletier, C., Valero, S., Inglada, J., Champion, N., Sicre, C. M., & Dedieu, G. (2017). Effect of training class label noise on classification performances for land cover mapping with satellite image time series. *Remote Sensing*, *9*(2). https://doi.org/10.3390/rs9020173

Pena, J. M., Gutierrez, P. A., Hervás-Mart\'\inez, C., Six, J., Plant, R. E., & López-Granados, F. (2014). Object-based image classification of summer crops with machine learning methods. *Remote Sensing*, *6*(6), 5019–5041.

Pena, M. A., & Brenning, A. (2015). Assessing fruit-tree crop classification from Landsat-8 time series for the Maipo Valley, Chile. *Remote Sensing of Environment*, *171*, 234–244. https://doi.org/http://dx.doi.org/10.1016/j.rse.2015.10.029

Peng, G., Deng, L., Cui, W., Ming, T., & Shen, W. (2009). Remote sensing monitoring of tobacco field based on phenological characteristics and time series image—A case study of Chengjiang County, Yunnan Province, China. *Chinese Geographical Science*, *19*(2), 186–193. https://doi.org/10.1007/s11769-009-0186-x

Petitjean, F., & Weber, J. (2014). Efficient Satellite Image Time Series Analysis Under Time Warping. *Geoscience and Remote Sensing Letters, IEEE*, *11*(6), 1143–1147. https://doi.org/10.1109/LGRS.2013.2288358

Qi, J., Chehbouni, A., Huete, A. R., Kerr, Y. H., & Sorooshian, S. (1994). A modified soil adjusted vegetation index. *Remote Sensing of Environment*, *48*(2), 119–126. https://doi.org/http://dx.doi.org/10.1016/0034-4257(94)90134-1

Reimers, N., & Gurevych, I. (2017). Optimal Hyperparameters for Deep LSTM-Networks for Sequence Labeling Tasks. Retrieved from http://arxiv.org/abs/1707.06799

Rembold, F., & Maselli, F. (2006). Estimation of inter-annual crop area variation by the application of spectral angle mapping to low resolution multitemporal NDVI images. *Photogrammetric Engineering & Remote Sensing*, *72*(1), 55–62.

Rondeaux, G., Steven, M., & Baret, F. (1996). Optimization of soil-adjusted vegetation indices. *Remote Sensing of Environment*, *55*(2), 95–107.

Sakamoto, T., Gitelson, A. A., & Arkebauer, T. J. (2014). Near real-time prediction of U.S. corn yields based on time-series {MODIS} data. *Remote Sensing of Environment*, *147*, 219–231. https://doi.org/http://dx.doi.org/10.1016/j.rse.2014.03.008

Sakamoto, T., Yokozawa, M., Toritani, H., Shibayama, M., Ishitsuka, N., & Ohno, H. (2005). A crop phenology detection method using time-series {MODIS} data. *Remote Sensing of Environment*, *96*(3–4), 366–374. https://doi.org/http://dx.doi.org/10.1016/j.rse.2005.03.008

Shang, J., McNairn, H., Champagne, C., & Jiao, X. (2008). Contribution of Multi-Frequency, Multi-Sensor, and Multi-Temporal Radar Data to Operational Annual Crop Mapping. In *Geoscience and Remote Sensing Symposium, 2008. IGARSS 2008. IEEE International* (Vol. 3, pp. III-378-III–381). https://doi.org/10.1109/IGARSS.2008.4779362

Shao, Y., & Lunetta, R. S. (2012). Comparison of support vector machine, neural network, and {CART} algorithms for the land-cover classification using limited training data points. *ISPRS Journal of Photogrammetry and Remote Sensing*, *70*, 78–87. https://doi.org/http://dx.doi.org/10.1016/j.isprsjprs.2012.04.001

Şimşek, Fatih Fehmi ;Teke, Mustafa;Altuntaş, C. (2016). Controlling of Product Declarations of Farmers Using Remote Sensing Techniques: The Harran Plain Case. In *6. Uzaktan Algilama ve CBS Sempozyumu - UZAL-CBS 2016* (pp. 276–286).

Son, N.-T., Chen, C.-F., Chen, C.-R., Duc, H.-N., & Chang, L.-Y. (2013). A phenology-based classification of time-series MODIS data for rice crop monitoring in Mekong Delta, Vietnam. *Remote Sensing*, *6*(1), 135–156.

Tang, K., Zhu, W., Zhan, P., & Ding, S. (2018). An Identification Method for Spring Maize in Northeast China Based on Spectral and Phenological Features. *Remote Sensing*, *10*(2), 193. https://doi.org/10.3390/rs10020193

Tatsumi, K., Yamashiki, Y., Torres, M. A. C., & Taipe, C. L. R. (2015). Crop classification of upland fields using Random forest of time-series Landsat 7 ETM+ data. *Computers and Electronics in Agriculture*, *115*, 171–179. https://doi.org/http://dx.doi.org/10.1016/j.compag.2015.05.001

Thenkabail, P., GangadharaRao, P., Biggs, T., Krishna, M., & Turral, H. (2007). Spectral matching techniques to determine historical land-use/land-cover (LULC) and irrigated areas using time-series 0.1-degree AVHRR Pathfinder datasets.

Photogrammetric Engineering & Remote Sensing, *73*(10), 1029–1040.

United Nations. (2015). *World Population Prospects: The 2015 Revision, Key Findings and Advance Tables. Working Paper No. ESA/P/WP.241*. Retrieved from http://esa.un.org/unpd/wpp/publications/files/key_findings_wpp_2015.pdf

Van Niel, T. G., McVicar, T. R., & Datt, B. (2005). On the relationship between training sample size and data dimensionality: Monte Carlo analysis of broadband multi-temporal classification. *Remote Sensing of Environment*, *98*(4), 468–480. https://doi.org/10.1016/j.rse.2005.08.011

Veloso, A., Mermoz, S., Bouvet, A., Le Toan, T., Planells, M., Dejoux, J. F., & Ceschia, E. (2017). Understanding the temporal behavior of crops using Sentinel-1 and Sentinel-2-like data for agricultural applications. *Remote Sensing of Environment*, *199*, 415–426. https://doi.org/10.1016/j.rse.2017.07.015

Waldner, F., Fritz, S., Di Gregorio, A., Plotnikov, D., Bartalev, S., Kussul, N., … Defourny, P. (2016). A Unified Cropland Layer at 250 m for Global Agriculture Monitoring. *Data*, *1*(1), 3. https://doi.org/10.3390/data1010003

Wardlow, B. D., Egbert, S. L., & Kastens, J. H. (2007). Analysis of time-series MODIS 250 m vegetation index data for crop classification in the U.S. Central Great Plains. *Remote Sensing of Environment*, *108*(3), 290–310. https://doi.org/10.1016/j.rse.2006.11.021

Xue, Z., Du, P., & Feng, L. (2014). Phenology-Driven Land Cover Classification and Trend Analysis Based on Long-term Remote Sensing Image Series. *Selected Topics in Applied Earth Observations and Remote Sensing, IEEE Journal Of*, *7*(4), 1142–1156. https://doi.org/10.1109/JSTARS.2013.2294956

Yan, L., & Roy, D. P. (2015). Improved time series land cover classification by missing-observation-adaptive nonlinear dimensionality reduction. *Remote Sensing of Environment*, *158*, 478–491. https://doi.org/http://dx.doi.org/10.1016/j.rse.2014.11.024

Yang, C., Everitt, J. H., & Murden, D. (2011). Evaluating high resolution {SPOT} 5 satellite imagery for crop identification. *Computers and Electronics in Agriculture*, *75*(2), 347–354. https://doi.org/http://dx.doi.org/10.1016/j.compag.2010.12.012

Yang, Y., Huang, Q., Wu, W., Luo, J., Gao, L., Dong, W., … Hu, X. (2017). Geo-Parcel Based Crop Identification by Integrating High Spatial-Temporal Resolution Imagery from Multi-Source Satellite Data. *Remote Sensing*, *9*(12), 1298. https://doi.org/10.3390/rs9121298

Yomralioglu, T., Inan, H. I., Aydinoglu, A. C., & Uzun, B. (2009). *Scientific research and essays. Scientific Research and Essays* (Vol. 4). Academic Journals. Retrieved from https://academicjournals.org/journal/SRE/article-abstract/92B8C7020073

Yonezawa, C. (2007). Maximum likelihood classification combined with spectral angle mapper algorithm for high resolution satellite imagery. *International Journal of Remote Sensing*, *28*(16), 3729–3737. https://doi.org/10.1080/01431160701373713

Yu, X., Zhuang, D., Chen, H., & Hou, X. (2004). Forest classification based on MODIS time series and vegetation phenology. In *International Geoscience and Remote Sensing Symposium (IGARSS)* (Vol. 4, pp. 2369–2372). https://doi.org/10.1109/igarss.2004.1369764

Zhang, X., Friedl, M. A., Schaaf, C. B., Strahler, A. H., Hodges, J. C. F., Gao, F., … Huete, A. (2003). Monitoring vegetation phenology using MODIS. *Remote Sensing of Environment*, *84*(3), 471–475. https://doi.org/https://doi.org/10.1016/S0034-4257(02)00135-9

Zheng, B., Myint, S. W., Thenkabail, P. S., & Aggarwal, R. M. (2015). A support vector machine to identify irrigated crop types using time-series Landsat NDVI data. *International Journal of Applied Earth Observation and Geoinformation*, *34*, 103–112. https://doi.org/http://dx.doi.org/10.1016/j.jag.2014.07.002

Zhong, L., Gong, P., & Biging, G. S. (2014). Efficient corn and soybean mapping with temporal extendability: A multi-year experiment using Landsat imagery. *Remote Sensing of Environment*, *140*, 1–13. https://doi.org/http://dx.doi.org/10.1016/j.rse.2013.08.023

Zhu, Z., & Woodcock, C. E. (2012). Object-based cloud and cloud shadow detection in Landsat imagery. *Remote Sensing of Environment*, *118*, 83–94. https://doi.org/10.1016/j.rse.2011.10.028

CURRICULUM VITAE

Mustafa Teke was born in Osmancık, Çorum in 1982. He graduated from Middle East Technical University, Department of Electrical and Electronics Engineering in 2005. He received his M.S. degree from METU, Informatics Institute in 2010. He has started to his PhD education in Informatics Institute in 2010. Since 2005, he has been working as software engineer in field of military defense sector with several companies. His current research interests are in the field of signal and image processing, pattern recognition and computer vision.